This study concerns Wheen parallel plates. 圆 mas achieved at whi travlence occurred. A fibrilence which strop Fresults indicate a h currence of strong veld was in boundary layers By means of an on-li esclosely investigated Sintermittent between a ^{) Teans} of condition sar 's characteristic of the A theoretical bounda Sate the characteristic Fing entrance region (

^{ler} a range of Reynolds

indicated go,

ABSTRACT

AN INVESTIGATION OF INCOMPRESSIBLE CHANNEL FLOW

Βv

Norbert Anthony Feliss

This study concerns the mechanism of the transition process of flow between parallel plates. An experimental critical Reynolds number of 7280 was achieved at which the flow became unstable and transition to turbulence occurred. A wave of 63 to 75 Hz. was amplified at the onset of turbulence which strongly suggests its role in the transition process. The results indicate a highly localized transition process involving the occurrence of strong velocity spikes which are similar to transition processes in boundary layers.

By means of an on-line data acquisition system the bursting process was closely investigated. The shape of the velocity profile when the flow is intermittent between a turbulent slug and a laminar flow was analyzed by means of condition sampling. The major portion of the burst profile is characteristic of the common "one-seventh" turbulent shape.

A theoretical boundary layer analysis was utilized in order to elucidate the characteristics of the developing velocity profile in the converging entrance region of the channel. Entrance lengths were calculated over a range of Reynolds numbers and compared with experimental values. The results indicated good correlation between theory and experiment.

IX

in partial

Departme

AN INVESTIGATION OF INCOMPRESSIBLE CHANNEL FLOW

Ву

Norbert Anthony Feliss

A THESIS

Submitted to
Michigan State University
in partial fulfillment of the requirements
for the degree of

DOCTOR OF PHILOSOPHY

Department of Mechanical Engineering

1973



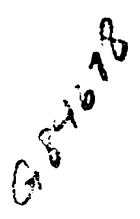
The author wishes to

1.0. Smith for assistar

Tanks are also due to 0
tise for serving as memt
Special appreciation

The financial support

Special Research made



ACKNOWLEDGEMENTS

The author wishes to thank his advisors, Drs. M. C. Potter and M. C. Smith for assistance throughout the course of this study.

Thanks are also due to Dr. J. V. Beck, Dr. N. L. Hills, and Dr. G. E. Mase for serving as members of the guidance committee.

Special appreciation is extended to Jim for his support and encouragement throughout the study.

The financial support which the author received from Division of Engineering Research made the continuation of graduate study possible.

.ST OF FIGURES :Vol. INTRODUCTION 2 1. Desa 2. Baci 2 THEORETICAL 1. Deve Bour 2. Sola 3. Res 3 EXPERIMENTAL 1. Cha 2. Ins 3. Dat Ļ EXPERIMENTAL 1. Ent

E

G H I

LIST OF TABLES

TABLE OF CONTENTS

																				Page
LIST	0F	TABL	.ES .			• •	• •				•		•		•		•	•	•	٧
LIST	0F	FIGU	IRES			• •	• • •				•		•		•		•	•	•	vi
CHAP	TER																			
1			INTR	ODUC	TION			• •			•		•		•		•	•	•	1
2				1.	Des Bac	crip kgro	otion ound	of •	Pro	ble	em •		•		•		•	•	•	1 2
2			THEO	RETI	CAL	ANAL	YSIS	FOF	R DE	VEL	OP I	NG	СНА	NNE	L F	LOW	١.	•	•	6
				1. 2. 3.	Bou Soli	ndar utic	oment by La on of of	yer the	Equ e Bo	ıati bund	ons ary	La	yer	Eq.	uat	ion	S		•	6 13 18
3			EXPE	RIME	NTAL	FAC	ILIT	'Y Ai	ND E	QU I	PME	NT	•		•		•		•	26
				1. 2. 3.	Ins	trun	Ass enta quis	tion	า้		•		•				•		•	26 27 29
4			EXPE	RIME	NTAL	RES	SULTS	. .			•		•		•		•	•	•	41
				1.	Α.	La Cr Cu	e an mina itic rve- amin	r Er al F Fitt	ntra Reyn ting	nce old to	Le s N Ve	ngt umb loc	hs er ity	 Pro	ofi		•	•	•	43
					Ε.	Tu Va	rbul riat	ent ion	Reg	ion Rey	s nol	ds	Num	ber	an	 d	•	•	•	53
					F.	Pr Va	obe riat	Posi ion	itio in	n Pre	•		•		•		•	•	•	56
					G. H. I.	Pr Si La	obe de W mina ectr	Posi all r Fl	itio Bou luct	n nda uat	ry ion	 Lay s B	er efo	 re]	Tra				•	56 60 65 75

	Pa	age
	 Mechanism of the Burst Process 8 A. Span-Wise and Length-Wise Variation 	2
	of the Burst Process	1
	C. Periodicity of Burst Process 9D. Velocity Profiles During Transition 9	9
5	DISCUSSION OF RESULTS	9
	 Conclusions	5 7
	APPENDICES	
	A - SYMBOLS FOR BOUNDARY LAYER ANALYSIS 11	8
	B - SYMBOLS USED IN EXPERIMENTAL RESULTS 12	1
	REFERENCES	3

- l. Variation of : channel . . .
- Variation of t channel . . .
- 3. Periodicity of

LIST OF TABLES

Table		Page
1.	Variation of burst process along length of channel	. 86
2.	Variation of burst process along width of channel	. 89
3.	Periodicity of burst process	96

... Two-dimension Illustration : Calculated dis for various Pe Calculated fre x-coordinate f Calculated ski x-coordinate f Comparison of lengths . . . Photograph of Schematic draw Photograph of Schematic draw Photograph of layer Probe . Schematic draw boundary layer Photograph of I Schematic drawi Variation of co function of the Comparison of t experimental er

Intensity varia function of the

LIST OF FIGURES

Figure		Page
1.	Two-dimensional inlet configuration	. 8
2.	Illustration of notation for boundary layer analysis	. 10
3.	Calculated displacement thickness versus x-coordinate for various Reynolds numbers	
4.	Calculated free stream velocity distribution versus x-coordinate for various Reynolds numbers	. 23
5.	Calculated skin friction coefficient versus x-coordinate for various Reynolds numbers	. 24
6.	Comparison of theoretical and experimental entrance lengths	. 25
7.	Photograph of experimental channel assembly	. 32
8.	Schematic drawing of experimental channel assembly .	. 33
9.	Photograph of motorized y-coordinate Probe	. 34
10.	Schematic drawing of motorized y-coordinate Probe	. 35
11.	Photograph of z-coordinate side wall boundary layer Probe	. 36
12.	Schematic drawing of z-coordinate side wall boundary layer Probe	. 37
13.	Photograph of IBM 1800 computer facility	. 38
14.	Schematic drawing of computer interface	. 39
15.	Variation of computer sampling rates as a function of the number of channels used	. 40
16.	Comparison of theoretical (Schlichting, 1962) and experimental entrance lengths	. 42
17.	Intensity variation (with the use of grids) as a function of the Revnolds number	. 44

- Computer print velocity profil
 Computer print velocity profil
 Computer print velocity profil
 Computer print
 Variation of Filaminar, burst
- Variation of F

 Comparison of the drop as a function
- ä. Side wall bour
- Intensity of 1 wall boundary
- Frequency spec various distan 0.340 inches
- Intensity of n Reynolds numbe
- ي Intensity vari Reynolds numbe
- Intensity vari $rac{Reynolds}{Reynolds}$ numbe
- Intensity vari Reynolds numbe
- Intensity var Reynolds numb
- Intensity var Reynolds numb
 - Mosaic of int range 3800 to range 6400 to
 - Frequency spe the hot wire

		P	age
18.	Computer printout of calculated and experimental velocity profiles (parabolic velocity)	•	4 8
19.	Computer printout of residuals	•	49
20.	Computer printout of calculated and experimental velocity profiles (non-parabolic profile)		51
21.	Computer printout of residuals	•	52
22.	Variation of Reynolds number with Probe position; laminar, bursting, and fully turbulent regions	•	54
23.	Variation of Pressure with Probe position	•	58
24.	Comparison of theoretical and experimental Pressure drop as a function of Probe position	•	61
25.	Side wall boundary layer thickness	•	62
26.	Intensity of laminar fluctuations for the side wall boundary layer	•	63
27.	Frequency spectra for the side wall boundary layer; at various distances from the wall: 0.010, 0.150, and 0.340 inches	•	64
28.	<pre>Intensity of natural disturbances as a function of Reynolds number; at X/d = 0</pre>	•	66
29.	Intensity variation as a function of X/d ; for the Reynolds number range 3800 to 7300	•	69
30.	Intensity variation as a function of X/d ; for the Reynolds number range 4200 to 7300	•	70
31.	Intensity variation as a function of X/d ; for the Reynolds number range 4800 to 7150	•	71
32.	Intensity variation as a function of X/d ; for the Reynolds number range 5000 to 7000	•	72
33.	Intensity variation as a function of X/d ; for the Reynolds number range 5400 to 6500 and 6400 to 7600 .	•	73
34.	Mosaic of intensity data: a) for the Reynolds number range 3800 to 6800, and b) for the Reynolds number range 6400 to 7600	•	74
35.	Frequency spectrum of 60 Hz. noise associated with the hot wire instrumentation		78

- Frequency spect of 6800 . . .
- Frequency spect of 7300 . . .
- # Frequency spectof 6800 . . .
- Schematic draw together with
- 4). Comparison bet sampling initi
- ". u' portion of z = -7.0 in. a
- u' portion of z = 15.5 in. a
- u' portion of z = 12.0 in. a
- u' portion of z = 14.5 in. a
- u' portion of z = 14.5 in. a
- . Mechanism of a
- Mosaic of vel
- Computer prin velocity prof
- S. Computer prin
- Velocity char during the bu
 - Perturbations burst process

		Page
36.	Frequency spectra at X/d of 336; for a Reynolds number of 6800	79
37.	Frequency spectra at X/d of 336; for a Reynolds number of 7300	80
38.	Frequency spectra at X/d of 144; for a Reynolds number of 6800	81
39.	Schematic drawing of Schmitt trigger circuit together with hot wire instrumentation	83
40.	Comparison between automatic and manual computer sampling initiation	84
41.	u' portion of computer sampled burst process at $z = -7.0$ in. and $z = 10.5$ in	87
42.	<pre>u' portion of computer sampled burst process at z = 15.5 in. and z = 2.0 in</pre>	90
43.	u' portion of computer sampled burst process at $z = 12.0$ in. and $z = 9.0$ in.; at X/d of 96	92
44.	u' portion of computer sampled burst process at $z = 14.5$ in. and $z = 1.0$ in.; at X/d of 120	93
45.	u' portion of computer sampled burst process at $z = 14.5$ in. and $z = 1.0$ in.; at X/d of 144	94
46.	Mechanism of the bursting process	97
47.	Mosaic of velocity profile during burst process	100
48.	Computer printout of calculated and experimental velocity profiles (1/7 power law profile)	103
49.	Computer printout of residuals	104
50.	Velocity changes near the wall and the centerline during the burst process	106
51.	Perturbations during the laminar portion of the burst process	107

The transition product of the experimental artisted at Michigan Statisted at Michigan St

- 1) A detailed exp veloped region lent flow. The this investiga
- An examination

 phenomenon of

 an on-line data
- A survey of the tal and theore profile.

CHAPTER 1

INTRODUCTION

1. Description of the Problem

The transition process of laminar flow between parallel plates is part of the experimental research effort on Plane Poiseuille flow being conducted at Michigan State University. The current study deals with a high aspect ratio channel facility which previously yielded Reynolds numbers greater than previously reported. The phenomenon of transition which is fundamental for the science of fluid mechanics has been studied experimentally since the full mechanism has not yet been established. Theoretical investigations of the development of the boundary layer in the entrance region of the channel can elucidate the characteristics of the developing velocity profile.

The thesis encompasses an extensive and explicit study of the following:

- 1) A detailed experimental study of the entrance region, fully developed region and the side wall region for laminar and turbulent flow. The approximate region of transition is located in this investigation.
- 2) An examination of the turbulent slug peculiar to channels. The phenomenon of the bursting process is explored with the aid of an on-line data acquisition computer facility.
- 3) A survey of the entrance flow region elucidating both experimental and theoretical investigations of the developing velocity profile.

] Bokground

in date, stability t

った "location" of tra

पक्ष) which profiles ar

derly small. It also c

खंड त्रेंड responsive an

Enameters such as wa

The the Schubauer-Skram

consted that in all ca

Thy of the laminar fl

The theoretical wor

"A between parallel p

Frintic expansions

Herage velocity and c

forbulence. L. H.

iritical Reynolds n

es sectormed by W. (

te amplitude in

recical technique

included that a re

er.

The process o

ix Kepanoff (13

thit wire mea.

2. Background

To date, stability theory can predict neither the details of the nonlinear process by which the flow changes from laminar to turbulent, nor the "location" of transition. What it can do is determine approximately which profiles are unstable providing the disturbances are sufficiently small. It also can identify those frequencies for which the system is most responsive and provides insight into how a change in the system parameters such as wave numbers or wave speeds can affect transition. Since the Schubauer-Skramstad (1943) experiments it has been generally accepeted that in all cases turbulence does indeed arise from an instability of the laminar flow for parallel shear flows.

The theoretical work of predicting the instability of Poiseuille flow between parallel plates was conducted by C. C. Lin (1945). Using asymptotic expansions he obtained a Reynolds number of 7,100 based on average velocity and channel height for the critical number at the onset of turbulence. L. H. Thomas (1953) using a numerical method calculated a critical Reynolds number of 7,700. A theoretical stability analysis was performed by W. C. Reynolds and M. C. Potter (1967) for a wave of finite amplitude in a parallel shear flow. Using a more sophisticated numerical technique they also determined a critical number of 7,700 and concluded that a relatively weak but finite disturbance markedly reduced this number.

The process of formation, growth, and coallescing of turbulent spots in a boundary layer has been studied in detail by Emmons (1951), Schubauer and Klebanoff (1955), Elder (1960), and Spangenberg and Rowland (1961). The hot wire measurements of Klebanoff et. al. (1962) indicated that

emir eddies") are i firly unstable and bre empinto random fluct Tani (1967) descri Deabsence of large di that stages in the following rces, (2) further non? Dent of high shear la indent randomness.) the appearance of we tary of laminar insta Previous work in a elin (1960), Patel : it the transition pr ್ಯೋಯ or less. She itilent slugs in a r ed his work and de Bofferent downstrea The stability of ^{हेंस} experimentally t ^{物質}tion. The crit far as the fluid. estillowed and break itheoretical an

artices generated by t

"hairpin eddies") are indicative of turbulent flow. These vortices are highly unstable and break down into smaller vortices which eventually develop into random fluctuations typical of turbulent flow.

Tani (1967) described the transition process in boundary layers, in the absence of large disturbuing influences, as a sequence of four distinct stages in the following order: (1) amplification of weak disturbances, (2) further nonlinear development of the disturbances, (3) development of high shear layer disturbances, and finally (4) development of turbulent randomness. Tani noted that the transition process is preceded by the appearance of weak oscillations of the type predicted by linearized theory of laminar instability.

Previous work in a rectangular channel such as those conducted by Sherlin (1960), Patel and Head (1969), and Breslin (1970) demonstrated that the transition process can take place at a critical Reynolds number of 3,000 or less. Sherlin determined the growth and propagation speed of turbulent slugs in a rectangular duct. Narayanan and Narayana (1968) extended his work and determined the characteristics of the bursting process at different downstream positions.

The stability of laminar flow in a rectangular channel was investigated experimentally by Kao and Park (1970) with and without artificial excitation. The critical Reynolds number was found to be 2,600 using water as the fluid. In particular, the progress of growing disturbances was followed and breaking was found to be the ultimate fate of a growing wave.

A theoretical analysis of a nonlinear instability burst in plane

gallel flow has recentl उनिर्मा the pressure Most approximat Te form of Prandtl isclution may be c Eference solution *:]sterle (1961), and Langhaar

series expa

em (1972). The object remmeron of transition may of the evolution of Wygranski and Champ mass in flow through arrary layer. They ex it detected the occurre mess. They demonstra south the leading and The development of my into a plane char in theory. It has a Feral features of vi त्र aminar flow in th E'r Schlichting's no iver equations by ex interces from the in parallel flow has recently been achieved by Stewartson, Stuart, and Brown (1972). The object of this investigation was to understand the phenomenon of transition by an extension of the linearized theory to the study of the evolution of arbitrary infinitesimal disturbances.

Wygnanski and Champagne (1970) found the behavior of the transition process in flow through circular tubes similar to that occurring in a boundary layer. They experimentally investigated the transition process and detected the occurrence of strong velocity spikes during the bursting process. They demonstrated for a pipe flow that the fluid was entrained at both the leading and trailing edges of the burst.

The development of a parabolic Poiseuille profile downstream of entry into a plane channel is one of the standard problems in laminar flow theory. It has attracted attention because it exemplifies certain general features of viscous flow. A determination of the entrance length for laminar flow in the inlet of a straight channel was initially treated in Schlichting's now classical paper (1934). He solved the boundary layer equations by expanding the stream function in a series for small distances from the inlet, starting with the Blassius solution, and matching with the pressure distribution for a uniform accelerating flow.

Most approximate analyses of the developing flow problem involve some form of Prandtl's boundary layer approximation. Four general methods of solution may be discerned in the literature: (1) numerical finite-difference solution of the boundary layer equations initiated by Bodoia and Osterle (1961), (2) linearization of the inertia terms, Boussinesq (1891) and Langhaar (1942), (3) integral expansions, Schiller (1922), and (4) series expansions, Schlichting (1934). An assumption common to

The way in which the limite parabolic velocifie non-uniformity of asymmetric studied.

Wilson (1971) re-exe

melast two methods is t

is of modern boundary 1 the entrance. The model ilel plates was found to laminar flow develop ix a paralle plate chang orbers. In this work th he use of boundary laye The first phase of * growth and developmen Herence methods were equations of mass; in layer methods comm (2) Cebeci and it rethod of Mellor ar ^{ीत, physical} soundnes ÷≎ en.

the last two methods is that the flow consists of boundary layers near the walls together with a central inviscid core in which the velocity increases downstream to satisfy continuity.

The way in which the boundary layers eventually merge to form the ultimate parabolic velocity distribution was considered by Van Dyke (1970). The non-uniformity of asymptotic expansions at large downstream locations was studied.

Wilson (1971) re-examined the work of Van Dyke (1970). The techniques of modern boundary layer theory were used to examine the region near the entrance. The model of uniform flow into an infinite cascade of parallel plates was found to be the most satisfactory.

Laminar flow development in the entrance region of a circular tube and a paralle plate channel was analyzed by Chen (1973) at low Reynolds numbers. In this work the momentum integral method was utilized without the use of boundary layer assumptions.

The first phase of this thesis includes a study of the boundary layer growth and development in the entrance region of a channel. Finite difference methods were utilized for solving the coupled partial difference equations of mass and momentum. The three finite difference boundary layer methods commonly used are those of: (1) Spalding and Pantankar (1968), (2) Cebeci and Smith (1968), and (3) Mellor and Herring (1969). The method of Mellor and Herring (1968) was chosen because of its accuracy, physical soundness, and adaptability to the particular application problem.

Clevelopment of the Studies of boundar me is the practical ne it the other is the de meron of boundary lay Tis thesis were design হালে techniques emplo For and Herring (196 In order to solve to Te free stream velocity in solution of the pro Tration was obtained

್ಯ two distinct region

is plate channel. In

ege until well into ti

in the law of conserva

THEORETICAL A

[া]ণ্ডল velocity. ing continuity

erefore,

feely is the free st it ree stream velocit ^{he shape} of the co

CHAPTER 2

THEORETICAL ANALYSIS FOR DEVELOPING CHANNEL FLOW

1. Development of the Potential Flow and Boundary Layer Equations

Studies of boundary layer flows have been made for two reasons:

one is the practical need for boundary layer solutions in design problems
and the other is the desire to achieve a better understanding of the phenomenon of boundary layer flows. The calculation methods described in
this thesis were designed to expedite both of these objectives. The numerical techniques employed in the analysis make use of the method of
Mellor and Herring (1968).

In order to solve the boundary layer equations a necessary input is the free stream velocity. Ordinarily, this is obtained from a potential flow solution of the problem. For the present channel facility this information was obtained in the following manner. The channel was divided into two distinct regions, the entrance section and the horizontal parallel plate channel. It was assumed that the boundary layers did not converge until well into the constant gap channel. For the contracting region the law of conservation of mass could be utilized to obtain the free stream velocity.

From continuity

$$\int \rho (\overrightarrow{U} \cdot \hat{\mathbf{n}}) dA = 0$$
 (2.1)

or

$$-\rho U_1 A_1 + \rho U_2 A_2 = 0$$

Therefore,

$$U_1 = (A_2/A_1) U_2$$
 (2.2)

where \mathbf{U}_1 is the free stream velocity in the contracting region and \mathbf{U}_2 is the free stream velocity at the entrance to the parallel plate region.

The shape of the contraction is a cantilever-cantilever beam

faction curve and is i

vere W is the force at the port of inertia, Lucrary constant. The bour

feeth is half the gap i

14/2, half the gap wid

1:

regeneral equation, the withe contracting reg

in oying continuity (2

the channel, U2.

A computer program is redified to including the present analys residue, two dimensis

deflection curve and is shown in Figure 1. the general formula for the deflections y at any point of a beam fixed at both ends is

$$y = \frac{Wx^2}{12EI} (3L - 2x) + C$$
 (2.3)

where W is the force at the fixed end, E the modulus of elasticity, I the moment of inertia, L the length of the contraction, and C an arbitrary constant. The boundary conditions are

$$x=0$$
, $y=h$ and $dy/dx = 0$

$$x=L$$
, $y=d*$ and $dy/dx = 0$

where h is half the gap width in the contraction at x = -6 ft., and d* is d/2, half the gap width in the channel. Employing these relations in (2.3) the following equation is obtained

$$\frac{W}{12EI} = \frac{d^*-h}{L^3} \tag{2.4}$$

The general equation, that describes the variation of y as a function of x in the contracting region is

$$y = \frac{d^*-h}{13} x^2 (3L-2x) + h$$
 (2.5)

Employing continuity (2.2) the potential flow velocity in the contraction, U_1 , can be expressed as a function of x and the potential flow velocity in the channel, U_2 .

$$U_{1} = \frac{d^{*}}{h - \frac{h - d^{*}}{13} x^{2} (3L - 2x)} U_{2}$$
 (2.6)

A computer program developed by H. J. Herring and G. L. Mellor (1970) was modified to include the calculation of the potential flow solution for the present analysis. The equations governing the flow of an incompressible, two dimensional, boundary layer illustrated in Figure 2,



Figure 1. Two-dir

Shape of Contraction

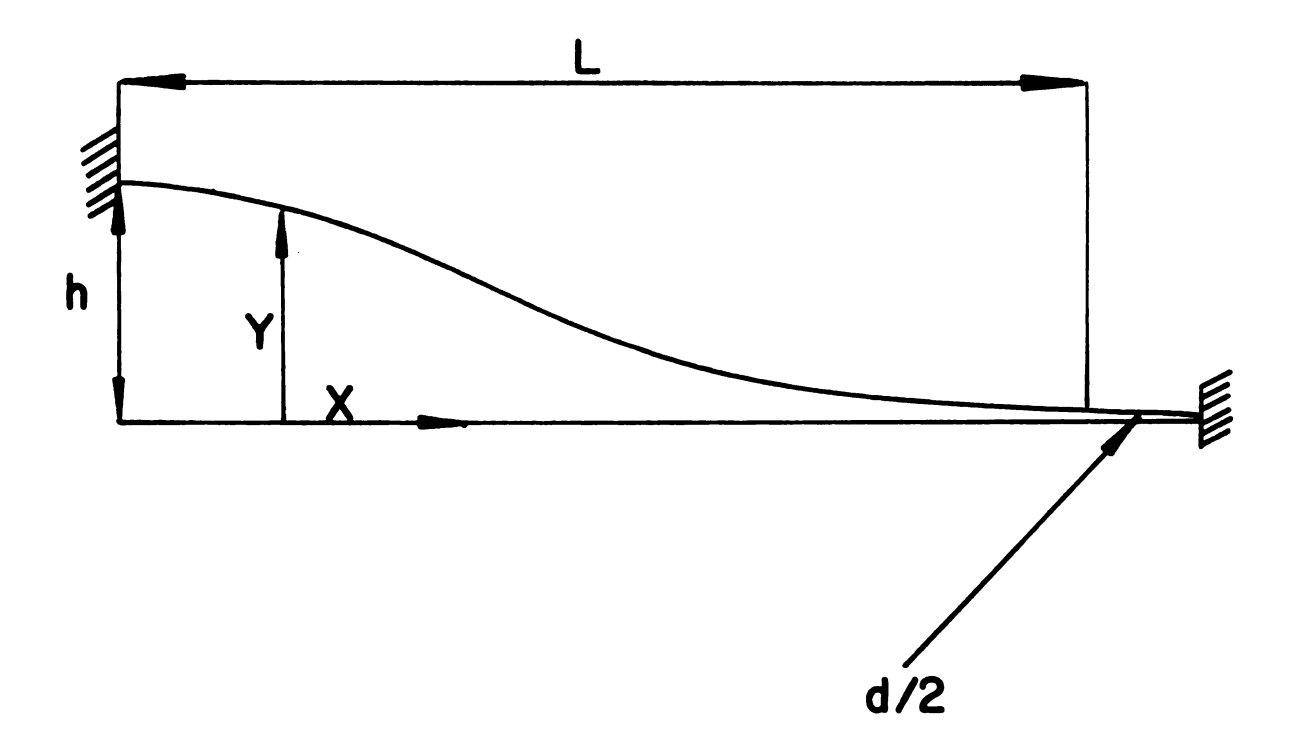


Figure 1. Two-dimensional inlet configuration

$$u \frac{3u}{3\overline{x}} +$$

$$\operatorname{def}(\overline{x},\overline{y}) = r_{W}(\overline{x}) + \overline{y}$$

intient boundary layer

rate -u'v' is the kinemater that the state of the state o

ree for laminar flow resundary conditions

$$\frac{1}{y} + \infty \quad 0$$

Sations (2.7) and (2

this transforman

are given by

$$\frac{\partial (ru)}{\partial \overline{x}} + \frac{\partial (rv)}{\partial \overline{y}} = 0 \tag{2.7}$$

$$u \frac{\partial u}{\partial \overline{x}} + v \frac{\partial u}{\partial \overline{y}} = U \frac{\partial U}{\partial \overline{x}} + \frac{1}{r} \frac{\partial (r \tau/\rho)}{\partial \overline{y}}$$
 (2.8)

where $r(\overline{x}, \overline{y}) = r_{\overline{W}}(\overline{x}) + \overline{y} \cos \alpha(\overline{x})$. The equations apply to laminar or turbulent boundary layer flow if the definition of τ/ρ is take to be

$$\tau/\rho = \nu \frac{\partial u}{\partial \overline{\nu}} - \overline{u'v'}$$
 (2.9)

where $-\overline{u^{\dagger}v^{\dagger}}$ is the kinematic Reynolds stress. The effective viscosity is defined by

$$\tau/\rho = \nu_{e} (\partial u/\partial \overline{y}) \tag{2.10}$$

where for laminar flow ν_{p} is equal to ν_{t} the kinematic viscosity.

The boundary conditions are

$$u(\overline{x},0) = 0 \tag{2.11a}$$

$$v(\overline{x},0) = 0 \tag{2.11b}$$

$$\frac{1}{v} = \frac{1}{v} \int_{-\infty}^{\overline{y}} \left[U(\overline{x}) - u(\overline{x}, \xi) \right] d\xi \text{ is bounded}$$
(2.11c)

Equations (2.7) and (2.8) are transformed with a variation of the Probstein-Elliott transformation.

$$x = \overline{x} \tag{2.12a}$$

$$y = \int_{0}^{\overline{y}} r(\overline{x}, \xi) / r_{W} d\xi$$
 (2.12b)

In the case of turbulent flow u is interpreted as a time average quantity. Using this transformation and the resulting relations

$$\frac{\partial}{\partial x} = \frac{\partial}{\partial x} + \frac{\partial y}{\partial x} \frac{\partial}{\partial y}$$

fire for laminar flow is soundary condition

 $\frac{\text{limit}}{y+\infty}$

Cations (2.7) and (

e case of turbul

are given by

$$\frac{\partial (ru)}{\partial \overline{x}} + \frac{\partial (rv)}{\partial \overline{y}} = 0 \tag{2.7}$$

$$u \frac{\partial u}{\partial \overline{x}} + v \frac{\partial u}{\partial \overline{y}} = U \frac{\partial U}{\partial \overline{x}} + \frac{1}{r} \frac{\partial (r \tau/\rho)}{\partial \overline{y}}$$
 (2.8)

where $r(\overline{x}, \overline{y}) = r_W(\overline{x}) + \overline{y} \cos \alpha(\overline{x})$. The equations apply to laminar or turbulent boundary layer flow if the definition of τ/ρ is take to be

$$\tau/\rho = \nu \frac{\partial u}{\partial \overline{y}} - \overline{u'v'}$$
 (2.9)

where $-\overline{u'v'}$ is the kinematic Reynolds stress. The effective viscosity is defined by

$$\tau/\rho = \nu_{e} (\partial u/\partial \overline{y})$$
 (2.10)

where for laminar flow ν_{e} is equal to $\nu,$ the kinematic viscosity.

The boundary conditions are

$$u(\overline{x},0) = 0 \tag{2.11a}$$

$$v(\overline{x},0) = 0 \tag{2.11b}$$

$$\frac{1}{v} = \frac{1}{v} \int_{-\infty}^{\overline{y}} \left[U(\overline{x}) - u(\overline{x}, \xi) \right] d\xi \text{ is bounded}$$
(2.11c)

Equations (2.7) and (2.8) are transformed with a variation of the Probstein-Elliott transformation.

$$x = \overline{x} \tag{2.12a}$$

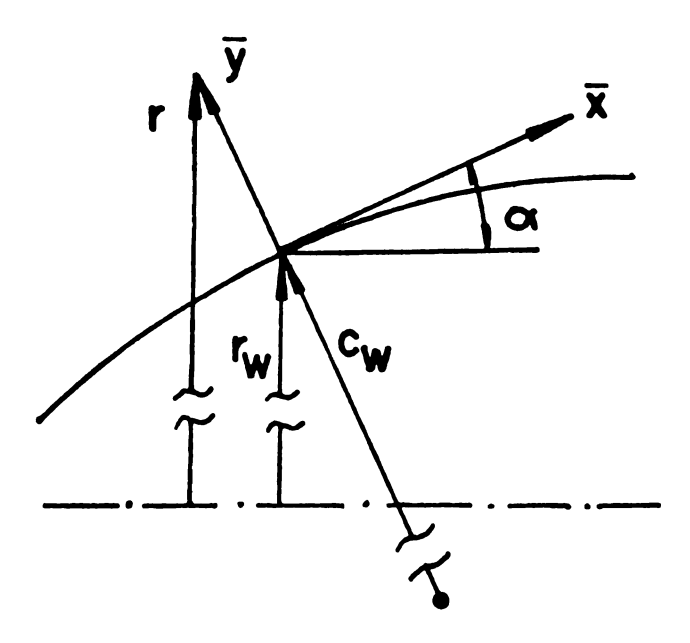
$$y = \int_{0}^{\overline{y}} r(\overline{x}, \xi) / r_{W} d\xi$$
 (2.12b)

In the case of turbulent flow u is interpreted as a time average quantity. Using this transformation and the resulting relations

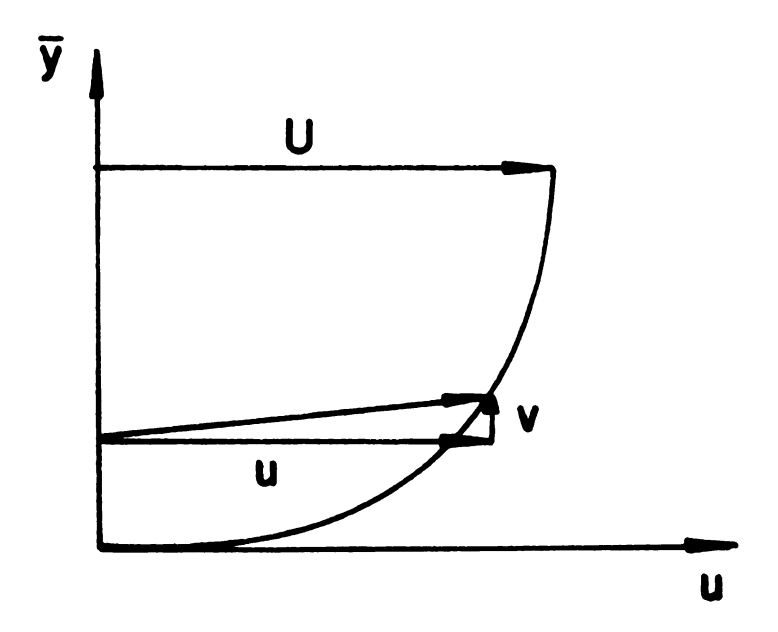
$$\frac{9x}{9} = \frac{9x}{9} + \frac{9x}{9} \frac{9x}{9}$$



Figure 2. N



Coordinate System



Velocity Profile

Figure 2. Notation for boundary layer analysis.

mations (2.7) and (2.8

$$u \frac{\partial u}{\partial x} + v$$

in the calculation pro Exity profile is exp Personnations

is the displace #

When rewritten in it (2.14) become

Yere, $P = 6* \frac{dU}{dx}/U$, C $\frac{1}{2} = \frac{2(6*/r_W)}{cos}$ Teboundary condition

$$\frac{\partial}{\partial y} = \frac{r}{r_w} \frac{\partial}{\partial y}$$

equations (2.7) and (2.8) become

$$\frac{1}{r_{w}} \frac{\partial (u \cdot r_{w})}{\partial x} + \frac{\partial v}{\partial y} = 0 \qquad (2.13)$$

$$u \frac{\partial u}{\partial x} + v \frac{\partial u}{\partial y} = U \frac{\partial U}{\partial x} + \frac{\partial}{\partial y} \left(\frac{r}{r_w} \frac{\tau}{\rho}\right) \qquad (2.14)$$

For the calculation procedure a new set of variables is introduced. The velocity profile is expressed in defect form according to the following transformations

$$\eta = y/\delta^* \tag{2.15a}$$

$$f'(x,\eta) = \frac{\partial f}{\partial \eta} = \frac{U(x) - u(x,\eta)}{U(x)}$$
 (2.15b)

where & is the displacement thickness.

When rewritten in terms of these new variables, equations (2.13) and (2.14) become

$$[(1 + C_{a}\eta) Tf'']' + [(Q + R)(\eta - f) - v_{w}/U]f'' + P(f' - 2)f' = \delta^{*}(1 - f') \frac{\partial f}{\partial x} + \delta^{*}f'' \frac{\partial f}{\partial x}$$
(2.16)

where, $P = \delta^* \frac{dU}{dx}/U$, $Q = \frac{d(\delta^*U)}{dx}/U$, $R = \delta^* \frac{dr_w}{dx}/r_w$,

$$C_a = 2(\delta^*/r_w) \cos , T = v_e/(U \delta^*)$$

The boundary conditions are

$$f'(x,0) = 1$$
 (2.17a)

$$f(x,0) = 0$$
 (2.17b)

Limit
$$f(x,\eta) \rightarrow 1$$
 (2.17c)

Testern I is the nondimental inner parameter \$\phi\$ a stivited into three discential and a defect layer.

Latities, \$\psi\$, \$\psi\$, and \$\parameter\$ is defined.

ithe outer, or defect it, y, and au/ay. Th

the two layer model,

The value $\kappa = 0.41$ is the experimentally observation is expressed at the common asymptote in can be written for

Fig.R = US*

The term T is the nondimensional effective viscosity and is a function of an inner parameter ϕ and an outer parameter Φ . The boundary layer is divided into three distinct regions: the wall layer, the overlap layer, and a defect layer. In the inner or wall layer, ν_e depends on three quantities, ν , y, and $\partial u/\partial y$ where ν_e is the effective viscosity. The inner function is defined as

$$\phi(\times) = \frac{v_e}{v}, \quad \times = \frac{\kappa \eta \delta^*}{v} \sqrt{\tau/\rho}$$
 (2.18a,b)

In the outer, or defect layer, v_e depends on the three quantities, (5*U), y, and $\partial u/\partial y$. The outer function can be defined as

$$\Phi(\chi) = \frac{v_e}{v}, \quad \chi = \frac{\kappa \eta}{U} \sqrt{\tau/\rho}$$
 (2.19a,b)

In the two layer model, there is a region where the layers overlap and both expressions for ν_e apply simultaneously.

$$v_e = v\phi = \delta * U \Phi = \kappa \eta \delta * \sqrt{\tau/\rho}$$

The value κ = 0.41 is the von Karman constant and is chosen to predict the experimentally observed logarithmic law of the wall. The composite function is expressed as the sum of the inner and outer functions minus their common asymptote. Thus, the nondimensional effective viscosity,

T, can be written for turbulent flow over the whole layer as

$$T = \phi(\times) + R_{\delta^*} \Phi(\frac{\times}{R_{\delta^*}}) - \times \qquad (2.20a)$$

$$T = \frac{1}{R_{\delta \star}} \phi(R_{\delta \star} \chi) + \Phi(\chi) - \chi \qquad (2.20b)$$

where $R_{\kappa^*} = \frac{U\delta^*}{v}$. For laminar flow $T = 1/R_{\delta^*}$.

1 Solution of the Bour Equation (2.16) wh Their parabolic partia igasolution is: conv enation using finite di multing equation by a An adaption of the Herivatives by finite iess stable. The erro 236) is written in te $\Re x$ position of the katulated, x_i . رِيِّ)] + [ريَّيْ (ريَّيْ)] + [ريَّيْ (ريَّيْ)

 $\frac{\overline{c}^*}{\Delta x}$ (1-

here the relation for Dation (2.23) can be

(jtc^a+) 14.,], ! = -

Cl = (5x + b + l C2 = b [1/2(fi C3 = (5* + 5* 1-1

C4 = (5* + 5*;--

2. Solution of the Boundary Layer Equations

Equation (2.16) which describes the boundary layer flow is a non-linear parabolic partial differential equation. The procedure of obtaining a solution is: conversion to an ordinary differential-difference equation using finite differences for the x-derivatives; and solving the resulting equation by a fourth order Runge-Kutta method.

An adaption of the Crank-Nicholson scheme is used to represent the x-derivatives by finite differences. This is an implicit method and is always stable. The error is of second order in the x-step size. Equation (2.16) is written in terms of average functions at a point halfway between the x position of the known profile, x_{i-1} , and that of the profile to be calculated, x_i .

where the relation $\overline{f}' = 1/2(f'_i + f'_{i-1})$ is used.

Equation (2.23) can be written in terms of functions at position x_i as follows

$$-[(1+C_{a}^{\eta}) Tf'']'_{i} = -\tau'_{b} + C_{1}(f''_{i} + f''_{i-1}) + C_{2}(f'_{i} + f'_{i-1}) - C_{3}(f'_{i} + f'_{i-1}) - C_{4}(f_{i} + f_{i-1})$$
(2.24)

where

$$C_{1} = (\overline{\delta}_{X}^{*} + \overline{P} + \overline{R})[\eta - 1/2(f_{i}^{+} + f_{i-1}^{-})] - (v_{w_{i}}^{+} + v_{w_{i-1}}^{-})/(U_{i}^{+} + U_{i-1}^{-})$$

$$C_{2} = P [1/2(f_{i}^{+} + f_{i-1}^{+}) - 2]$$

$$C_{3} = (\delta_{i}^{*} + \delta_{i-1}^{*}) [1 - 1/2(f_{i}^{+} + f_{i-1}^{+})]/\Delta x$$

$$C_{4} = (\delta_{i}^{*} + \delta_{i-1}^{*}) 1/2(f_{i}^{*} + f_{i-1}^{*})/\Delta x$$

.

 $\tau_b^* = -[(1 + C_a \tau)]$

The resulting form of

$$[b_5f'']_1^! = b_4 + b_4$$

were the coefficients

b₁ = -C₄

 $b_2 = c_2 - c_3$

b₃ = C₁

 $b_4 = -\frac{1}{1}b + C_1f_{1-}^{**}$

b₅ = -(1 + C_a, -

it solution of (2.26)

The coeffi

*previous iteration

ecf. The displacer

ime specified accurac

et the effective visc

Equation (2.26)

Eure used for solving tation is rewritten

`:er,

`exundary condition

$$\tau_b' = -[(1 + C_a^n) Tf'']_{i-1}'$$
 (2.25a,b,c,d,e)

The resulting form of the nonlinear ordinary differential equation is

$$[b_5f'']_i' = b_4 + b_3f_i'' + b_2f_i' + b_1f_i$$
 (2.26)

where the coefficients are

$$b_{1} = -C_{4}$$

$$b_{2} = C_{2} - C_{3}$$

$$b_{3} = C_{1}$$

$$b_{4} = -\tau_{b}' + C_{1}f_{i-1}'' + (C_{2} + C_{3})f_{i-1}' + C_{4}f_{i-1}$$

$$b_{5} = -(1 + C_{a_{i}})^{\eta} T_{i}$$
(2.27a,b,c,d,e)

The solution of (2.26) is carried out iteratively because of its non-linearity. The coefficients b_1 to b_5 are evaluated using the result of the previous iteration. The resulting linear equation is solved for f' and f". The displacement thickness δ^* is adjusted so that $f(\infty) = 1$ to some specified accuracy. The parameters P,Q,R, and C_a are recalculated and the effective viscosity function, T, is also recalculated.

Equation (2.26) is solved with a Runge-Kutta method which is a procedure used for solving first order ordinary differential equations. The equation is rewritten as a set of first order equations as follows.

$$f^{(1)} = f, \quad f^{(2)} = f', \quad f^{(3)} = b_5 f''$$

$$\frac{\partial f^{(1)}}{\partial \eta} = f^{(2)}, \quad \frac{\partial f^{(2)}}{\partial \eta} = f^{(3)}/b_5$$

$$\frac{\partial f^{(3)}}{\partial \eta} = b_4 + b_3 (f^{(3)}/b_5) + b_2 f^{(2)} + b_1 f^{(1)}$$
(2.28a,b,c)

The boundary conditions (2.17a) and (2.17b) are applied at the wall and

汉制 is applied at tr tra method requires th per of the operational eda particular solutio mundary conditions at t inthe particular solut

 $\frac{1}{2}$ $x_i(0)$ is reset to f" Stores progressively c Sertial but it does re in the homogeneous solu

iea corposite numerica etion

esa free parameter V The outer be tierge n which is an ! the appropriate ter

issution of (2.32) car

(2.17c) is applied at the outer edge of the layer. Since the Runge-Kutta method requires three boundary conditions at the wall advantage is taken of the operational linearity of equation (2.26). Both a homogeneous and a particular solution are calculated which satisfy the following boundary conditions at the wall:

For the particular solution

$$f_p^{"}(x,0) = f^{"}(x,0)$$
, (from the previous iteration) (2.29a)

$$f_n'(x,0) = 1.0$$
 (2.29b)

$$f_{D}(x,0) = 0.0$$
 (2.29c)

 $f_p^{"}(x,0)$ is reset to $f^{"}(x,0)$ each time so that the particular solution becomes progressively closer to the complete solution. This step is not essential but it does result in an increase in accuracy.

For the homogeneous solution

$$f_b^{"}(x,0) = 1.0$$
 (2.30a)

$$f_h^i(x,0) = 0.0$$
 (2.30b)

$$f_h(x,0) = 0.0$$
 (2.30c)

The a composite numerical solution is constructed according to the relation

$$f' = f'_p + A_f f'_h \tag{2.31}$$

 A_f is a free parameter which is determined by matching the outer boundary condition. The outer boundary condition is the solution of equation (2.16) at large η which is an improved outer boundary condition of equation (2.17c). With the appropriate terms omitted (f' small, $f \approx 1$) equation (2.16) is $[(1 + C_a \eta) T_\infty f'']' + (Q + R)(\eta - 1)f'' - 2Pf' = \delta^* \frac{\partial f'}{\partial x}$ (2.32)

A solution of (2.32) can be written $f'(\eta) = f'(\eta_a) \exp\left[\frac{(\eta_a - 1)^2 - (\eta - 1)^2}{2s(x)(1 + C_a \eta)}\right] \qquad (2.33)$

were s(x) is a solution

is 1.0 for a two-difference is the value of reasymptotic solution for (2.34), replaces

rere

reparameter s(x) is (

s_i = 2

iserting equation (2.

in the range $(0 < n < n_a)$, is solution can then (33).

Occasionally, the street that equation its. For example, o forms, if f becomes thin general approact

where s(x) is a solution of the equation

$$(\delta^*/2) \frac{ds}{dx} + C_s(Q + R)s = T_{\infty}C_s^2$$
 (2.34)

 C_s is 1.0 for a two-dimensional flow and 0.5 for an axisymmetric flow, and n_a is the value of n at which the numerical solution is matched to the asymptotic solution. Therefore, equation (2.33), where s is obtained from (2.34), replaces (2.17c) as the outer boundary condition. From equation (2.33), at some point n_a , near the edge of the layer

$$f''(\eta_a) = -A_s f'(\eta_a)$$
 (2.35a)

where

$$A_{s} = \frac{(\eta - 1)}{s(x)(1 + C_{a}\eta)} \left[1 - \frac{(\eta - 1)C_{a}}{2(1 + C_{a}\eta)} \right] \qquad (2.35b)$$

The parameter s(x) is obtained from the approximate solution of equation (2.34)

$$s_{i} = \frac{2(\Delta x/\overline{\delta}^{*})\overline{T}_{\infty}C_{S}^{2} + s_{i-1}\left[1 - (\overline{Q}+\overline{R}) C_{S}(\Delta x/\overline{\delta}^{*})\right]}{1 + (\overline{Q}+\overline{R}) C_{S}(\Delta x/\overline{\delta}^{*})}$$
(2.36)

Inserting equation (2.35a) into (2.31) and rearranging yields,

$$A_{f} = \frac{f_{p}^{"}(\eta_{a}) + A_{s}f_{p}^{"}(\eta_{a})}{f_{h}^{"}(\eta_{a}) + A_{s}f_{h}^{"}(\eta_{a})}$$
(2.37)

In the range $(0<\eta<\eta_a)$, f' (and f,f") may be calculated from equation (2.31). The solution can then be extended out to any value of η using equation (2.33).

Occasionally, the solutions f_p' and f_h' become so large before η_a is reached that equation (2.31) no longer gives numerically significant results. For example, on a computer carrying numbers of seven significant figures, if f_p' becomes larger than 10^4 , f' given by equation (2.31) will not in general approach zero at the edge of the boundary layer to three

emition (2.29a). If a motion (2.29a). If a motion (2.29a). If a motion, this indicate all have no noticeable at its permissable to remain allow a more accorded several timescurate.

significant figures. To overcome this problem, a recalculation is performed using the same coefficients (2.27), but resetting the boundary condition (2.29a). If, recalculation fails to produce a small enough f_p' solution, this indicates that changes in the outer portion of the profile will have no noticeable effect on the f_p' solution near the wall. Therefore, it is permissable to reset f_p'' at some point, n_s , further out in the layer which will allow a more accurate calculation of f_p' . Recalculation may be performed several times with n_s further and further out as f_p' becomes more accurate.



: Results of the B By using the f ::: to the boundar the entrance region whes prior to the tat the boundary la thing influence ger Safilter device v fastraw chamber 1 if the boundary layer In order to co rescribe the veloc Palation. The v Tr flow over a fla Spated boundary 1 Tream velocity. [tream velocity tha itions were all ba A more accura facement thick ϵ ll should be dis

^{tt: accelerated.} ignoids number is i'el plate channe

Tis numbers. A Pirance region as

3. Results of the Boundary Layer Analysis

By using the free stream velocity obtained from continuity as an input to the boundary layer analysis the growth of the boundary layer in the entrance region was computed. The calculations were initiated seven inches prior to the beginning of the contracting region. It was assumed that the boundary layer growth was small up to this point because of the mixing influence generated by the filter assembly. The settling chamber is a filter device which is attached to the contraction. It is made up of a straw chamber followed by a series of five screens. The calculation of the boundary layer was begun at the junction of the final screen.

In order to compute a boundary layer solution it was necessary to prescribe the velocity profile in the boundary layer at the start of the calculation. The velocity profile resulting from a similarity solution for flow over a flat plate was assumed. During the calculation the first computed boundary layer solution was utilized to recalculate a new free stream velocity. Usually four iterations were necessary to obtain a free stream velocity that remained invariant after recalculation. The calculations were all based upon a laminar boundary layer.

A more accurate measure than the boundary layer thickness is the displacement thickness. The displacement thickness is that distance the wall should be displaced outwards so that the external potential flow is not accelerated. The displacement thickness, DT, as a function of x and Reynolds number is presented in Figure 3. At the beginning of the parallel plate channel the displacement thickness is a minimum for all Reynolds numbers. A maximum displacement thickness is observed in the entrance region at x = -5 ft.. The distributions indicate that the

replacement thickness
This observation correl
affat plate.

The calculated from the witers between -6 ft. to 2.8 ft./sthe velocity incresers and represents and represent

A large increase involds numbers start in 2 ft. At small Remains were early and the high Reynolds numbers in an incommon until after

A laminar velocing calculations of the transition region

the calculation

The numerical temperature to the preceding bounds

region of maxim

resses sharply. F

displacement thickness is inversely proportional to the Reynolds number.

This observation correlates with the Blassius solution for flow over a flat plate.

The calculated free stream velocity is presented in Figure 4. A linear increase in the free stream velocity is observed for all Reynolds numbers between -6 ft. and -3 ft. The velocity increases from 1.3 ft./sec. at -6 ft. to 2.8 ft./sec. at -3 ft. for a Reynolds number of 7300. This represents a slope, dU/dx, of 0.5 sec. -1. For the Reynolds number of 2550 the velocity increases from 0.5 ft./sec. to 1.0 ft./sec. over the same region and represents a slope of 0.2 sec. -1.

A large increase in the free stream velocity is evident for all Reynolds numbers starting at x = -2 ft. and increasing to a maximum at x = 2 ft. At small Reynolds numbers the free stream velocity reaches a maximum very early and remains constant at approximately x = 2 ft. At the high Reynolds numbers it is observed that the velocity does not reach a maximum until after 5 ft.

A laminar velocity profile is considered in all cases since theoretical calculations were not employed to predict a transition from a laminar to a turbulent flow. From previous experiments it was observed that the transition region did not occur until approximately x = 5 ft. Therefore, the calculations at the large Reynolds numbers can be based upon a laminar boundary layer profile prior to this region.

The numerical prediction of the skin friction coefficient based upon the preceding boundary layer calculations is depicted in Figure 5. At the region of maximum velocity, x = -2 ft., the friction coefficient decreases sharply. For all Reynolds numbers, a constant friction coefficient

folis attained at a The boundary laye frwich the velocity green velocity. The 5 eixity is attained to larger than the displac 'ayer for all Reynolds ile plate channel. A ⊯tmo boundary layers where the boundary la The entrance leng The was calculated for Merimental values. A esths is presented in 'mital values appear t ers above 3000 the the ेशिश्चीly observed. TH all sped when the bour $^{\frac{1}{2}}$ way in which the bo રવામાં velocity dis-Taily matching of the The boundary layer. * resence of vortic Tion also complicate Ter is increased.

of 0.1 is attained at approximately x = 2 ft.

The boundary layer thickness was calculated based upon a distance for which the velocity in the boundary layer reaches 99.5% of the free stream velocity. The boundary layer thickness over which the potential velocity is attained to within 1 percent is approximately three times larger than the displacement thickness. The thickness of the boundary layer for all Reynolds numbers is a minimum at the entrance to the parallel plate channel. A fully developed velocity profile is achieved when the two boundary layers eventually converge. For the small Reynolds numbers the boundary layers quickly converge.

The entrance length necessary to develop a parabolic velocity profile was calculated for a number of Reynolds numbers and compared to the experimental values. A plot of experimental and theoretical entrance lengths is presented in Figure 6. At the low Reynolds numbers the theoretical values appear to correlate well with experiment. At Reynolds numbers above 3000 the theory predicts a shorter entrance length than experimentally observed. The assumption that the velocity profile is fully developed when the boundary layers come together is not entirely correct. The way in which the boundary layers eventually merge to form the ultimate parabolic velocity distribution is a problem that was considered by Van Dyke (1970) and Wilson (1971). The problem to be solved involves the critically matching of the boundary layer solution into the speed at the edge of the boundary layer. This can be done by means of asymptotic expansions. The presence of vorticity induced in the inviscid core by the inlet condition also complicates the problem. This effect increases as the Reynolds number is increased. Thus the boundary layers come together and after a

The ability to prescribe ability to prescribe ability to prescribe ability to prescribe attending the mechanics carrels.

short distance the profile is parabolic.

The ability to predict the boundary layer solution based upon a calculated free stream velocity provides the analyst with an extremely useful tool. This investigation can be extended to optimize and design better entrance regions. This could provide better insight for understanding the mechanics of developing flows in the entrance regions of channels.

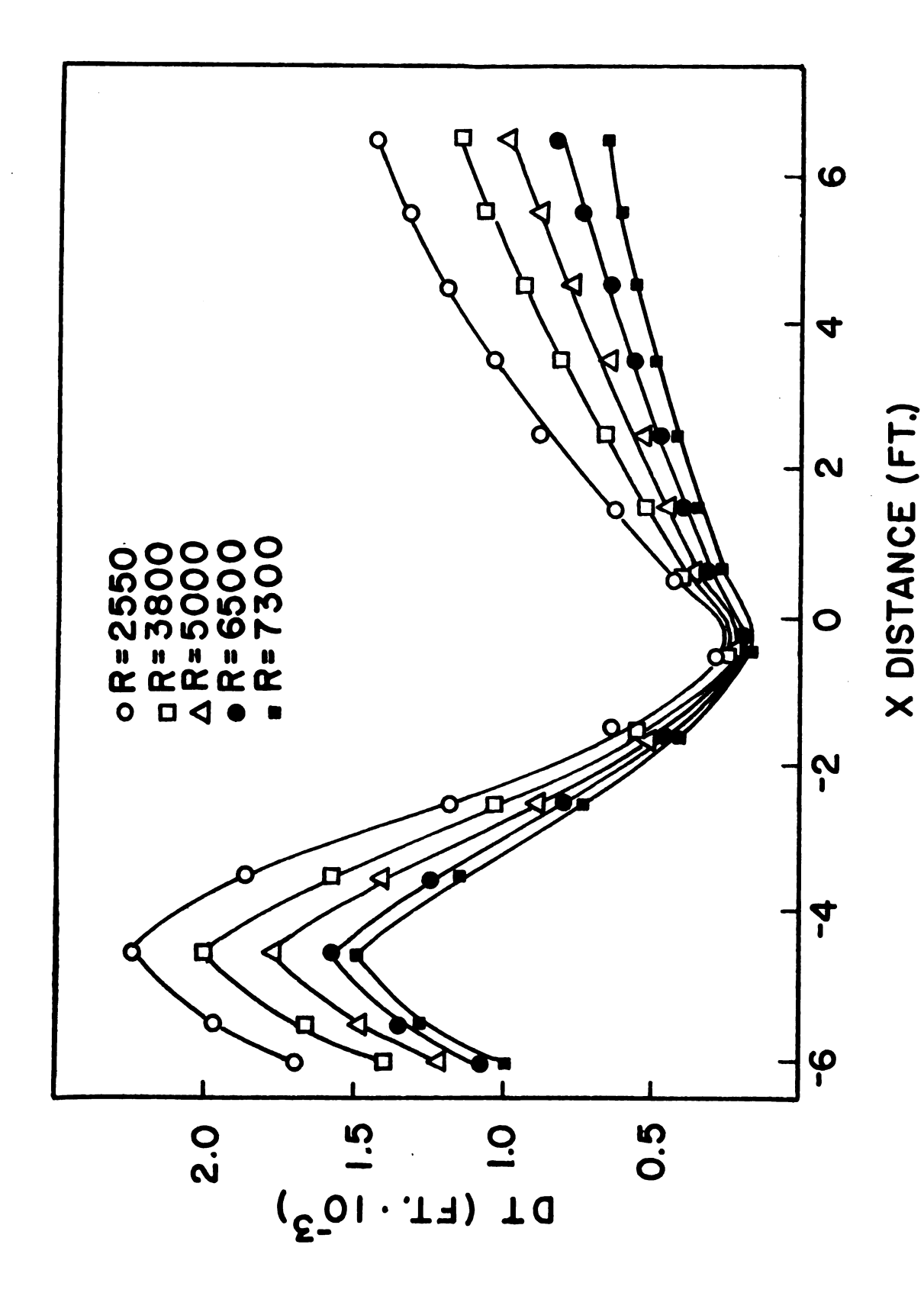


Figure 3. Calculated displacement thickness for various Reynolds numbers.

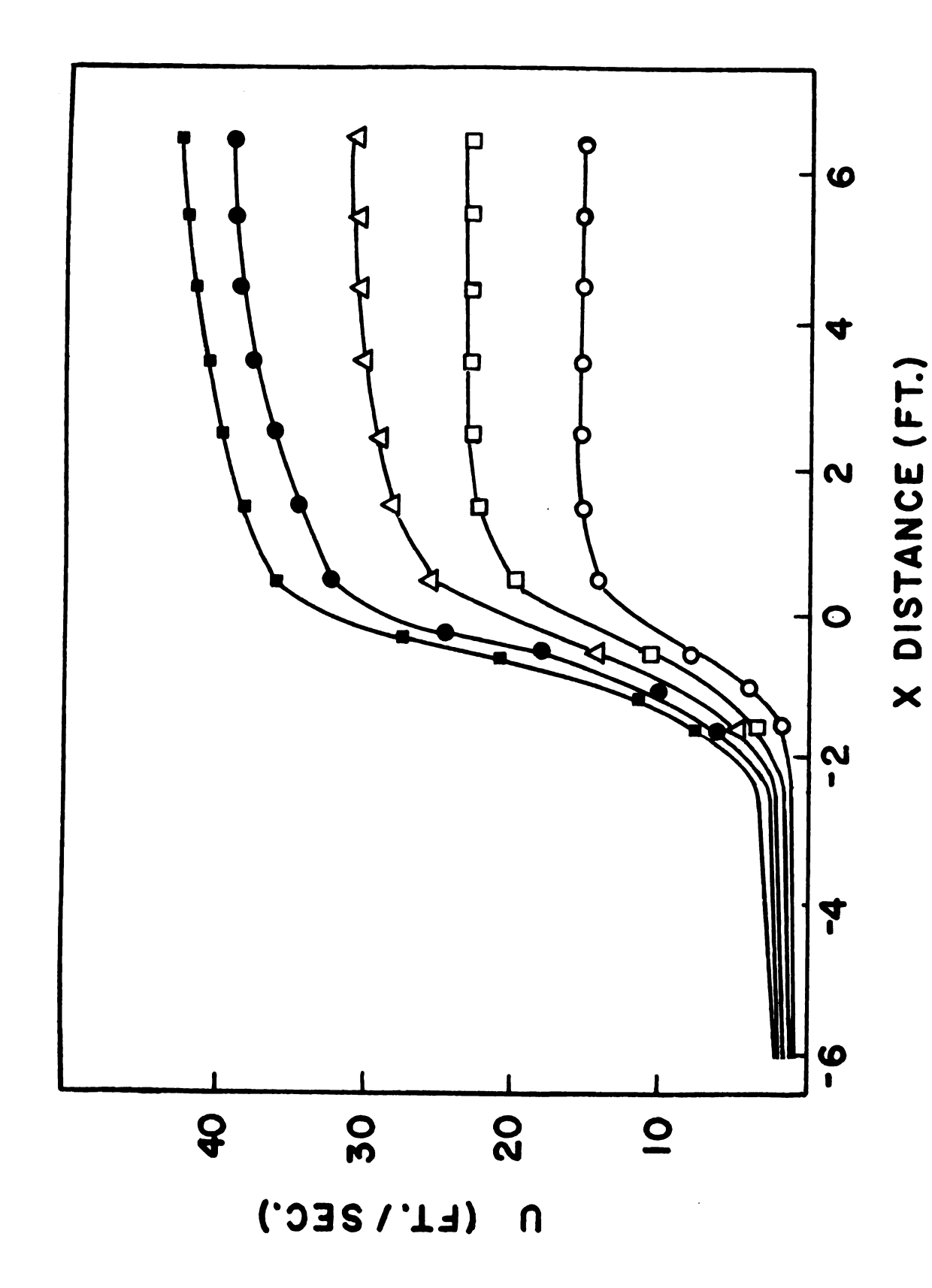


Figure 4. Calculated free stream velocity for various Reynolds numbers.

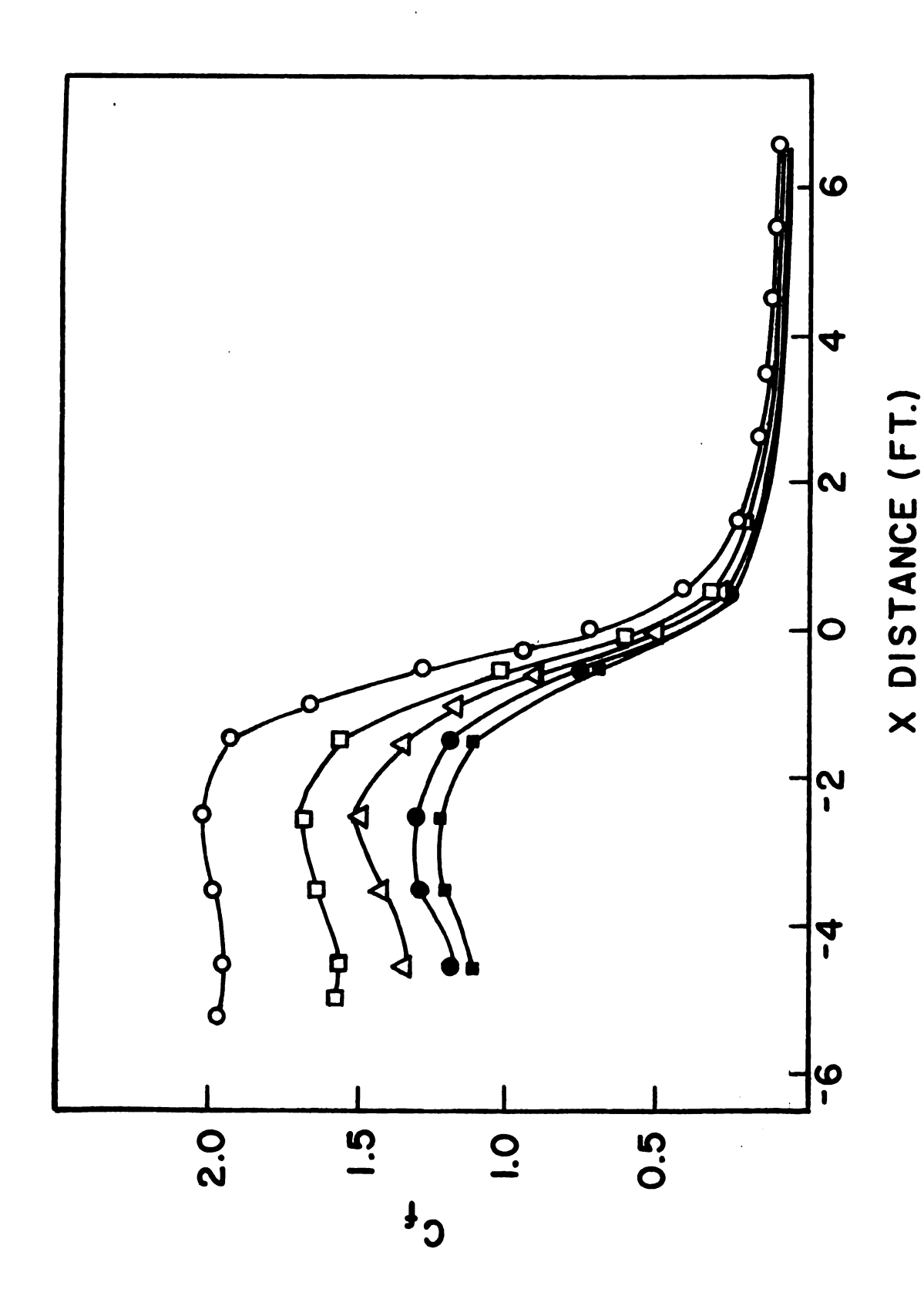


Figure 5. Calculated skin friction coefficient for various Reynolds numbers.

R 4000

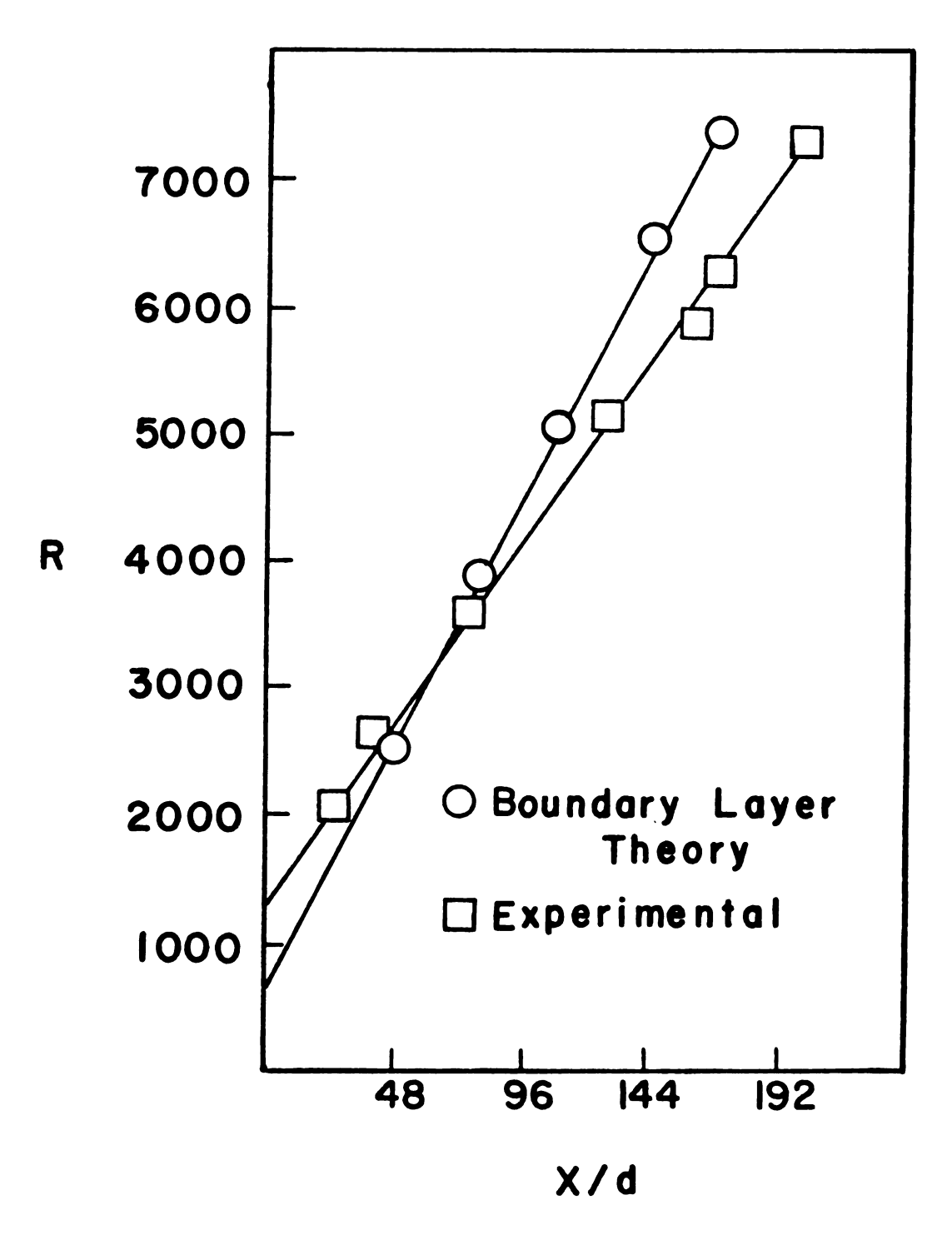


Figure 6. Comparison of theoretical and experimental entrance lengths.

CHAPTER 3

EXPERIMENTAL FACILITY AND EQUIPMENT

1. Channel Assembly

Experiments were carried out in a rectangular parallel-sided channel 24 ft. long, 35 in. wide, with a gap width of 1/2 in. The entire assembly consists of an entrance region, a parallel plate region, and a plenum chamber. A settling chamber 1 ft. by 3 ft. in cross section and 5 ft. long together with a contraction 6 ft. long, 3 ft. wide, "smoothly" drawing together from 1 ft. to 1/2 in. and 36 in. to 35 in. constitutes the entrance region to the parallel plate channel. The rear assembly of the channel consisted of a plenum chamber 8 ft. by 5 ft. by 4 ft. and a centrifugal fan assembly attached to the plenum chamber. The details of this system are presented in Figures 7 and 8.

The settling chamber is a filter device which consists of a large fiberglass gauze filter, two honeycomb straw sections completely filled with straws, 8 & 1/4 in. long, 1/4 in. in diameter, and a series of 5 screens, 7 in. apart, with mesh sizes of 40, 40, 80, 100, and 120 respectively. The contracting region beginning 7 in. following the 120 mesh screen, is constructed of sheet metal and wood. A strong matrix of wood and fiberglass on the outside of the sheet metal serves to strengthen the device and to dampen vibrations.

The experimental test section consists of two large horizontal plates separated by a width of 1/2 in. The bottom plate is a series of 3 rolled and polished aluminum plates which are sealed at the joints and polished smooth. The side walls are aluminum strips (except for a short section, 4 ft. long on the right hand side between X/d of 120 and 216, of acrylic

plastic) 1/2 in. by 1/2 in. and 24 ft. long. Thirteen supporting members consisting of aluminum bars 1 in. by 1 in. by 48 in. are fastened at intervals of 23 in. across the width of the top plate. Their function is to insure the top and bottom plates are kept at a constant distance apart. The top plate can be displaced up and down by adjusting the bolts in these supports. A special gapping instrument is used to measure the displacement of the top plate with respect to the bottom plate. The sensitivity of this instrument is such that variations of .005 in. can be detected. In this manner the gap width of the channel was adjusted to 0.500 \pm 0.010 in.

The plenum chamber not only serves as an exhaust chamber but also allows entry for the analyst to insert special test equipment into the channel region. During the course of an experiment this chamber is sealed shut. To eliminate vibrations and noise both the plenum chamber and the exhaust fan assembly are well insulated.

2. Instrumentation

A. Velocity Measuring Devices

Measurements of the mean flow profiles were obtained by means of a hot wire anemometry system. The hot wires were mounted on a unique probe system that traversed the flow field in either the y or z directions. Three probes were designed for this purpose and two of these probes were capable of traversing in the y-direction and the third in the z-direction. A motorized probe capable of traversing the flow in the y-direction through electronic pulses generated manually or automatically is shown in Figures 9 and 10.

The motorized probe is operated by means of a small stepping motor

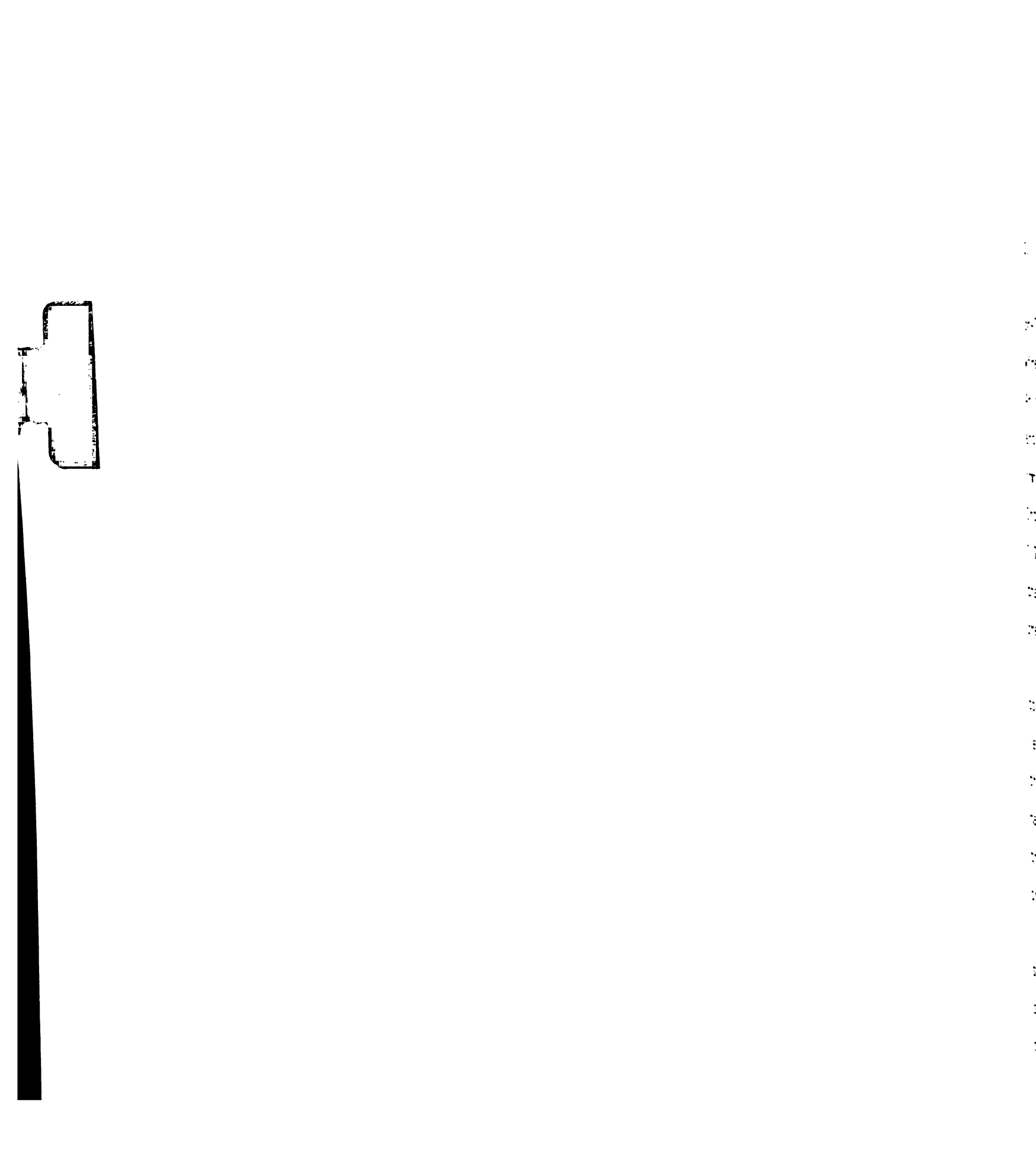
which moves an inclined plane. A shaft is spring loaded against this plane. Small movements of the plane in the x-direction cause equally small movements of the shaft in the y-direction. With this type of system it is possible to accurately step the probe across the narrow gap width of 1/2 in. in increments of 0.013 in. A strain guage mounted on the shaft loading spring provides a feedback mechanism for the location of the probe in the y-direction.

In order to accurately measure the effects of the side wall boundary layer a probe system was designed that had the capability of traversing in the z-direction. A strong magnet is used to control the movement of the probe through the plexiglass plate. The probe assembly is shown in Figures 11 and 12. The probe is situated along the centerline of the channel and is swung in a large arc towards the side wall.

B. Commercially available Equipment

In conjunction with the previously mentioned equipment the following list describes the complete system of instrumentation:

- 1) 2 Disa 55D05 constant temperature hot wire anemometers with Disa 55D15 and 55D10 linearizers.
- 2) A Disa 55D35 RMS voltmeter with RMS and RMS squared outputs permitting readings of intensity.
- 3) A Thermosystem model 1657 high and low pass filter allowing for signal conditioning.
- 4) A Quan-Tech 304T wave analyzer with RMS voltage versus frequency providing a sweep between 0 and 6500 Hz.
- 5) A Tektronix 564B fast writing storage oscilloscope coupled with a Tektronix C-40 camera providing a visual and hard copy display.



- 6) A Decker Delta Model 308 differential pressure instrument with a 0.3 and 3.0 in. transducer for pressure and calibration measurements.
- An Ellis strain gage meter.

3. Data Acquisition

An IBM 1800 computer with an A-D converter was utilized for fast on-line data acquisition and processing of the analog signals from the hot wire anemometry system. The computer system is shown in Figure 13.

An interface system was designed that enabled the signals to be amplified and conditioned. This system employed a trigger mechanism that signaled immediate data sampling whenever a large negative spike was generated. Interfacing with the IBM 1800 permitted use of 16 inputs, 4 amplifiers, 1 low pass filter (0-400 Hz.) and a comparator circuit, a Schmitt trigger, that enabled the process interrupt signal. A schematic of this system is presented in Figure 14.

A computer program was written that made it possible for the user to select one of two modes of operation: a semi-automatic mode that converted the data to the users specifications, printed, plotted, and punched the data immediately following an experimental run; or a completely automatic mode that enabled the user to perform a number of experiments while the computer stored the information on cards for future conversion and processing.

A fast and slow data sampling program was written that enabled sampling rates from 169 microsec./sample to 20 sec./sample. The fastest sampling rate varied with respect to the number of analog inputs, called channels, that were used by the analyst. Figure 15 presents the computer

were available that enabled the analyst to initiate the sampling program and efficiently process the raw data. The following is a list of the commands:

- 1) DATA initiates the data sampling program and allows the analyst to input important parameters such as rate of sampling, number of channels desired, number of points, and the starting channel.
- 2) CONVERT DATA file X_i = channel Y_i , a_0 , a_1 , a_2 , ..., a_{13} allows the raw data from channel Y_i to be stored in file X_i and multiplies each data point by the polynomial $a_0 + a_1x + a_2x^2 + ... + a_{13}x^{13}$ where x is a data point.
- 3) PRINT FILE file X_1 , file X_2 , ..., file X_{11} prints contents of converted data stored in files X_1 through X_{11} .
- 4) PRINT RAW DATA prints contents of unconverted data present in the specified channels.
- 5) PUNCH FILE file X_i punches contents of converted data stored in file X_i in F10.4 format.
- 6) PUNCH FILES -punches contents of converted data of all files first in binary format then in F10.4 format.
- 7) PUNCH RAW DATA punches contents of unconverted data of all channels in binary format.
- 8) READ RAW DATA reads contents of unconverted data of all channels which is in binary format.

9,

10)

11.)

12)

13)

]4]

15)

- 9) READ FILES reads contents of converted data of all files which is in binary and F10.4 format.
- 10) TYPE called from the card reader, this command directs the computer to read a command from the typewriter.
- 11) CARD called from the typewriter, this command directs the computer to read a command from the card reader.
- 12) CREATE FILE file X_i , a_0 , a_1 , ..., a_{13} creates a file of artificial points generated by a polynomial and is stored in file X_i .
- 13) FILE CHANGE +-/* file X_i , file X_j , file X_k (a_0,a_1,\ldots,a_{13}) allows the addition, subtraction, division, and multiplication of two files, file X_i and file X_j , and stores the information in file X_k which may be operated on by the polynomial.
- 14) AXIS three modes for plotting an axis are available by this command.
- 15) PLOT file X_i (min, max), file X_j (min, max) the minimum to maximum points specified for file X_i are plotted versus the minimum to maximum points of file X_j . If the minimum and maximum points are not specified the computer searches for these points.
- 16) STATISTICS file X_i (min, max), file X_j (min, max), ... the minimum to maximum points of file X_i are averaged and a standard deviation is given.



Figure 7. Photograph of experimental channel assembly.

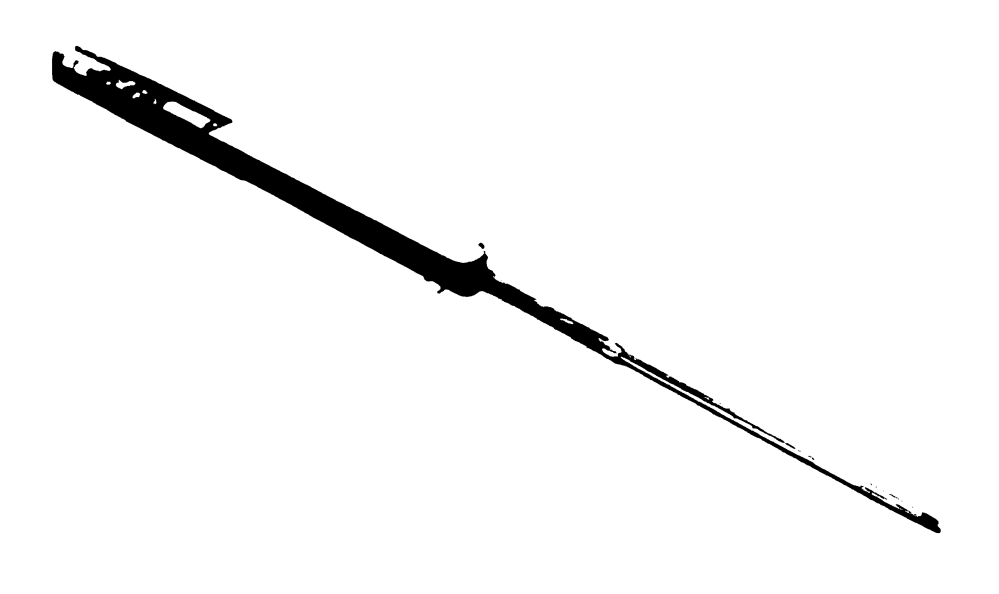
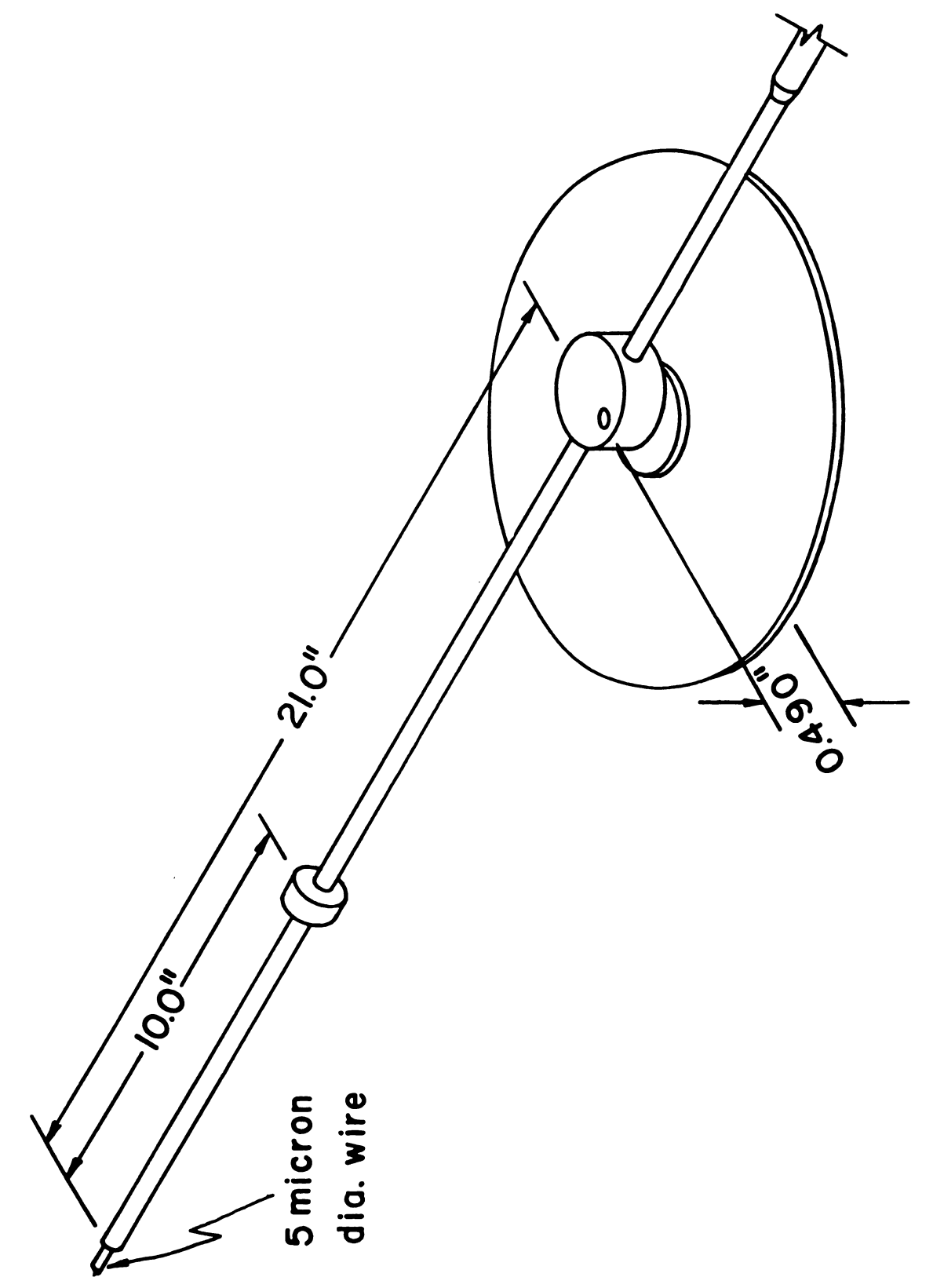


Figure 9. Photograph of motorized y-coordinate Probe.

Figure 10. Schematic drawing of motorized y-coordinate Probe.



Figure 11. Photograph of z-coordinate side wall boundary layer Probe.



Schematic drawing of z-coordinate boundary layer Probe. Figure 12.



Figure 13. Photograph of IBM 1800 computer facility.

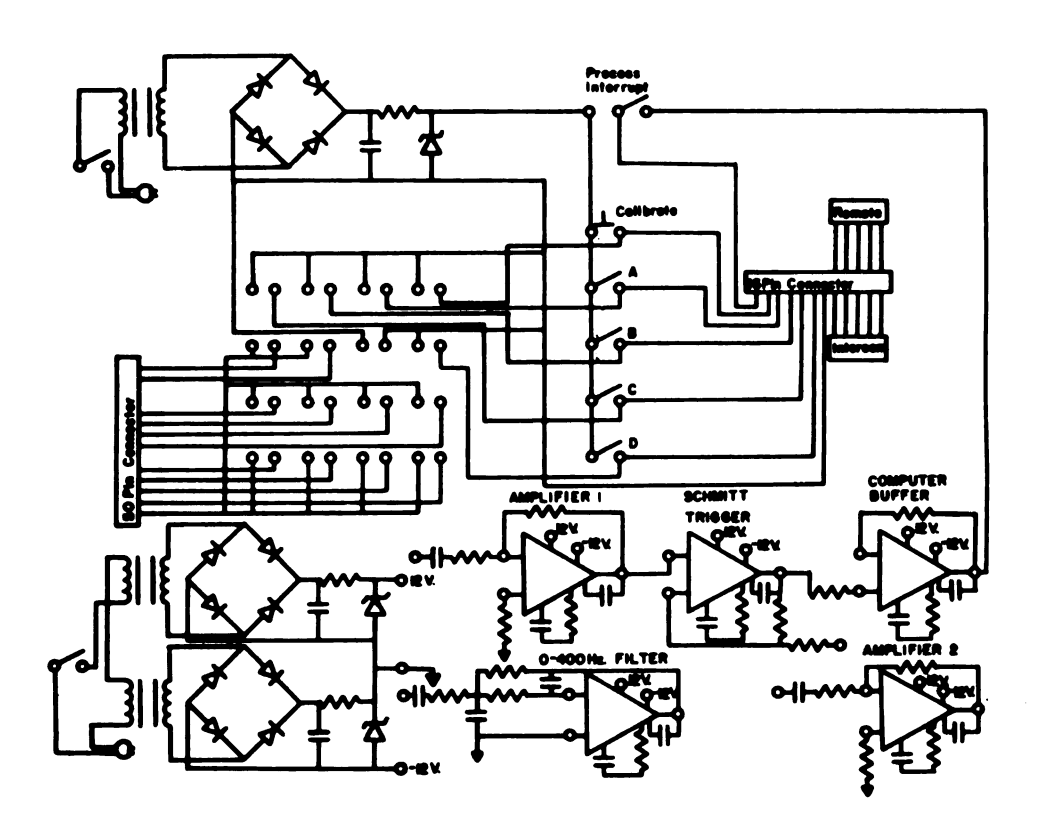


Figure 14. Schematic of computer interface.

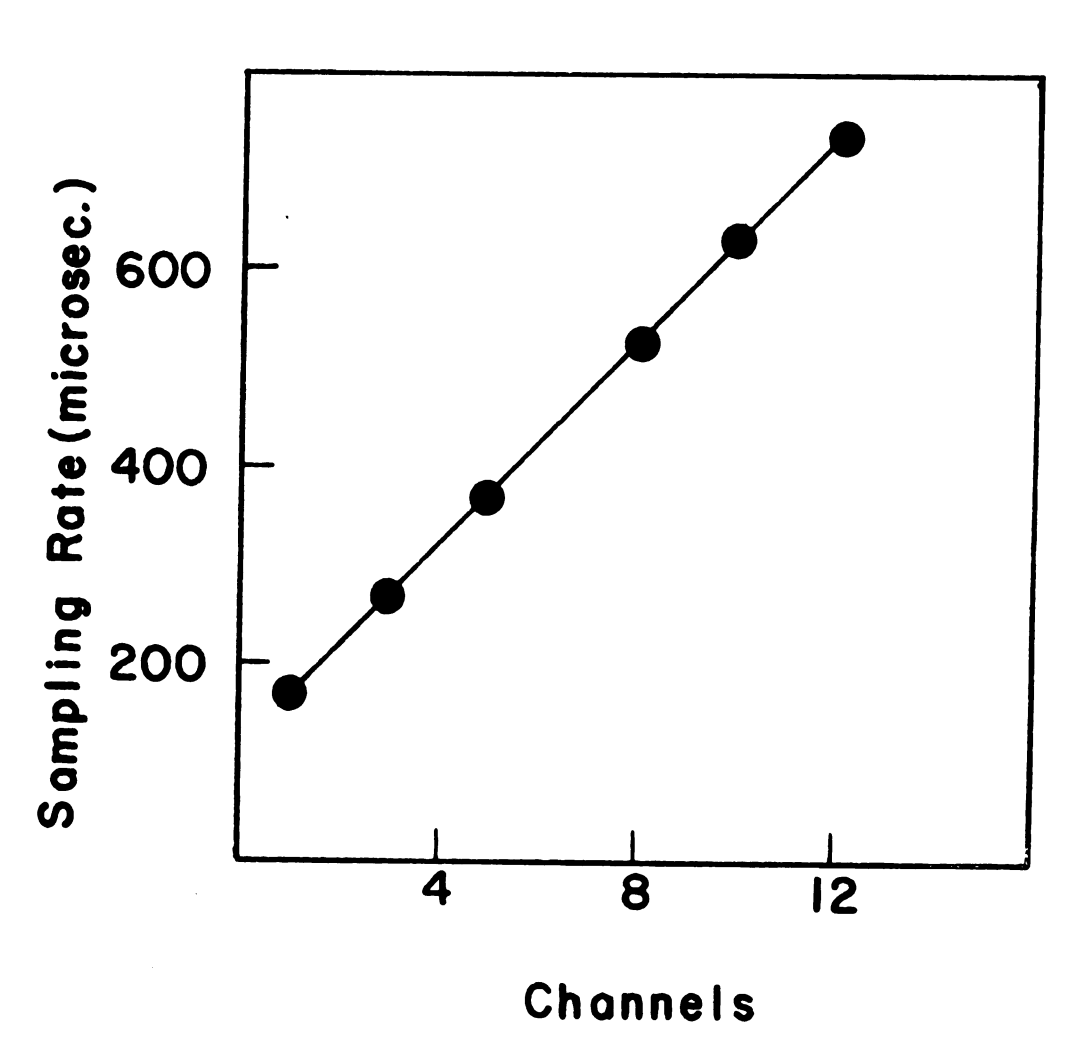


Figure 15. Variation of computer sampling rates.

CHAPTER 4

EXPERIMENTAL RESULTS

1. Entrance and Transition Regions

In order to understand the transition process it is necessary to investigate the developing region and the fully developed region for both laminar and turbulent flow. Information about the loaction of the transition region can be obtained from this investigation.

A. Laminar Entrance Lengths

In the present facility the parabolic velocity profile can be achieved up to a critical experimental Reynolds number of 7300. Figure 16 shows the linear relationship between the entrance length and Reynolds number. At the critical Reynolds number of 7300 the profile is fully developed at X/d = 204. The fully developed situation is achieved when the velocity profile is parabolic. Experimental constraints which are described in Section C are imposed in order to determine whether the velocity profiles are parabolic. A comparison is made between the experimental data and the analytical prediction of the entrance length by Schlichting (1962). This solution is based upon the developing two-dimensional flow in a straight channel without a converging entrance region. If it is assumed that the converging entrance region partially develops the flow before entry to the constant gap channel then the analytical solution may be translated a specified number of channel widths to coincide with the experimental results. An inspection of Figure 16 reveals that the slopes of the experimental and analytical entrance lengths versus Reynolds number deviate by less than 15%. Using a Reynolds number of 4800 as a point of reference the analytical line had previously been translated a distance of

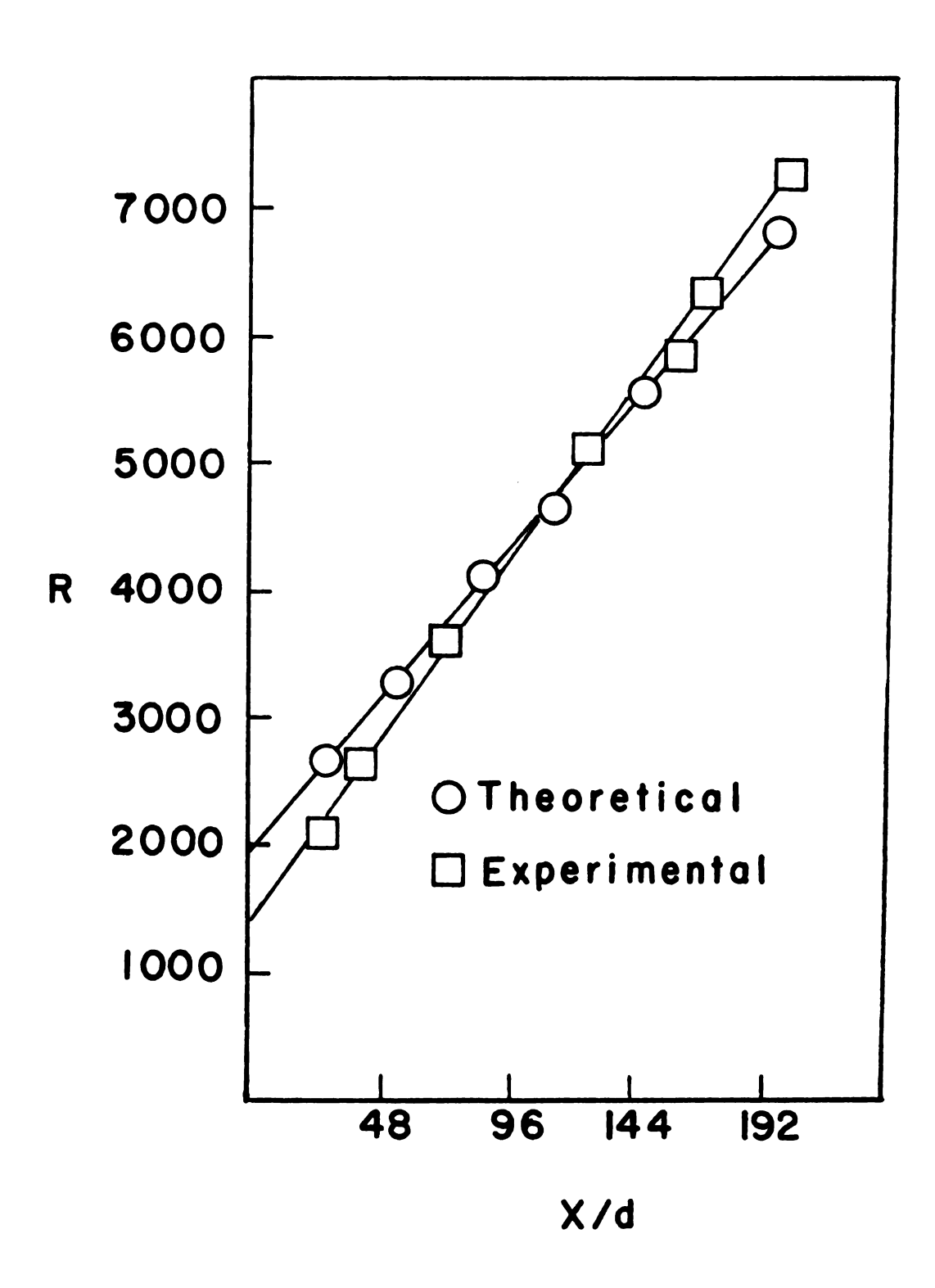


Figure 16. Comparison of theoretical and experimental entrance lengths.

3:

ergi 34 on

asser

: V:

Care

.

la pr

`\$\$. ?€?€

;

84 channel widths (3.5 ft.) along the abscissa. Therefore, a 6 ft. converging entrance region has developed the flow an equivalent length of 84 channel widths for a Reynolds number of 4800. For the present channel assembly the laminar entrance length $\ell_{\rm e}$ can be related as

$$\ell_{\rm p} = (1.42 \times 10^{-3}) \text{ R} - 1.86 \text{ ft.}$$
 (4.1)

and a similar relationship can be derived from the analytical solution

$$\ell_{\rm e} = (1.67 \times 10^{-3}) \, \text{R} - 3.00 \, \text{ft}.$$
 (4.2)

B. Critical Reynolds Number

The burst Reynolds number of the flow in the present facility can be influenced by controlling the intensity level of the free stream velocity fluctuations. Grids of different diameters and mesh sizes were placed in the entrance region and the fluctuation levels were measured at X/d = 168 before the onset of turbulence. A plot of intensity level versus critical Reynolds number is presented in Figure 17. The curve monotonically decreases to an intensity of 0.13% for a Reynolds number of 7280. This is the natural intensity level for the channel assembly. At the Reynolds number of 7280 no grid was utilized to disturb the flow. Inspection of the curve reveals that at large Reynolds numbers it becomes almost parallel to the abscissa. Since the theoretical Reynolds number for transition is 7700 a sudden decrease at this point in the curve is indeed a possibility. This has been predicted by Reynolds and Potter (1967). Unfortunately, the present channel assembly does not provide flow stability at Reynolds numbers above 7280.

C. Curve-Fitting to the Velocity Profiles

A statistical treatment of the data has been prepared to give information about the developing profiles, the nature of the fully developed

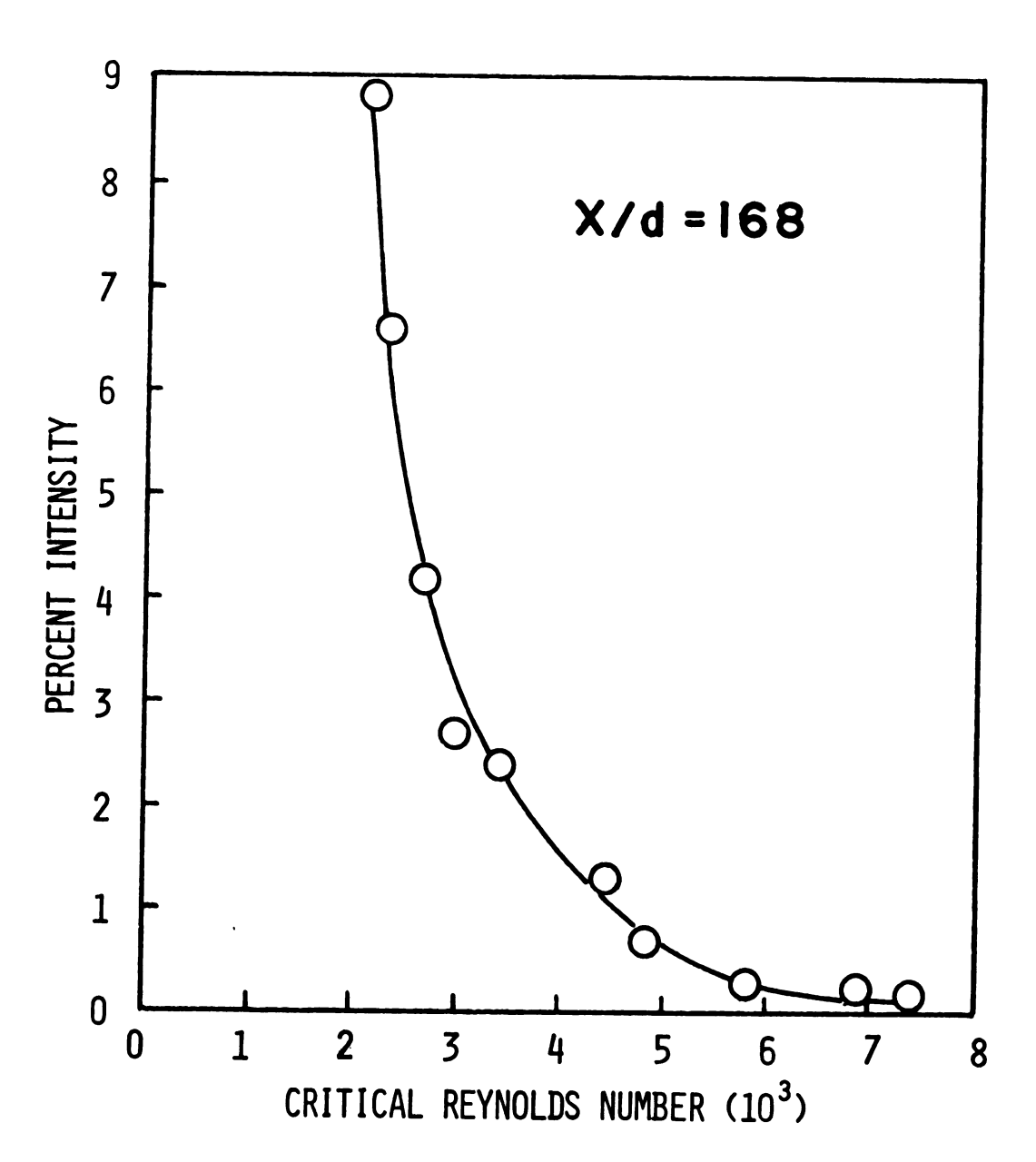


Figure 17. Intensity variation (with the use of grids) as a function of Reynolds number.

:r:"le

is based #1

:::'tion

: specia

ay to d

it was c

tter me

fors at

"ile ma

infile

In Starmel

5 E LO.;

÷ the

piète of

rere ul

profile and an accurate estimate of the channel gap width. This analysis is based upon standard curve-fitting and parameter estimation techniques.

Although the horizontal plates of the channel can be accurately positioned to give a channel gap width of 0.500 ± 0.010 in. by means of a special gapping instrument, changes in temperature and humidity from day to day can change these measurements by more than 0.015 in. Therefore, it was considered desirable to obtain an estimation of the gap width by other means. Velocity profile data were collected at different X/d stations at z=0 along the length of the channel and a curve-fitting technique was employed to obtain information not only about the nature of the profile but also of the channel width itself.

In the case of two-dimensional, steady, fully developed flow in a channel with two parallel flat walls a very simple equation is obtained from a solution of the Navier-Stokes equations and continuity.

$$\frac{dP}{dx} = \mu \frac{d^2u}{dy^2}$$
 (4.43a)

$$\frac{dP}{dy} = 0 (4.43b)$$

For the present study the coordinate system was established at the bottom plate of the channel. Thus the boundary conditions are

$$u(y=0) = 0$$
 (4.44a)

$$u(v=d) = 0$$
 (4.44b)

where $u(y=d/2) = u_{max}$. The solution to equation (4.43a) is

$$u = 4 u_{max} y/d (1-y/d)$$
 (4.5)

In parameter estimation the model

$$Y_{i} = \beta_{1}X_{i} + \beta_{2}X_{i}^{2} + \varepsilon_{i}$$
 (4.6)

ar be

:: 613

irdinar rere'y,

, -: r

it

÷ rę

rifre 1

can be studied by the method of least squares, Beck (1966). Comparison to equation (4.5) allows

$$Y_{i} = u_{i}$$

$$\beta_{1} = 4 u_{max}/d$$

$$\beta_{2} = -4 u_{max}/d^{2}$$

$$X_{i} = y_{i}$$

$$(4.7a,b,c,d)$$

Ordinary least squares is used to find the estimates of β_1 and $\beta_2,$ namely, b_1 and $b_2.$ A sum of the squares is defined by

$$S = \sum_{i=1}^{n} \epsilon_{i}^{2} = \sum_{i=1}^{n} [Y_{i} - E(Y_{i})]^{2}$$
 (4.8a)

$$S = \sum_{i=1}^{n} [Y_i - \beta_1 X_i - \beta_2 X_i^2]$$
 (4.8b)

By minimizing S with respect to β_1 and β_2 the estimates b_1 and b_2 are obtained. These are defined by the following equations

$$b_{1} = \frac{\sum X_{i}^{4} \sum X_{i}Y_{i} - \sum X_{i}^{3} \sum X_{i}^{2}Y_{i}}{\sum X_{i}^{2} \sum X_{i}^{4} - (\sum X_{i}^{3})^{2}}$$
(4.9)

$$b_{2} = \frac{\sum X_{i}^{2} \sum X_{i}^{2} Y_{i} - \sum X_{i} Y_{i} \sum X_{i}^{3}}{\sum X_{i}^{4} - (\sum X_{i}^{3})^{2}}$$
(4.10)

$$\overline{Y} = \frac{1}{n} \Sigma Y_i$$
, $\overline{X} = \frac{1}{n} \Sigma X_i$ (4.11a,b)

The residual $\mathbf{e_i}$ is the measured value of $\mathbf{Y_i}$ minus the predicted value

$$e_{i} = Y_{i} - \hat{Y}_{i} \tag{4.12}$$

where the predicted value of Y_i is denoted \hat{Y}_i

$$\hat{Y}_{i} = b_{1}X_{i} + b_{2}X_{i}^{2} \tag{4.13}$$

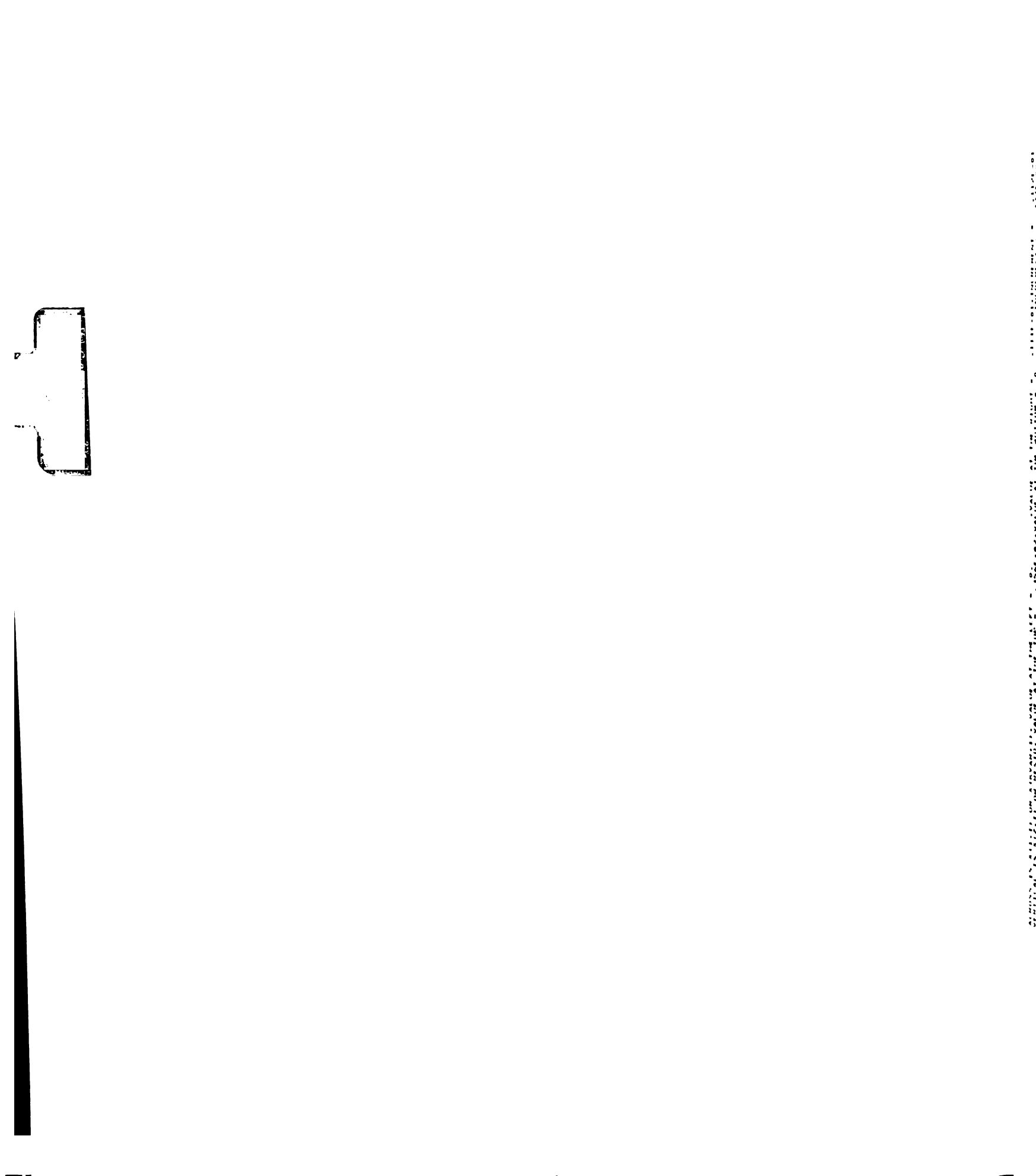
1:1:5 nii i ricen o aned a 5:¹-8: eiter tirve-f de goo inc do Biera] : rinj i Bret is less : ::alo is pres ispenial

: •es ·:::5.

In this manner both the gap width of the channel and the maximum velocity could be estimated. Knowing the value of the maximum velocity the gap width of the channel could then be established. In practice a sophisticated computer program written by Nicely and Dye (1971) was utilized to estimate these parameters. This program handles problems which are either linear or non-linear in the adjustable parameters.

The residual e; is minimized with respect to the parameters by the curve-fitting routine. This is an important parameter which indicates the goodness of fit of the model to the data. If the residuals are large and do not give a mean of zero then the model is either incorrect or several parameters in the model exhibit linear dependency. The criterion of minimum residuals is used to establish when the flow is fully developed. A parabolic velocity profile is determined when the sum of the residuals is less than ±0.8. In Figure 18 a typical computer printout is presented of calculated and experimental values. The experimental values fit very well to the theoretical curve. A standard residual plot of this same data is presented in Figure 19. The sum of the residuals for this particular experiment is -0.5161. This curve reveals a random scatter of residuals which indicates a good fit.

The run test (also called the Wald-Wolfowitz test) can be applied to residuals and other data to investigate the independence of the measurements. This type of test was utilized to determine the randomness of the residuals in Figure 19. This experiment gave rise to a 95% confidence arrangement of residuals. Therefore, the results show a good fit to equation (4.6). This data and analysis is accepted as defining the flow parabolic and therefore fully developed.



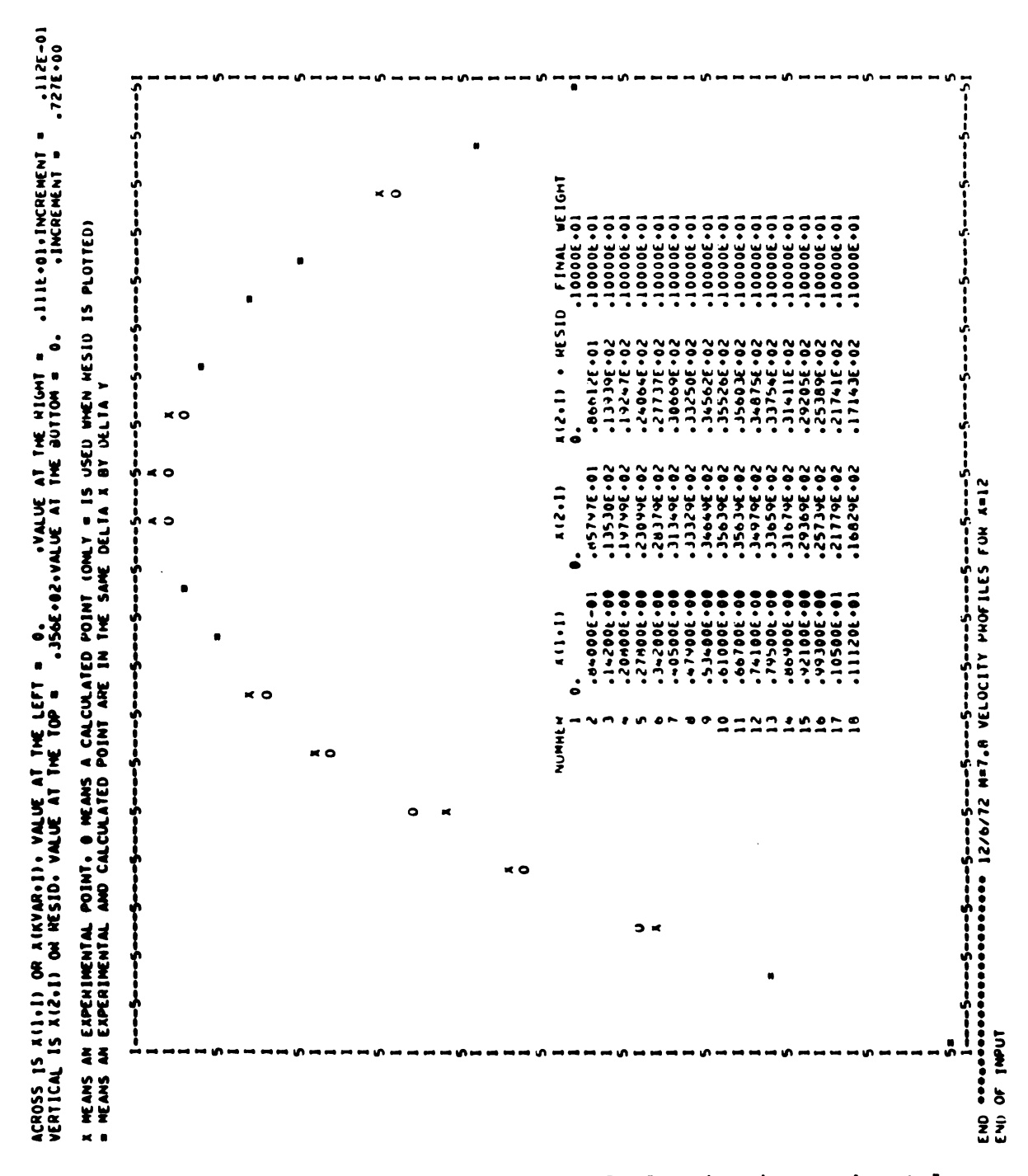


Figure 18. Computer printout of calculated and experimental velocity profiles (parabolic profile).

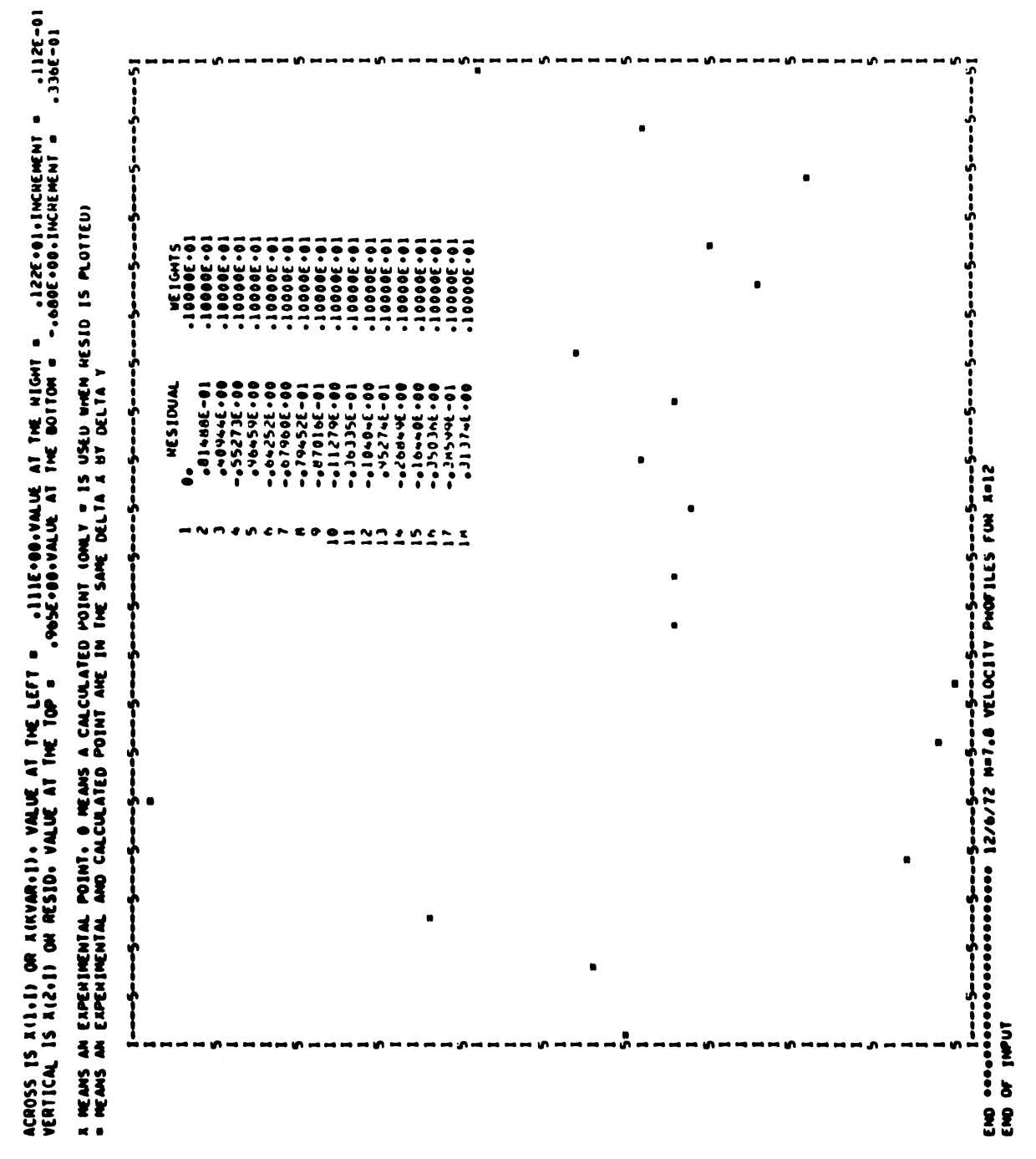


Figure 19. Computer printout of residuals.

•18

:ie ut

k"à

æ's

.3`5

-62;

fry

izta ! UD

in the state of th

é :re

N

A problem arises when the velocity profile is not fully developed. The model in equation (4.6) cannot be utilized to give information about the gap width. Figure 20 is a typical example of this case. The Reynolds number is 6800 and the X/d station is 96. At this Reynolds number a parabolic velocity profile is not realized until X/d is 192. The residuals for this experiment are plotted in Figure 21. The sum of the residuals is -26.0 and the run test does not indicate a random arrangement of residuals.

from polynomial regression. An nth degree polynomial is fitted to the data in the same manner as described previously. The linear regression of y upon a single variable x can be extended to the multiple regression

$$Y_i = \beta_0 + \beta_1 X_i + \beta_2 X_i^2 + ... + \beta_n X_i^n + \epsilon_i$$
 (4.14)

In the model, X_i are known precisely and Y_i are subject to random error which is normally distributed about the regression line with constant variance σ^2 . The procedure to estimate the parameters β_i is again to minimize the sum of the square

$$S = \sum_{i=1}^{n} \varepsilon_i^2 = \sum_{i=1}^{n} [Y_i - E(Y_i)]^2$$

$$S = \sum_{i=1}^{n} [Y_i - \beta_0 - \beta_1 X_i - \dots - \beta_n X_i^n]^2$$

The result is a system of n simultaneous linear normal equations which are conveniently solved by inversion of an $(n \times p)$ coefficient matrix $\underline{x}^T \times \underline{x}$, where p represents the number of parameters. In matrix notation equation (4.14) can be expressed as

$$Y = X\beta + \varepsilon \qquad (4.16)$$

and the least squares linear unbiased estimate of $\underline{\beta}$, designated \underline{b} , is

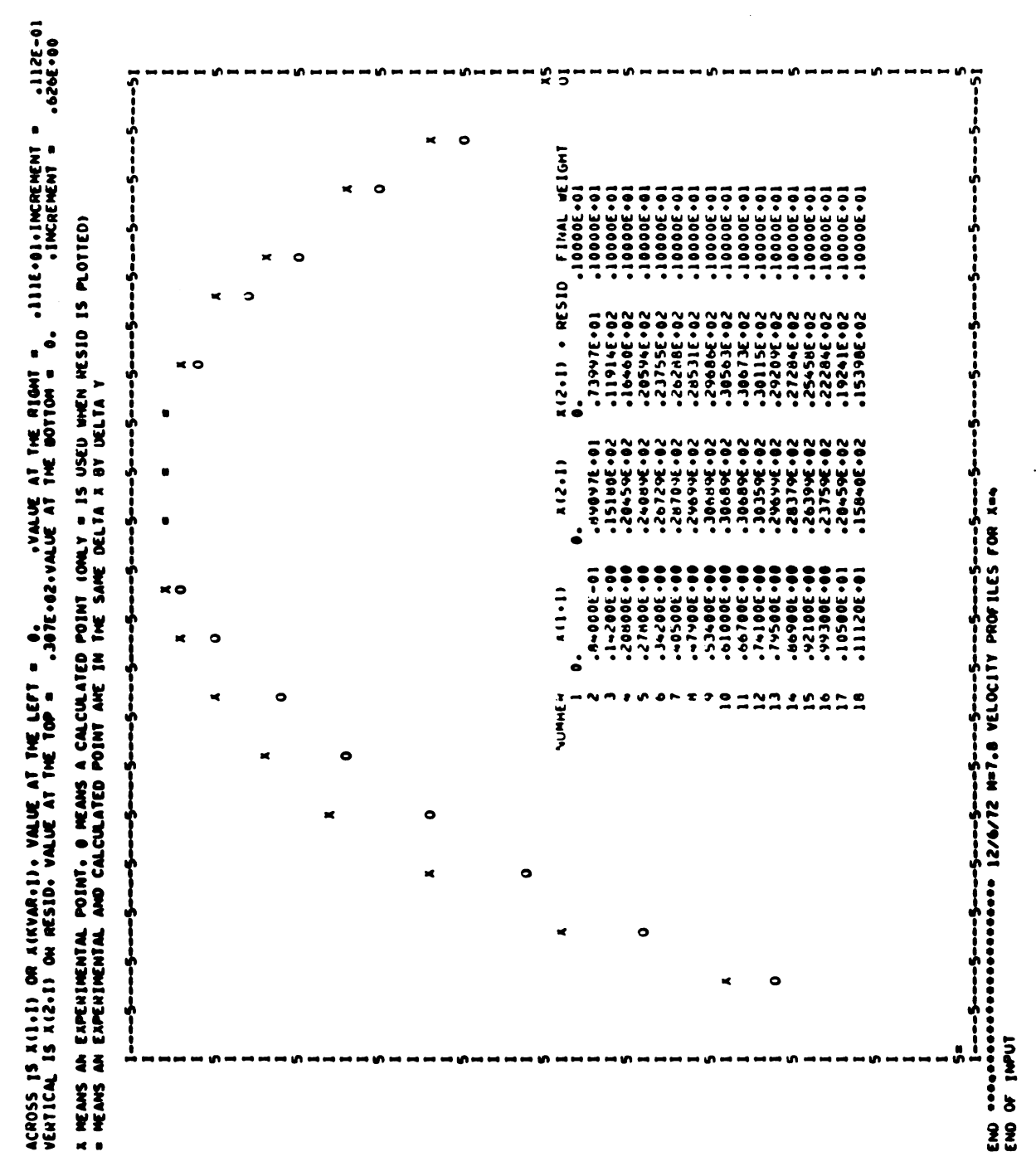
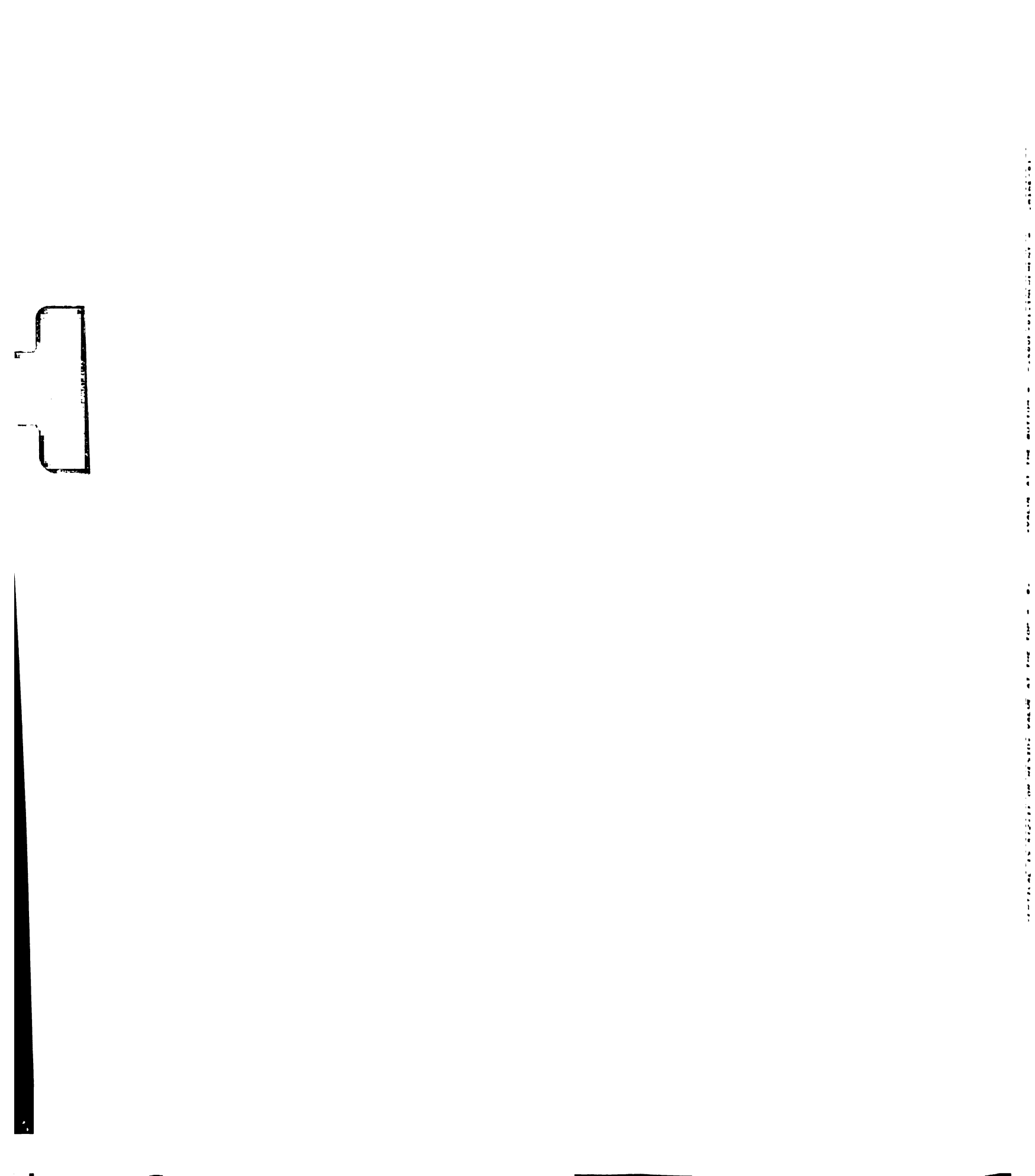


Figure 20. Computer printout of calculated and experimental velocity profiles (non-parabolic profile).



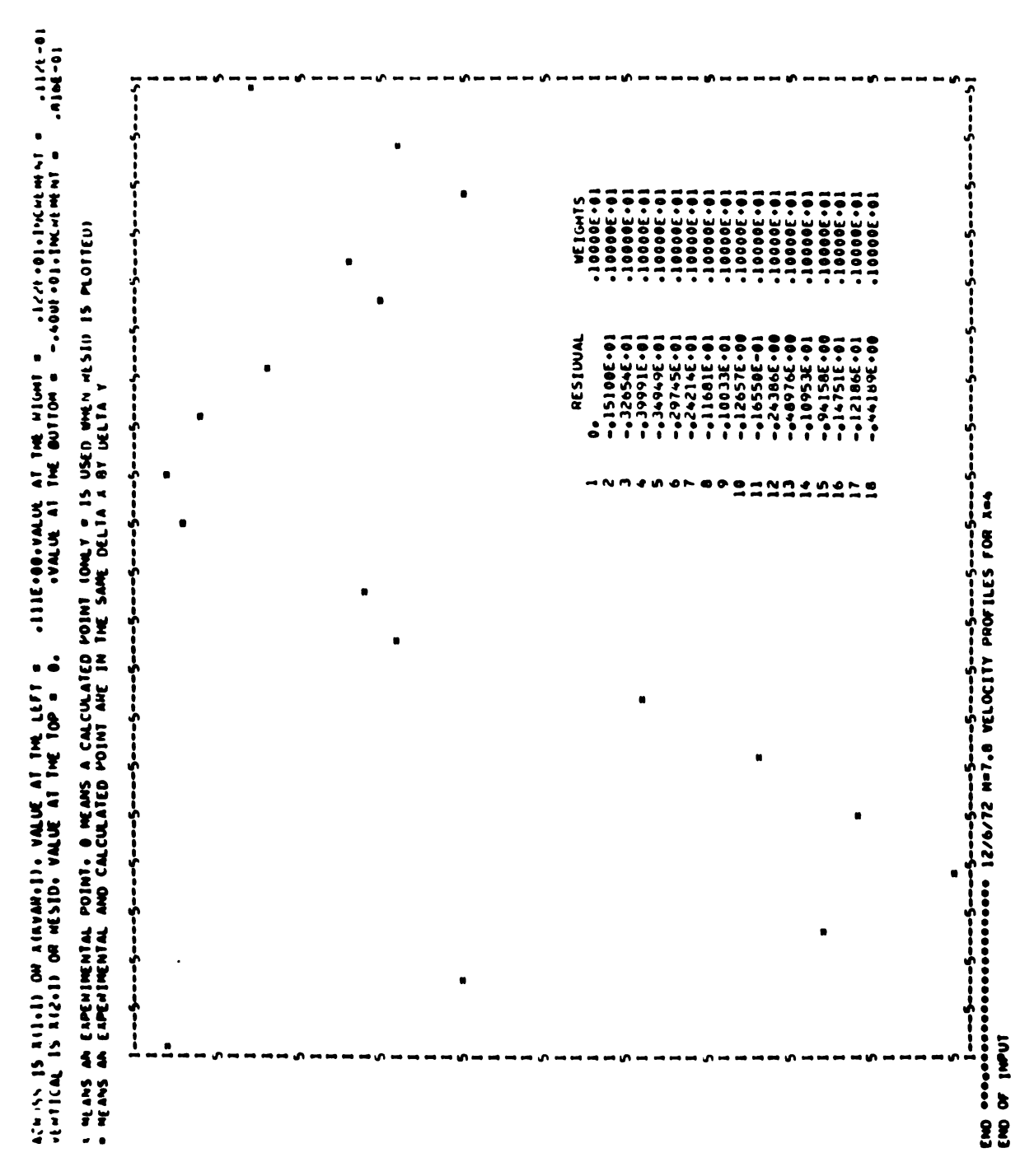


Figure 21. Computer printout of residuals.

$$\underline{S}(\beta) = (\underline{Y} - \underline{X} \underline{\beta})^{\mathsf{T}} (\underline{Y} - \underline{X} \underline{\beta}) \tag{4.17}$$

The well known least squares estimator is the result of the minimization procedure (Beck, 1966).

$$\underline{b}_{LS} = (\underline{x}^{\mathsf{T}} \underline{x})^{-1} \underline{x}^{\mathsf{T}} \underline{Y}$$
 (4.18)

The (n x n) symmetrical variance-covariance matrix of the estimates is

$$cov(\underline{b}_{LS}) = (\underline{x}^{T} \underline{x})^{-1} \sigma^{2}$$
 (4.19)

where σ^2 is estimated from

$$\sigma^2 = \frac{\underline{Y}^T \underline{\dot{Y}} - \underline{b}^T \underline{X}^T \underline{Y}}{n-p}$$
 (4.20)

In practice, a computer routine was utilized that employs a least squares fit of the data by five successive polynomials, n=1, 2, 3, 4, 5 and the standard deviation σ about the regression line was examined in each case. It was observed that σ decreased fairly rapidly with increasing n until a good fit was obtained. Further increases in n actually increased σ again due to the reduction of the degrees of freedom in the denominator of (4.20). The best fit to the experimental data occurred for n=3.

D. Examination of Laminar and Turbulent Regions

The procedure of parameter estimation was utilized to establish the gap width in those regions where the velocity profile was not fully developed. The average velocity which is a function of the gap width was obtained by a numerical procedure. For a parabolic profile the average velocity was simply $2/3 u_{\text{max}}$. At each X/d station a Reynolds number based upon the estimated gap width and the average velocity was calculated. A collection of curves representing the Reynolds number as a function of X/d and different flow rates is presented in Figure 22.

Examination of Figure 22 reveals that the channel Reynolds number

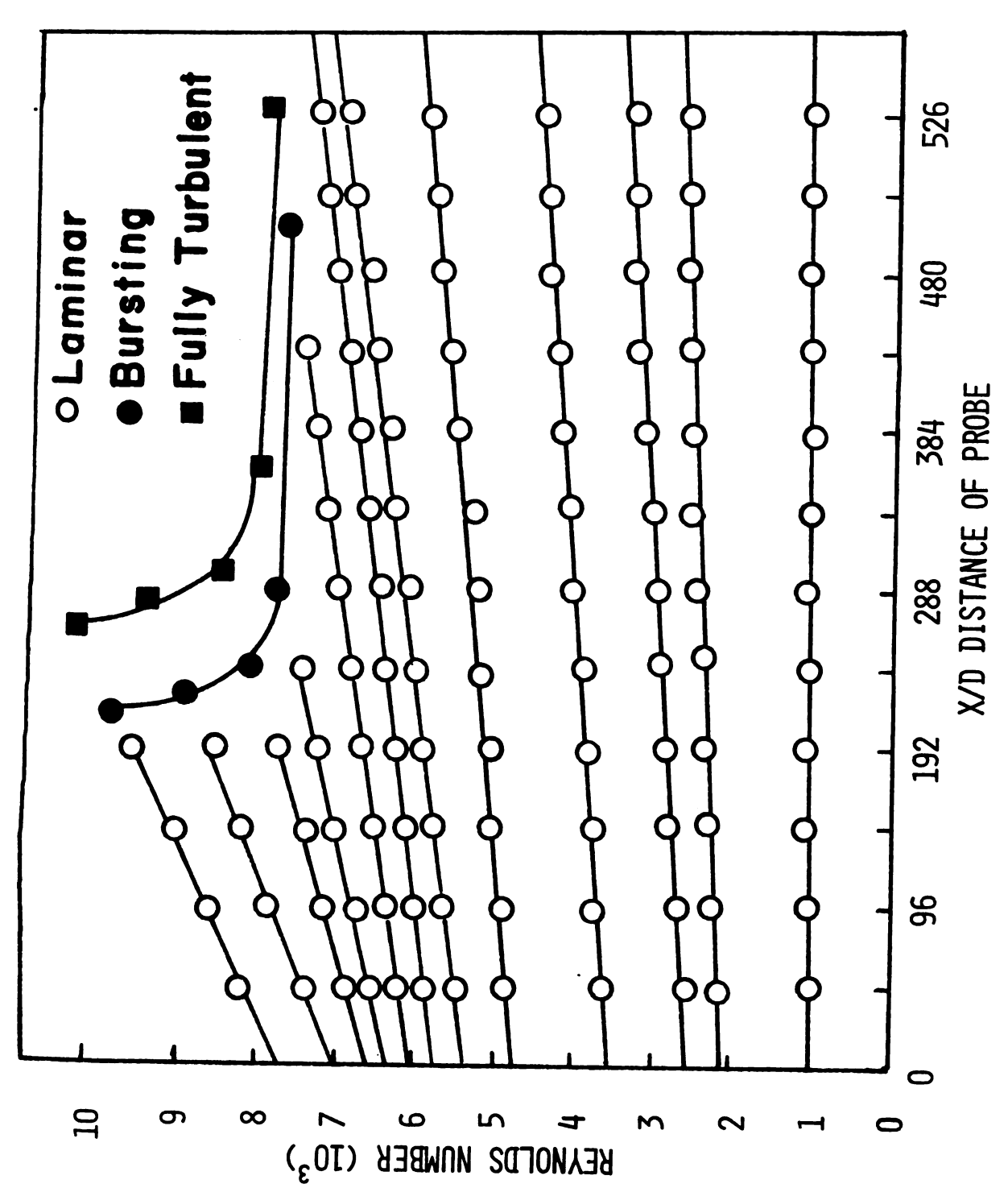


Figure 22. Variation of Reynolds number with Probe position.



varies linearly as a function of the probe position for a constant setting of the fan speed. Investigations in the regions of developing and fully developed flow have resulted in the experimental evidence that the wakeeffects of the probe assembly result in the flow being fully turbulent in the downstream direction of the probe. The wake quickly spreads across the entire width of the channel (2 to 3 ft. downstream of the position of the probe assembly). This effect results in an increase of the wall shear stress in the turbulent region behind the probe. Since the pressure drop is a direct function of the shear stress the actual positioning of the probe in either the downstream or upstream direction acts as a flow meter by increasing or decreasing the pressure drop. Therefore, the average channel velocity and Reynolds number is a function of the probe position for a given fan control setting. This effect is also a function of the initial fan setting or flow rate and becomes more predominant at the higher flow rates. Thus, in Figure 22 the slopes of the lines appear to increase rapidly at the higher Reynolds numbers. It can be shown that this increase in the slopes is linear with an increase in the Reynolds number.

A laminar, a bursting, and a fully turbulent region are exhibited at different Reynolds numbers in Figure 22 and because of the interference of the probe, at different X/d locations. The first burst occurs at a Reynolds number of 7300 at X/d of 432. Higher Reynolds numbers move the observed transition location upstream until a constant X/d value is obtained for Reynolds numbers above 9000. An X/d station of 170 represents this region as shown by the solid circles. A similar effect is achieved for the fully turbulent region which is represented by the closed rectangles.



An average X/d distance of 50 is obtained between the intermittent bursting zone and the fully turbulent zone. For Reynolds numbers above 10,500 a constant fully turbulent zone is evident at the X/d location of 240; no bursting is observed.

E. Variation in Reynolds Numbers and Probe Location

Information about the change in the average velocity as a function of the probe's position can be achieved from an analysis of Figure 22. The average velocity is observed to be a function of the position of the probe in the channel when the fan speed is held constant. Utilizing the curve-fitting procedure mentioned previously two models were developed which predict the variation in the average velocity for a given position of the probe assembly. The initial condition of the average velocity at probe positions of x = 0 and x = 23 ft. are also utilized.

$$U_{ave}(X) = (0.0270 U_0 - 0.1362) X + (1.00 U_0 + 0.9121) (4.21)$$
and
$$U_{ave}(X) = (0.0173 U_{23} - 0.1133) X + (0.605 U_{23} + 0.2753)$$
(4.22)

where U_0 and U_{23} indicate the average velocities at probe positions of x = 0 and x = 23 ft. respectively.

These two equations (4.21) and (4.22) can be utilized to predict the Reynolds number as the probe is either pushed upstream or pulled downstream to different X/d locations.

F. Variation in Pressure Drop and Probe's Position

It has been established that the positioning of the probe in either the upstream or downstream direction acts as a flow meter by increasing or decreasing the pressure drop when the fan speed is held constant. Experiments monitoring the pressure drop as a function of probe's position



have verified this phenomenon. A total pressure probe was positioned at various X/d locations and the pressure was monitored at each location. Figure 23 presents a family of curves of pressure drop versus X/d for different Reynolds numbers. The Reynolds numbers depicted for each curve were realized at x = 23 ft. If the probe presented no interference to the flow then -dP/dx must be constant since the average velocity would be constant. From the family of curves -dP/dx is non-linear and this non-linearity increases as a function of Reynolds number.

The effect of the probe's position on the average velocity can also be verified analytically by observing the pressure gradient changes. A friction coefficient for laminar flow and fully established turbulent flow is a commonly employed parameter for determining pressure drops. The friction coefficient for laminar flow in a channel is

$$f = 24/R*$$
 (4.23)

where R* is the Reynolds number based on twice the gap width.

$$R^* = 2d U_{ave}/v \qquad (4.24)$$

A friction coefficient for fully established turbulent flow in a smooth walled channel can be deduced by utilizing the equations that describe the universal turbulent velocity profile. The complete universal profile is given by Kays (1966).

$$y^{+} < 5$$
, $u^{+} = y^{+}$
 $5 < y^{+} < 30$, $u^{+} = -3.05 + 5.00 \text{ lny}^{+}$
 $y^{+} > 30$, $u^{+} = 5.5 + 2.5 \text{ lny}^{+}$ (4.25a,b,c)
 $u^{+} = u/u^{+}$, $u^{+} = \sqrt{\tau_{0}/\rho}$
 $y^{+} = yu^{+}/\nu$ $d^{+} = du^{+}/\nu$ (4.26a,b,c,d)

where

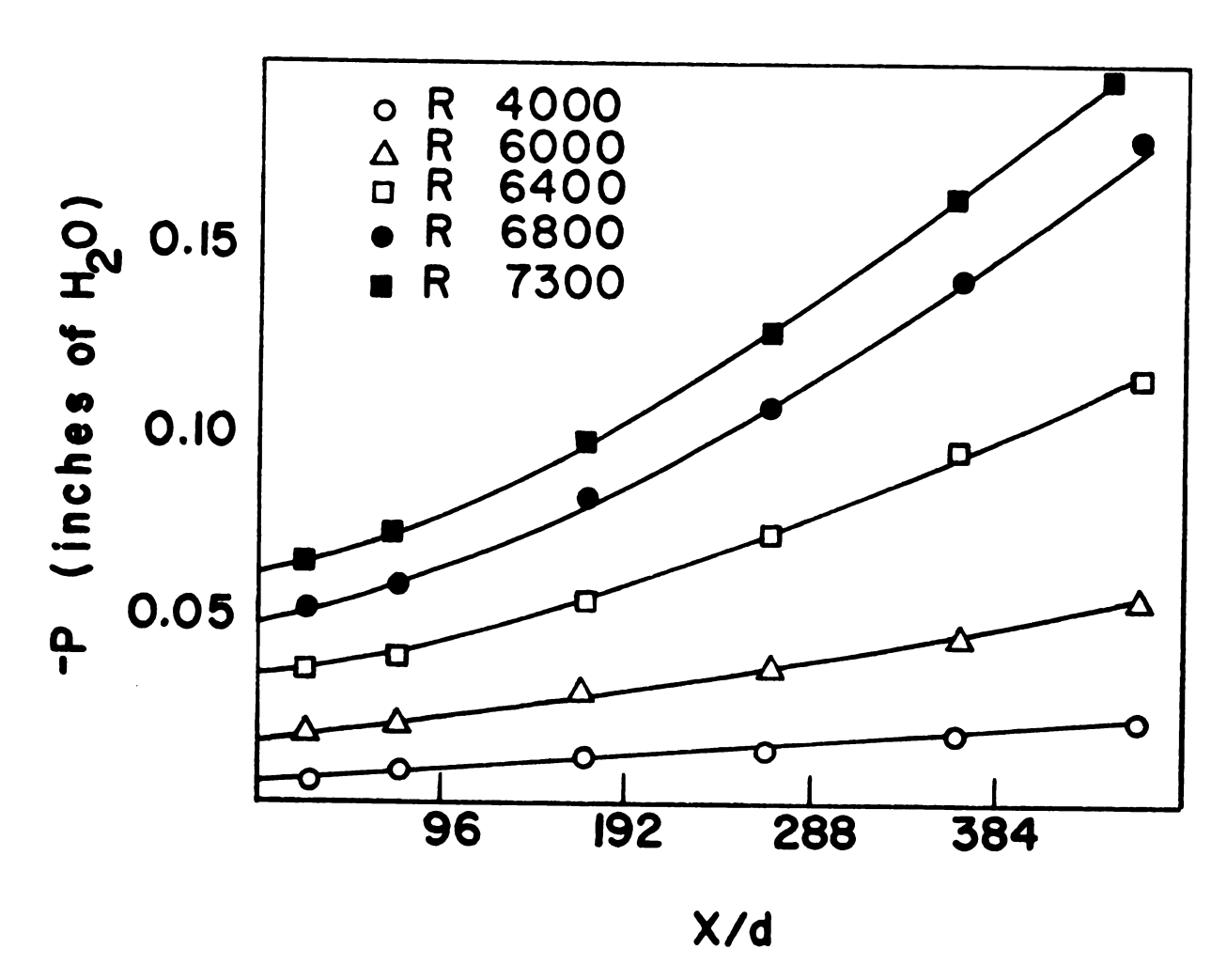


Figure 23. Variation of pressure with Probe position.

The friction factor is derived employing equation (4.25c) to evaluate a bulk mean velocity. Equation (4.25c) should not be used for $y^+<30$ but since little of the mass flow passes inside of $y^+=30$ little error is introduced. The bulk mean velocity is defined by the relation

$$U_{ave} = 1/d \int_0^d u \, dy = u^*/d^+ \int_0^{d^+} u^+ \, dy^+$$
 (4.27a,b)

The friction factor is, by definition

$$f = \frac{\tau_0}{\rho U_{ave}^2/2} = 2u^{*2}/U_{ave}^2$$
 (4.28a,b)

The result of the integration is a relation for the turbulent friction factor

$$(2/f)^{1/2} = 3.0 + 2.5 \ln \left[\frac{R^*}{2}(f/2)^{1/2}\right] (4.29)$$

The shear stress at the wall is a linear function of the pressure gradient and is related by the following equation

$$\tau_0 = \frac{d}{2} \left(-dP/dX \right) \tag{4.30}$$

The pressure gradient is evaluated by substituting equation (4.30) into (4.28a) to give

$$-dP/dX = \frac{f}{d} \rho U_{ave}^2$$
 (4.31)

and in terms of the Reynolds number

$$-dP/dX = f \frac{\rho v^2}{4 d^3} R^{*2}$$
 (4.32)

By appropriate substitution of the laminar and turbulent friction factor the pressure drop can be evaluated and compared to the experimental values. The following model for the pressure drop as a function of the probe's distance is utilized

$$-\Delta P = -\Delta P_{lam}(X+2) - 0.75 \Delta P_{turb}(24-X-2)$$
 (4.33)

 ΔP_{lam} and ΔP_{turb} represent the laminar and turbulent pressure drops. The turbulent wake generated by the probe fills approximately 75% of the total channel area. Therefore, the model encompasses the laminar region in front of the probe and 75% of the turbulent region behind the probe.

Figure 24 depicts the experimental and theoretical pressure changes as a function of the probe's position and Reynolds number. The analytical results correlate well with the experimental values except at the high Reynolds numbers. At the high Reynolds numbers for small X/d locations the flow is not fully developed. Since the velocity profiles used to develop the relations for the friction factors are based upon fully developed profiles the friction coefficients are not valid for the higher Reynolds numbers.

G. Side Wall Boundary Layer

The influence of the side wall boundary layer on the mean flow was determined by observing the growth of the boundary layer and the intensity of the fluctuations in the boundary layer as a function of the Reynolds number. The growth of the boundary layer can be compared with the Blassius solution for flow over a flat plate. For $u = 0.99 \ U_{\infty}$ the boundary layer thickness is defined as

$$\delta = 5\sqrt{VX/U_{\infty}} \tag{4.34}$$

This relation predicts a thickness of 0.77 in. for a length of 24 ft. and an average velocity of 24 ft./sec. corresponding to a Reynolds number of 6100. Figure 25 presents the experimental values of the boundary layer thickness as a function of the Reynolds number. A thickness of 0.670 in. is observed for a Reynolds number of 6200. However, a minimum thickness is observed for a Reynolds number of 2500 which increases to a maximum

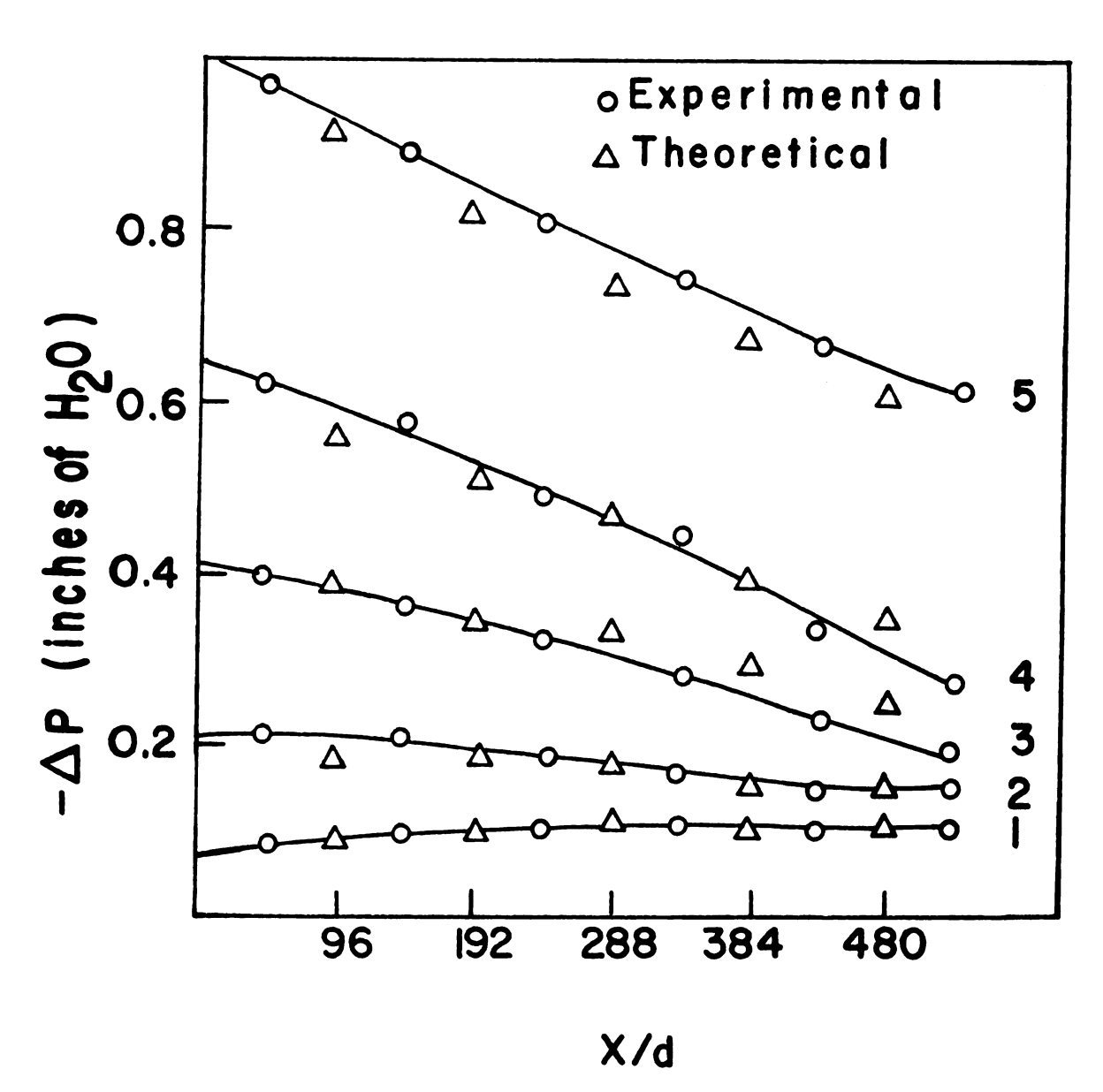


Figure 24. Comparison of theoretical and experimental pressure drop as a function of Probe position.

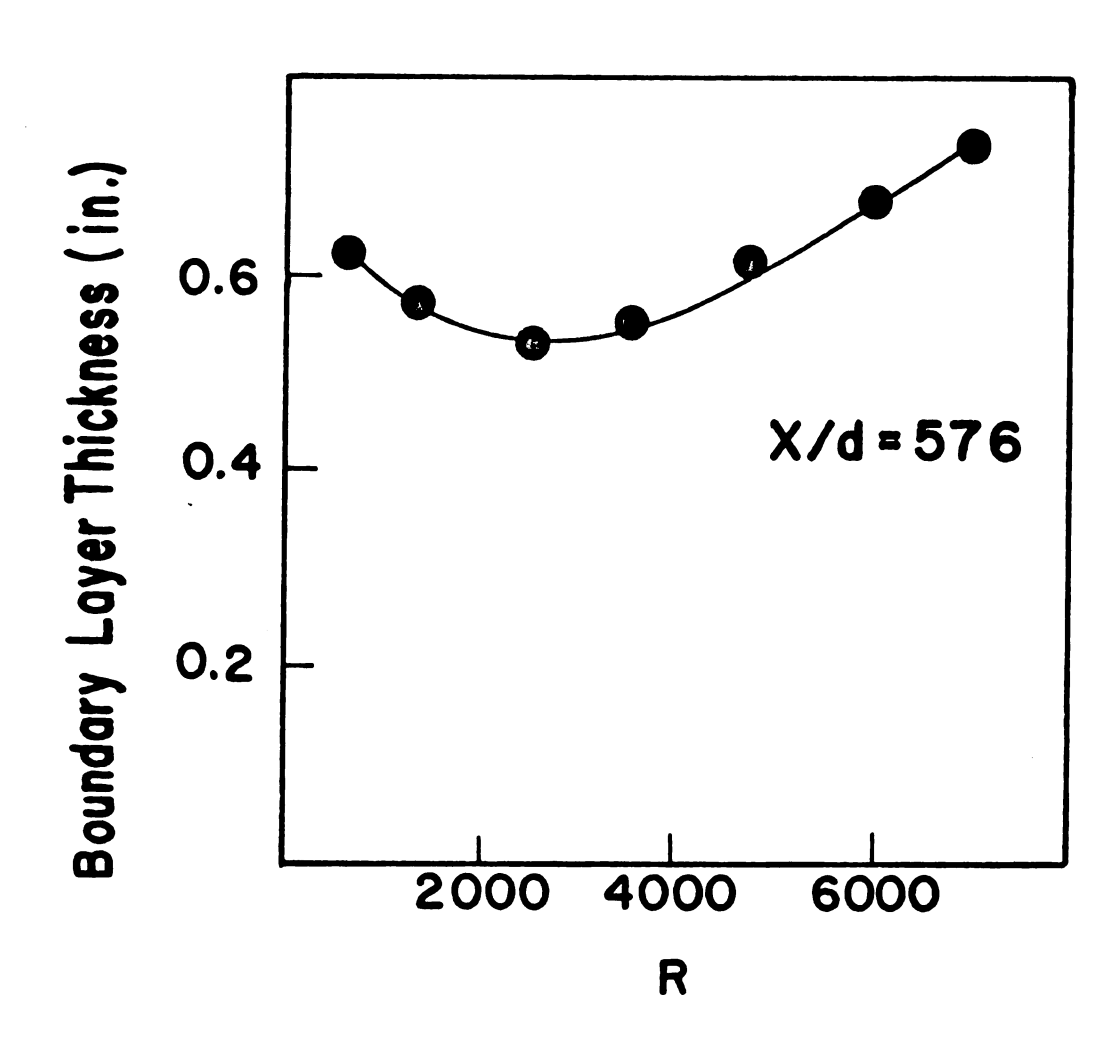


Figure 25. Variation of the side wall boundary layer thickness as a function of the Reynolds number.

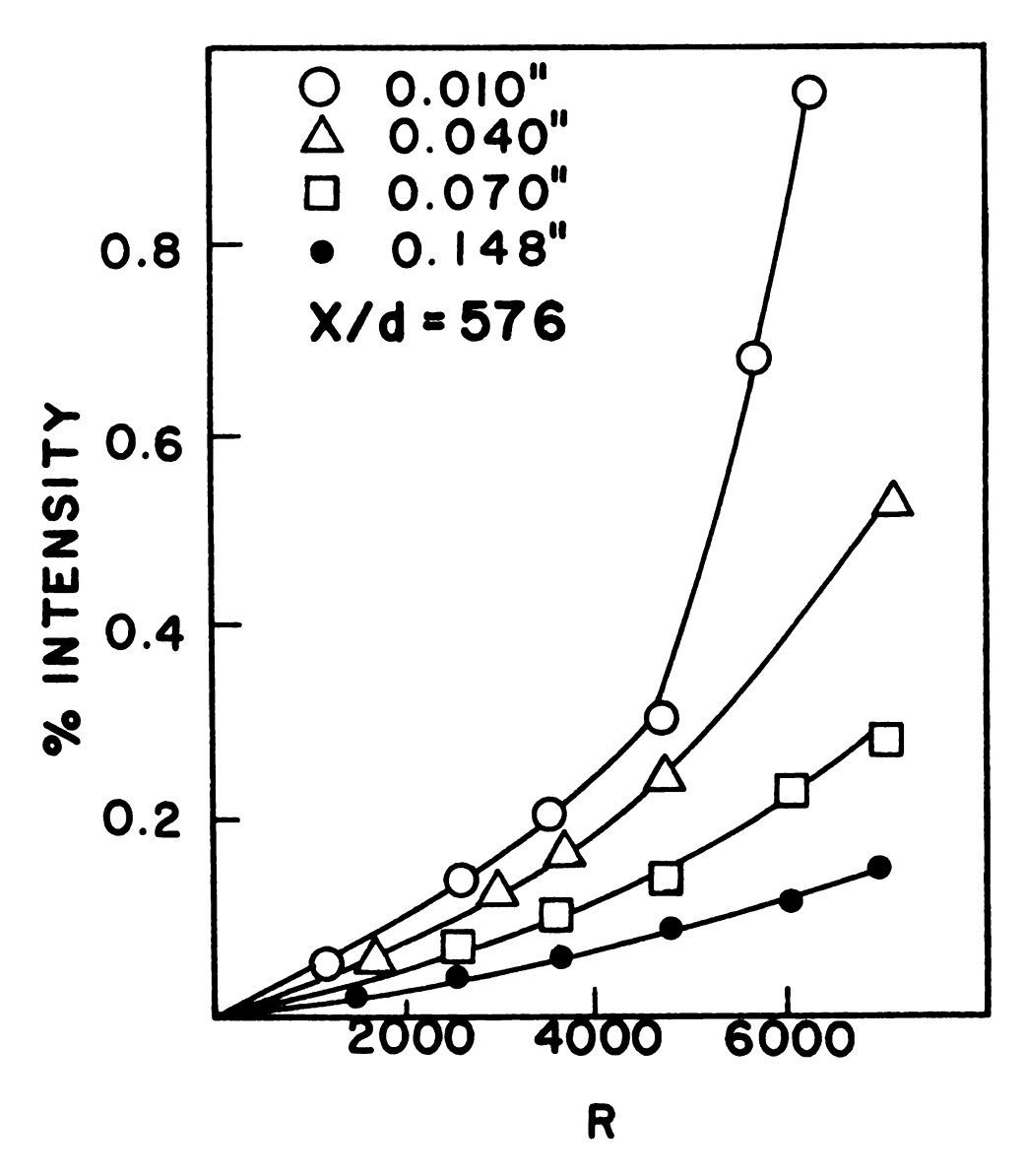


Figure 26. Intensity of laminar fluctuations for the side wall boundary layer as a function of Reynolds number.

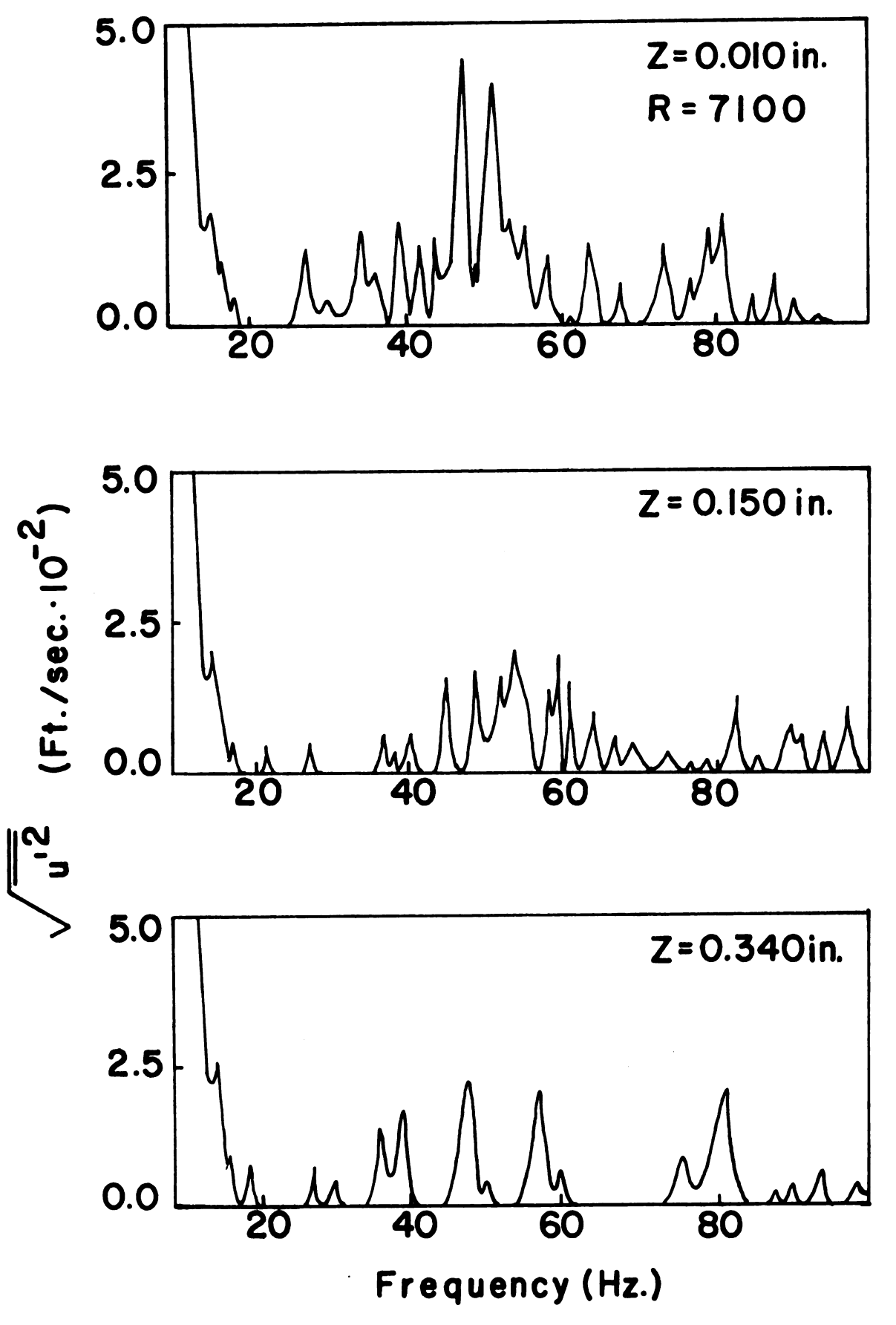


Figure 27. Frequency spectra for the side wall boundary layer.

laminar fluctuations in the boundary layer. Bursting occurs simultaneously in the boundary layer and the mean flow when the critical Reynolds number is reached (one probe located at 0.010 in. from the side wall and another at Z=0 determined the simultaneity of the burst process).

H. Laminar Fluctuations before Transition

Investigation of the growth and decay of laminar disturbances with increasing Reynolds number was made possible with a wave analyzer and an RMS voltmeter. Intensity data were obtained along the centerline at various X/d stations. The intensity is defined as

$$%I = 100 \sqrt{\frac{1}{u^2}} / U_{ave}$$
 (4.35)

where ${\bf u'}$ is the fluctuation about the mean and ${\bf U}_{{\bf a}{\bf v}{\bf e}}$ is the average channel velocity.

The disturbances generated naturally in the developing region of the channel appear to damp as they move downstream. However, this effect is due to increasing U_{ave} as the probe is pulled downstream. The decrease in intensity is a result of increasing U_{ave} and not a decrease in $u^{\frac{1}{2}}$. Damping does occur whenever the Reynolds number is increased. Figure 28 reveals this decrease in intensity of the natural disturbances at X/d = 0 for a range of Reynolds numbers. For the experimentally critical Reynolds number of 7300 the intensity at the inlet is approximately 0.12%.

In Figures 29 through 33 the intensity of the laminar fluctuations is presented as a function of X/d. The data is shown at three y-locations representing the position of the probe at y = d/12, the closest position of the hot wire to the wall, y = d/4, a position midway between the centerline and the wall, and y = d/2, the centerline of the channel. The symbol d represents the gap width of the channel which in this case is

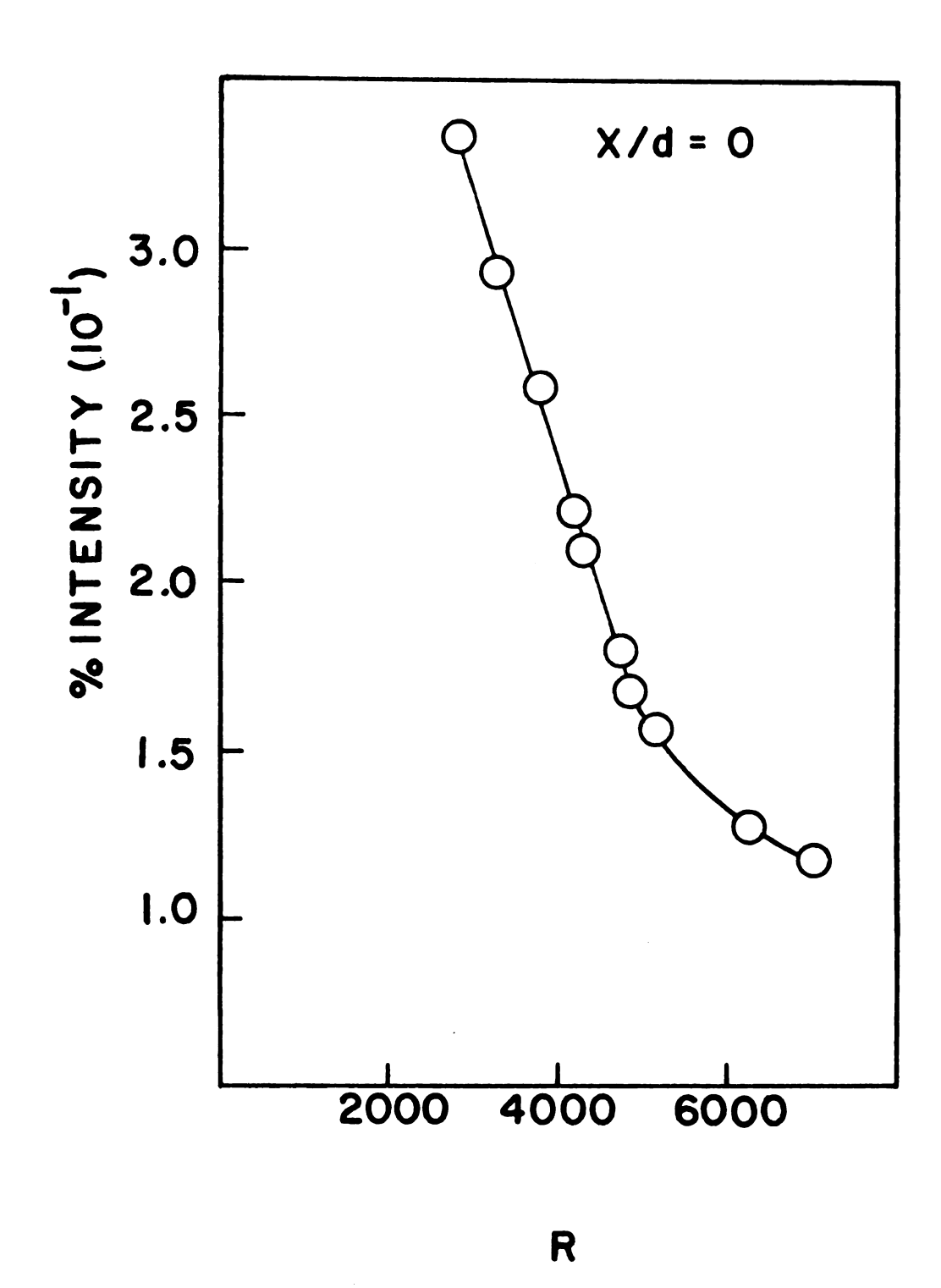


Figure 28. Intensity of natural disturbances as a function of the Reynolds number. X/d = 0

with Reynolds number and X/d before the onset of transition. The range of Reynolds numbers in each figure represents the changing flow rate due to the positioning of the probe at various X/d stations.

The intensity of the disturbances versus X/d for the Reynolds number ranges 3800 to 6800, and 4200 to 7300 are depicted in Figures 29 and 30 respectively. All three y-locations appear to have approximately the same intensity with small variations between each curve. In both Figures the intensity at the centerline, y = d/2, crosses over the intensity curve represented by the region close to the wall, y = d/12, at X/d of 330. After 330 gap widths the centerline region appears to have the maximum intensity.

Figure 31 represents the range of Reynolds numbers for which transition will occur. When the probe is pulled downstream to X/d of 384 a burst is observed. It is interesting to note that the centerline contains the most intense fluctuations at all X/d locations. The regions close to the wall, y = d/12 and y = d/4, represent a lower intensity level, but only slightly so.

A similar behavior is exhibited in Figure 32 for the Reynolds number range 5000 to 7000. The maximum intensity is located at the centerline while the minimum is at y = d/4, the region midway between the centerline and the wall. The location near the wall, y = d/12, represents the next largest intensity. A linear decrease in intensity occurs for all three locations until X/d of 312 at which point transition to turbulence occurs.

A strikingly dissimilar intensity curve is recognized in Figure 33 for the Reynolds number range of 5400 to 6500. At X/d of 96 the regions

y = d/12 and y = d/4 suddenly increase in intensity whereas the centerline continues to linearly decrease in intensity. The maximum intensity appears to be at the wall region before transition to turbulence occurs.

A similar behavior is indicated for the final Reynolds number range of 6400 to 7600. The increase in intensity at the location near the wall, y = d/12, for X/d of 96 is more pronounced. The centerline appears to be the most stable region at these high Reynolds numbers.

The two dissimilar sets of intensity data represent two different mechanisms for transition to turbulence. In the lower Reynolds number ranges the wall region appears to contain the maximum intensity. At large X/d locations the centerline becomes the region of maximum intensity. Linear stability theory predicts that the location near the wall permits a particular frequency of disturbance to grow in amplitude. Transition occurs because of this instability close to the wall. In the present channel at the critical Reynolds number of 7300 the flow becomes unstable and a burst originates near the point of instability. This first mechanism for transition is based upon the fact that the velocity profile becomes unstable due to a growing instability.

At the larger Reynolds numbers the second mechanism for transition is apparent. It was observed that the regions y = d/12 and y = d/4 suddenly become very unstable at X/d of 96, whereas the centerline remained very stable. At this specific value of X/d the developing boundary layers have not converged. Therefore, it appears that these boundary layers become unstable in the developing region. Turbulence is generated due to the growth of disturbances in the boundary layer.

A mosaic of the instantaneous intensity distributions is presented

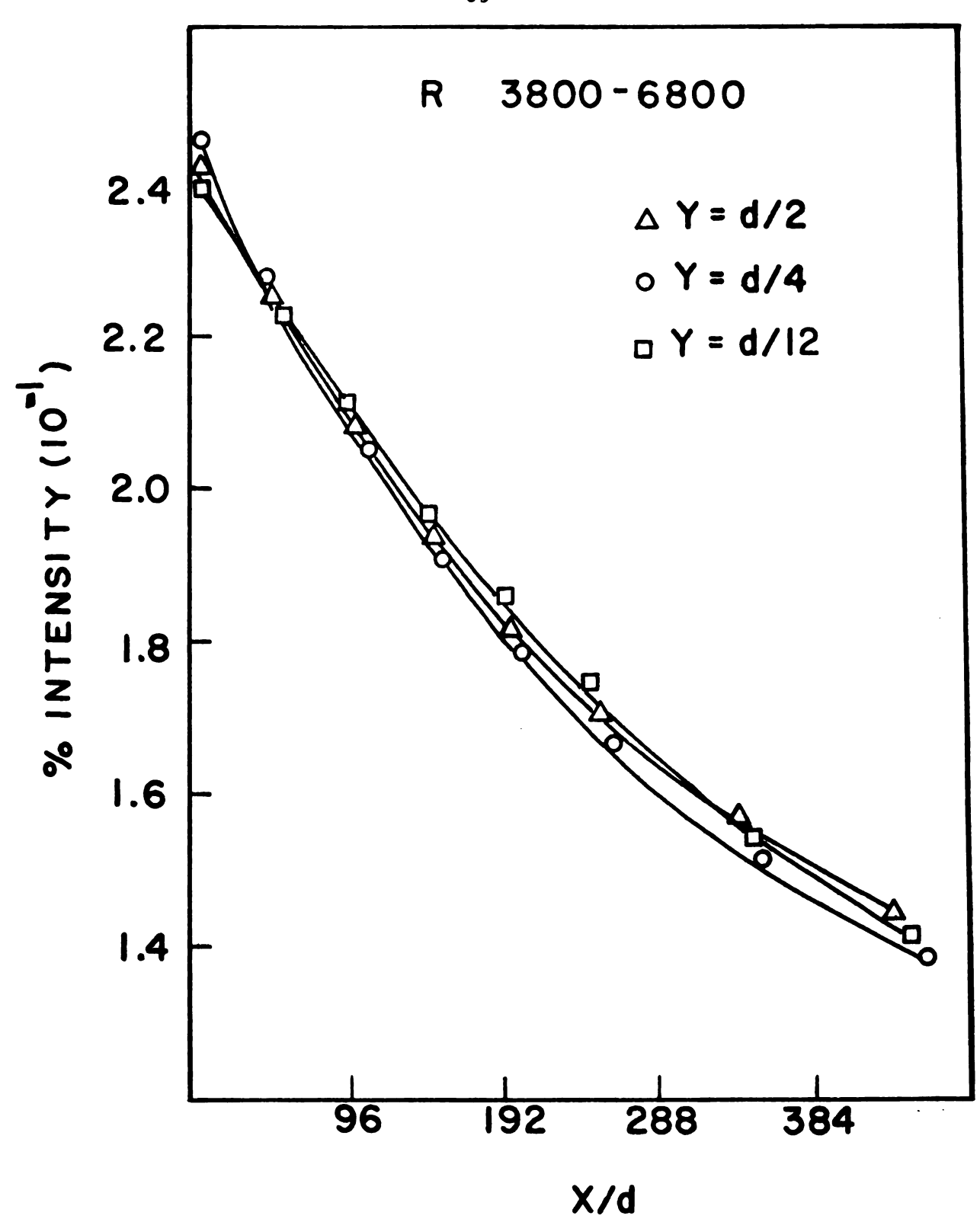


Figure 29. Intensity variation as a function of X/d; for the Reynolds number range 3800 to 6800.

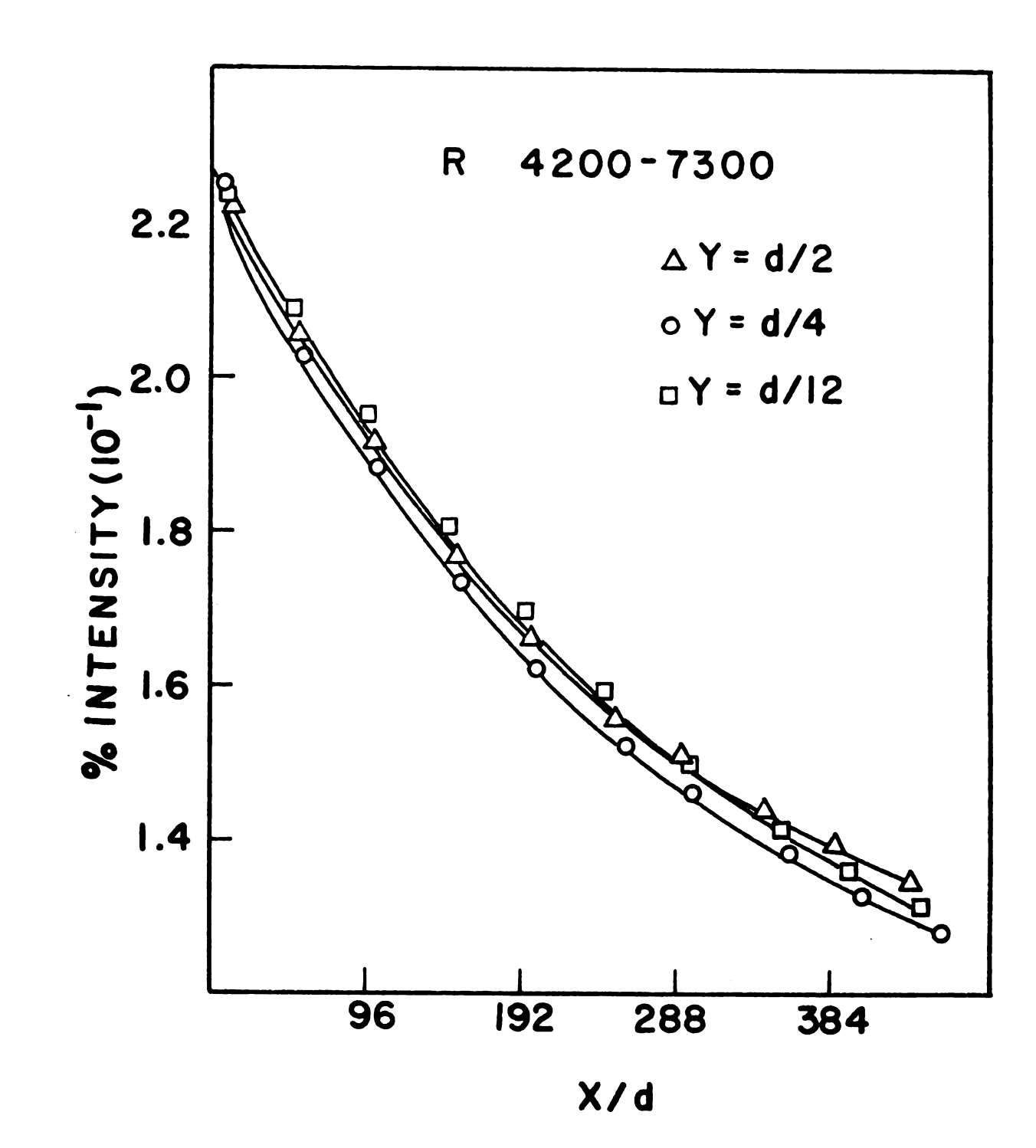


Figure 30. Intensity variation as a function of X/d; for the Reynolds number range 4200 to 7300.

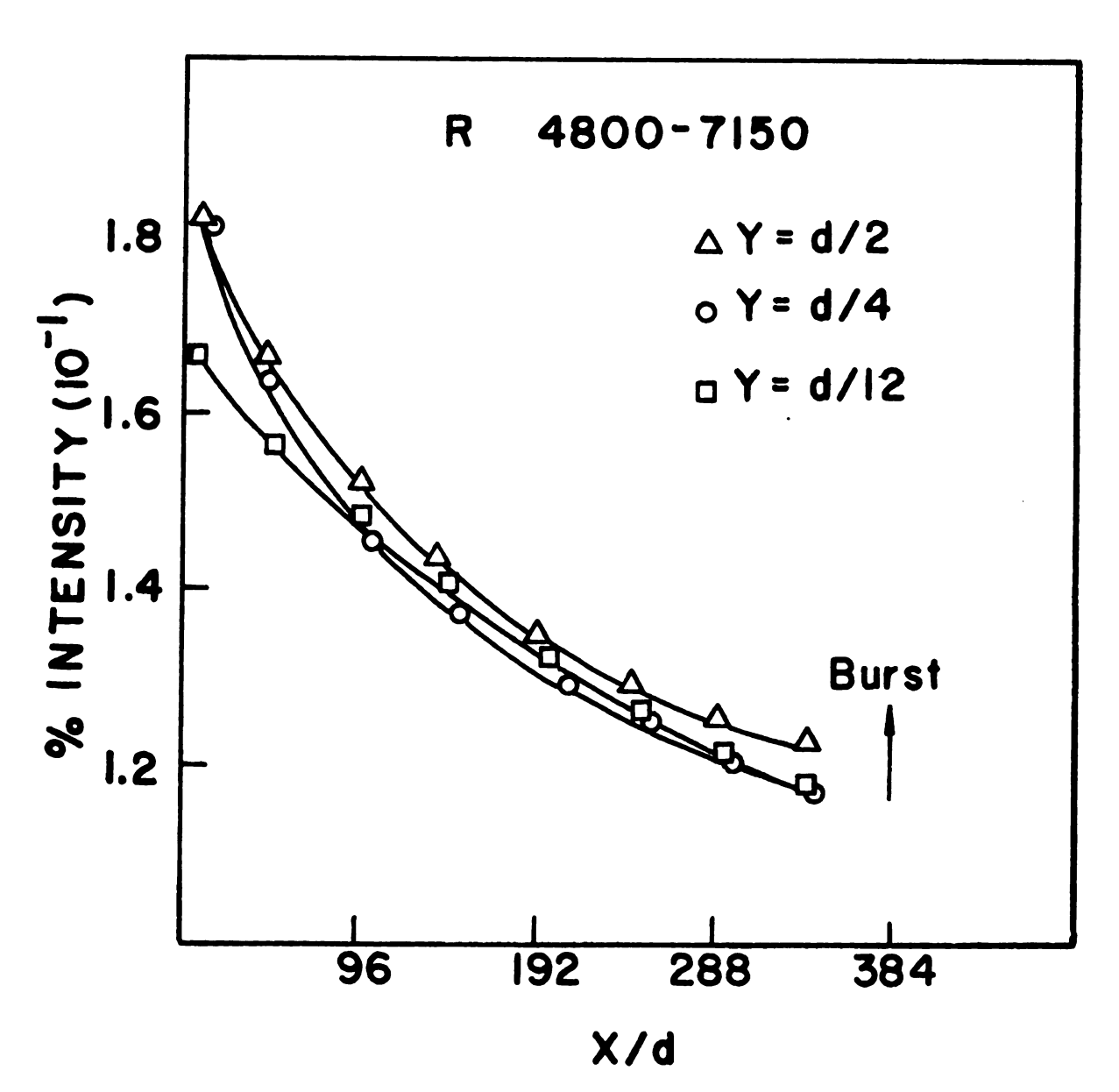


Figure 31. Intensity variation as a function of X/d; for the Reynolds number range 4800 to 7150.

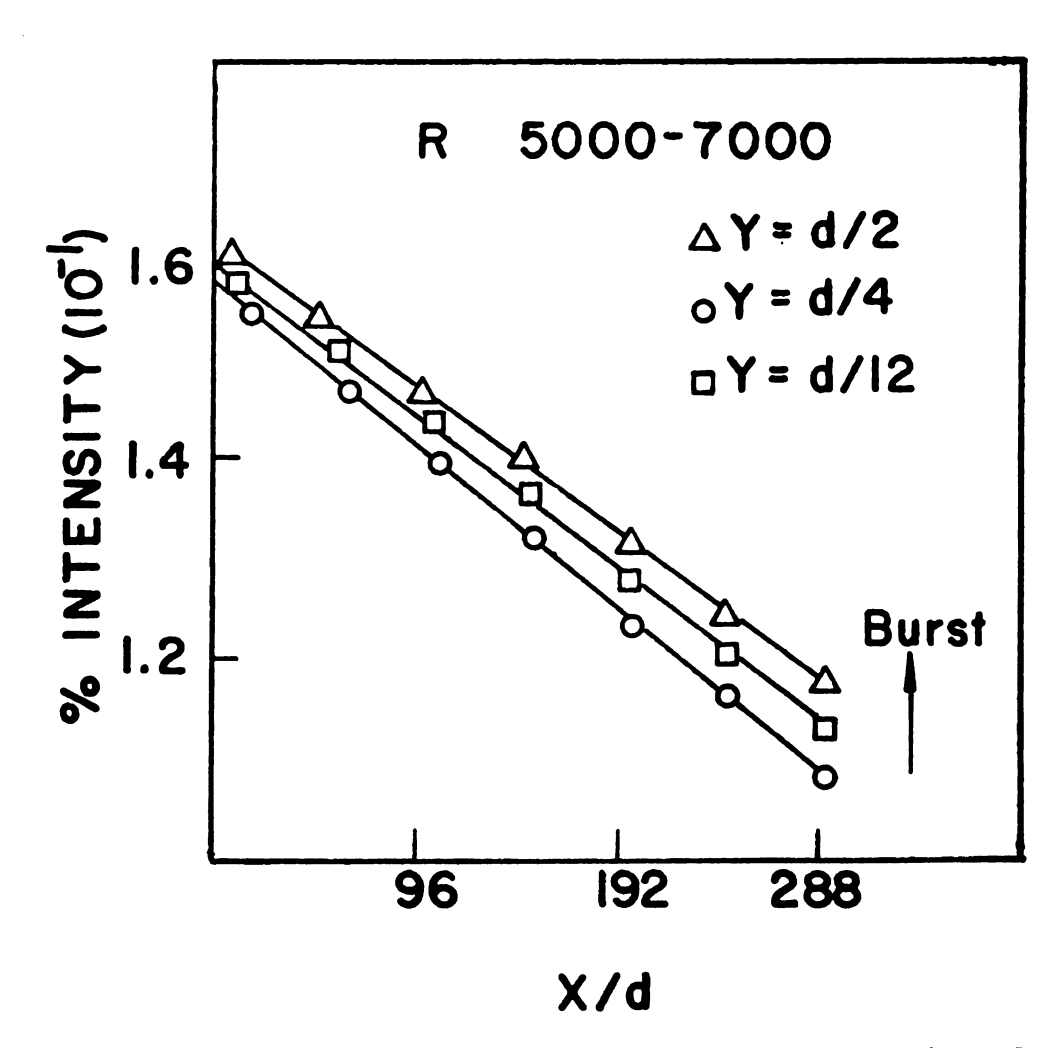


Figure 32. Intensity variation as a function of X/d; for the Reynolds number range 5000 to 7000.

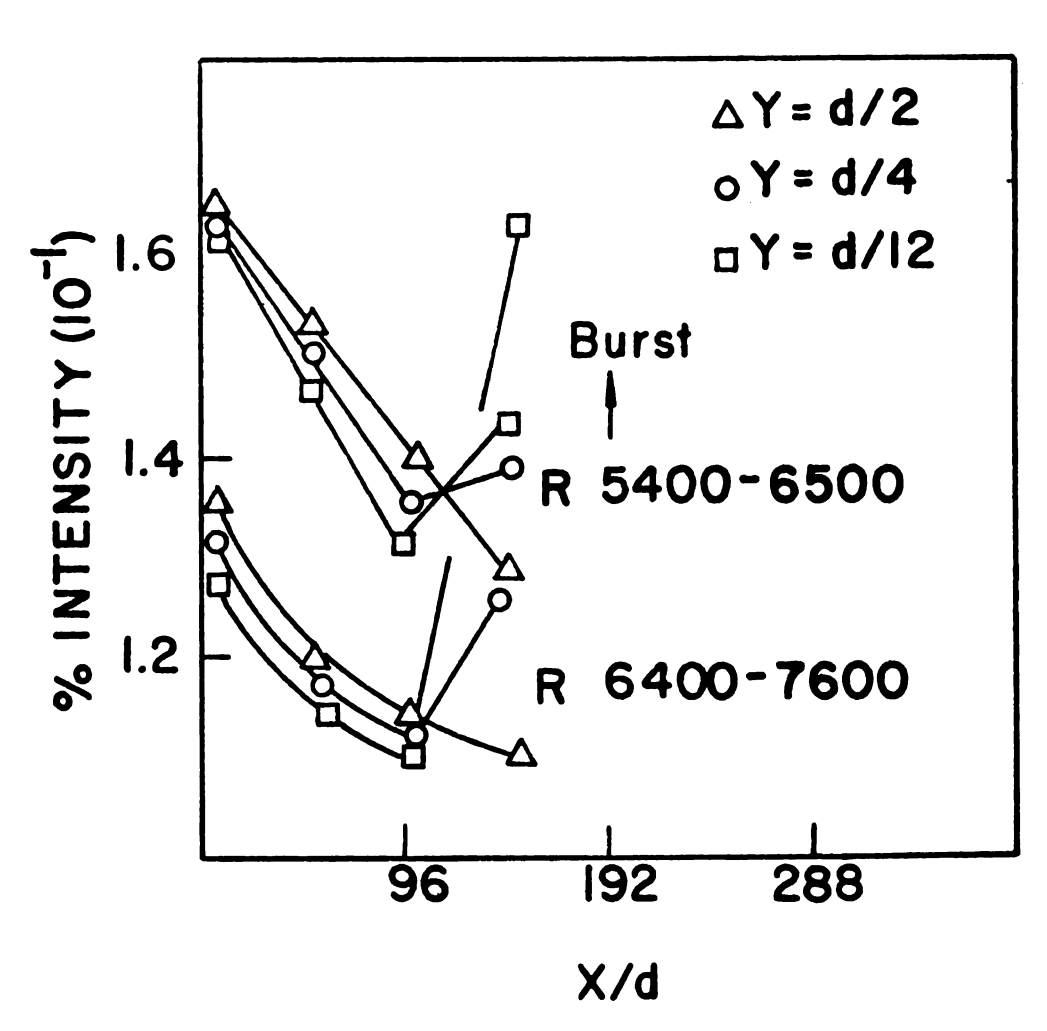


Figure 33. Intensity variation as a function of X/d; for the Reynolds number range 5400 to 6500 and 6400 to 7600.

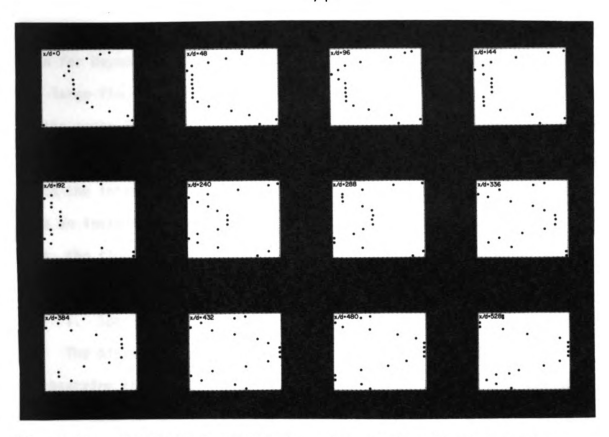


Figure 34a. Mosaic of intensity data; for the Reynolds number range $3800\ to\ 6800.$

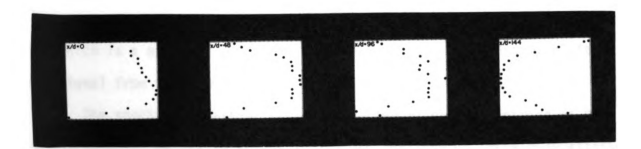


Figure 34b. Mosaic of intensity data; for the Reynolds number range $6400\ to\ 7600.$

in Figure 34. The first mosaic represents a typical intensity distribution for Reynolds numbers before transition such as shown in Figure 29. The large fluctuations close to the walls and the growing fluctuations at the centerline can be clearly observed. In the developing region the maximum fluctuations are localized at y = d/12. The second mosaic represents the intensity distribution at Reynolds numbers large enough to produce an instability in the boundary layer such as shown in Figure 33. Thus, the fluctuations near the wall are clearly being amplified in the last two frames of the mosaic.

I. Spectral Analysis

The disturbances at the wall and the centerline have been studied by observing the intensity of the u' fluctuations. A spectral analyzer also was used in conjunction with the RMS voltmeter to observe the appearance of the dominating waves before transition. In all spectral experiments a strong signal is observed at the frequencies of 55 to 65 Hz. This signal is associated with the 60 Hz. noise level of the hot wire instrumentation. The amplitude of this signal is 0.2 millivolts which is large enough to be detected by the analyzer. This is evident in Figure 35 which is a spectral analysis of the output from the linearizer with no signal from the hotwire.

The spectral investigations were performed at three ranges of Reynolds numbers, at X/d locations of 336 and 144, and at three y-locations. Typical spectra before the onset of transition for the Reynolds number range of 4000 to 7100 are presented in Figure 36. The X/d location is 336 and the Reynolds number at this location is 6800. As indicated by the three curves the number of dominating waves is a maximum at the region

near the wall, y = d/12, decreasing in number to the centerline, y = d/2. The dominating frequencies near the wall occur up to 80 Hz. The location midway between the wall and the centerline is associated with frequencies up to 40 Hz.

In all spectral investigations the low frequencies occurring between 10 and 30 Hz. determine the maximum amplitude of disturbances. Therefore, the intensity at the centerline is greater than the intensity at the wall since the maximum amplitude of disturbances occur between 10 and 30 Hz.

The spectra presented in Figure 37 are realized at the onset of transition for the Reynolds number range of 5130 to 7300. The X/d location is 336 and the Reynolds number at this location is 7300. As indicated previously the maximum number of dominating waves are localized near the wall, y = d/12. Karnitz (1971), in a previous investigation, has ascertained that the flow disturbance oscillates between 25 and 35 Hz. to 50 and 70 Hz. Because the period of oscillation between these two signals is small compared with the analyzer integration time the instrument averages the signal and shows all frequencies. Near the centerline the 63 to 80 Hz. waves disappear.

The Reynolds number range of 5800 to 700 associated with X/d locations of 0 to 192 represents the range for which disturbances will grow until transition is reached. The spectra for the X/d location of 144 and a Reynolds number of 6800 are presented in Figure 38. A very large disturbance is observed near the wall, y = d/12, at a frequency of 63 to 75 Hz. The amplitude of this disturbance is attenuated at y = d/4 and is entirely missing at the centerline. The spectral investigation presented at this location can be compared with the intensity data in Figure 33.

The intensity at X/d of 144 is a maximum for the region near the wall, y = d/12, decreasing to the centerline, y = d/2. The large intensity is probably associated with the 63 to 75 Hz. signal.

The large signal of 63 to 75 Hz. observed in Figure 38 is absent at locations upstream of X/d = 144. Since the initiation of turbulence is observed at X/d = 192 the large growth of the 63 to 75 Hz. signal must occur between these two locations.

The large growth of the 63 to 75 Hz. wave strongly suggests its role in the transition process. This wave is present at the smaller Reynolds numbers before the onset of transition. Linear stability theory determines that at the minimum critical Reynolds number of 7700 the frequency of the wave that amplifies as it progresses into unstable conditions is 92.5 Hz. Although a 25% difference exists between the predicted and the experimentally observed frequency the 63 to 75 Hz. signal does possess the characteristics of a perturbed wave being amplified at the onset of transition.

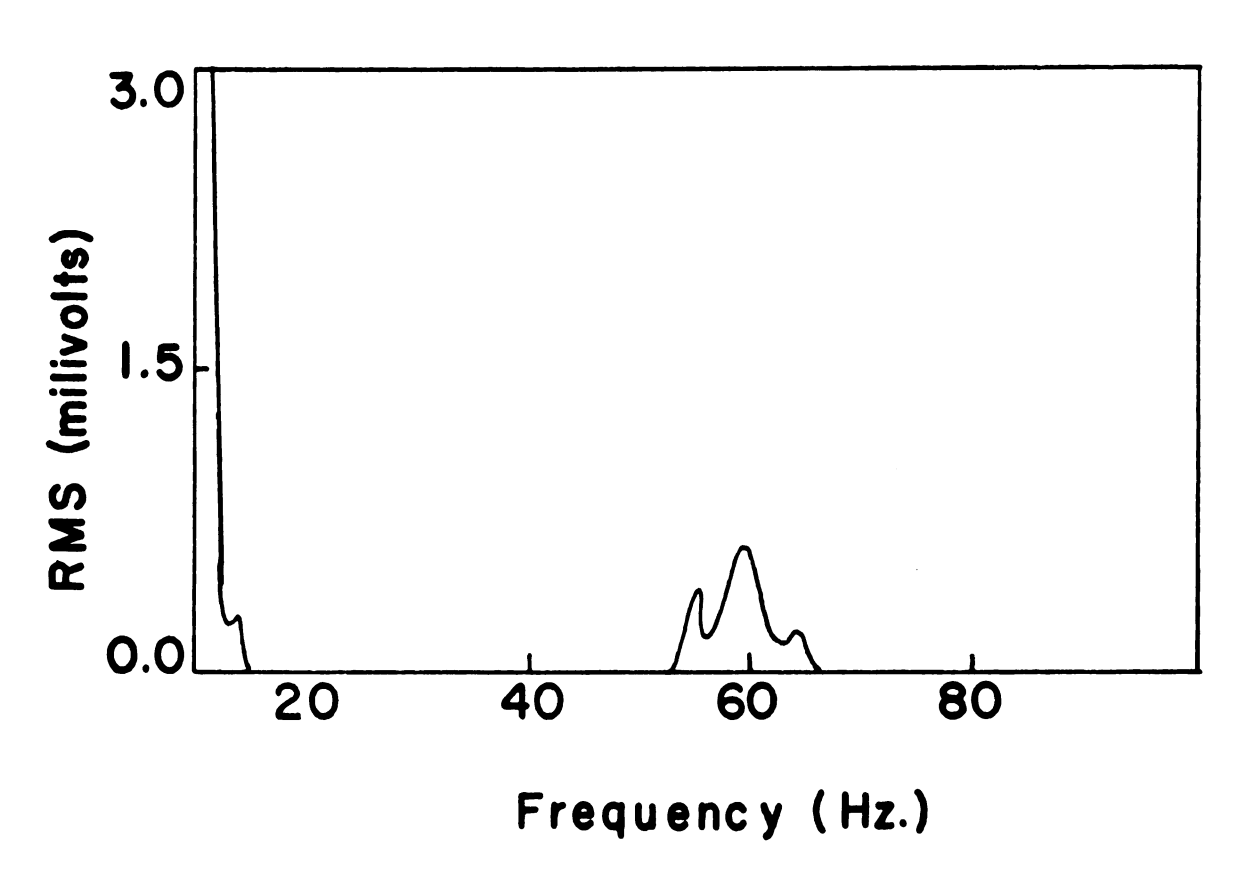


Figure 35. Frequency spectrum of 60 Hz. noise associated with the hot wire instrumentation.

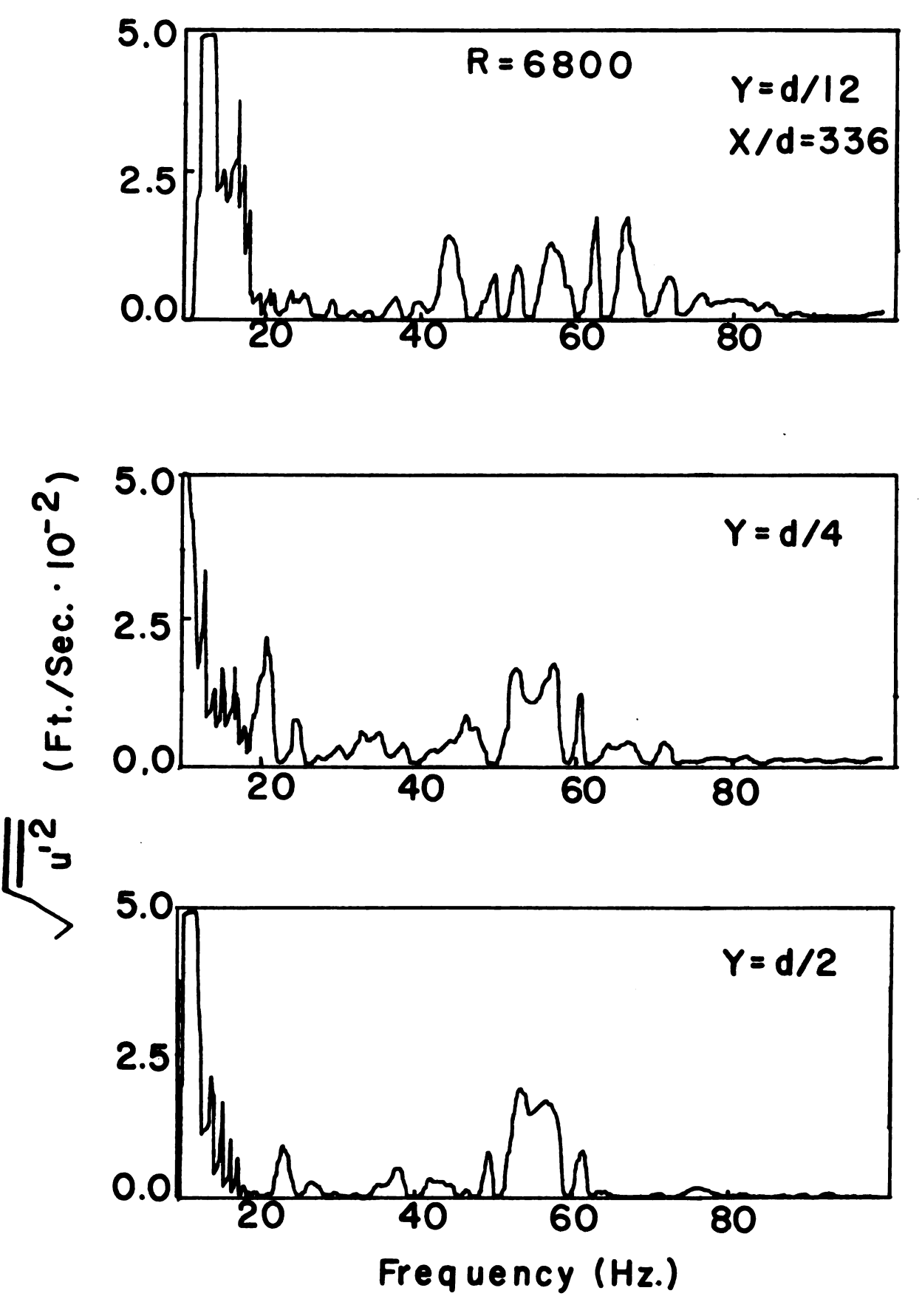


Figure 36. Frequency spectra at X/d of 336; for a Reynolds number of 6800.

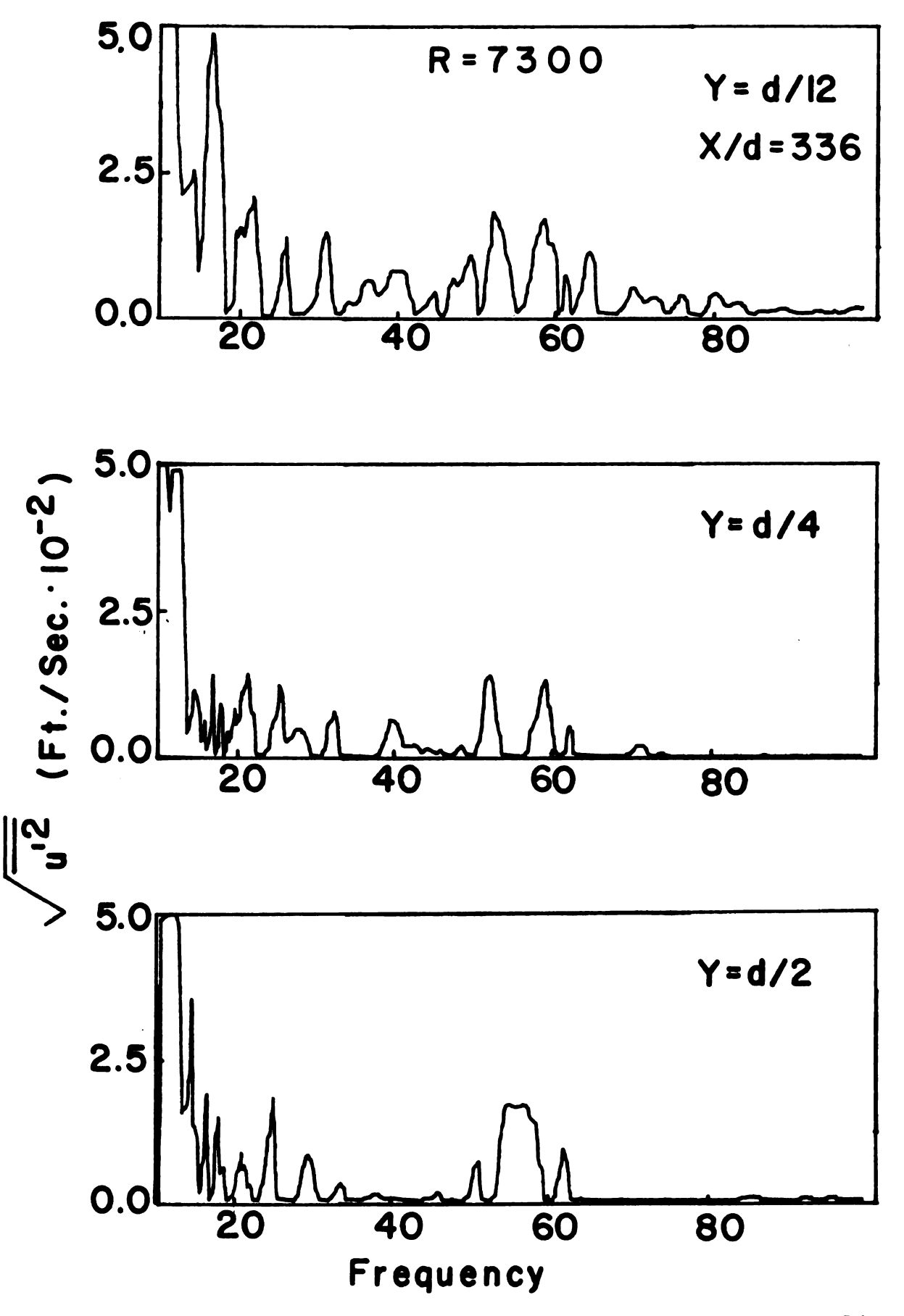


Figure 37. Frequency spectra at X/d of 336; for a Reynolds number of 7300.



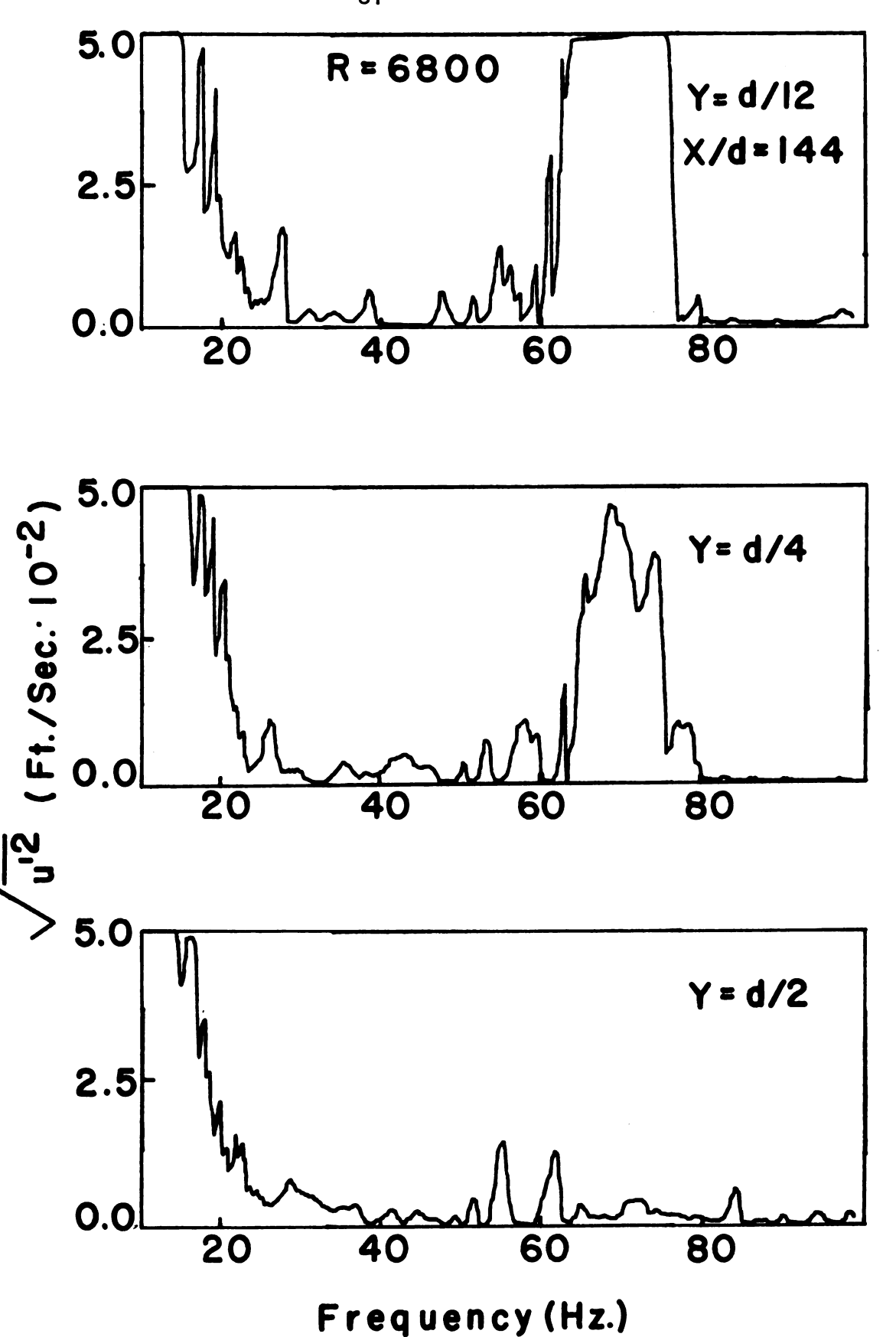


Figure 38. Frequency spectra at X/d of 144; for a Reynolds number of 6800.

2. Mechanism of the Burst Process

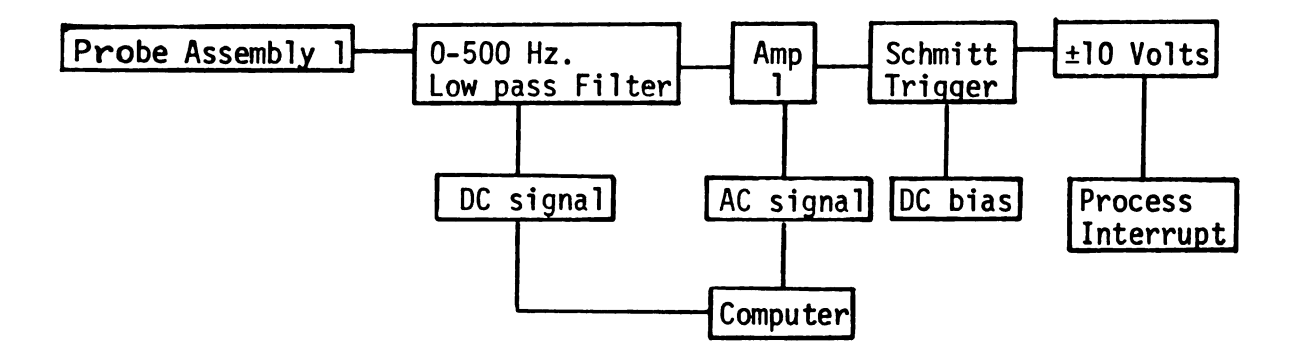
A. Span-Wise and Length-Wise Variation of the Burst

The turbulent burst was studied in a qualitative manner elucidating its role in the transition process. Before the bursting process occurs there is a parabolic velocity profile in the fully developed region of the channel at a sufficiently low Reynolds number. At the critical Reynolds number the flow becomes unstable and a burst develops and grows as it washes from the channel. Karnitz (1971), in a previous investigation, determined that the burst was uniformly distributed across the width of the Channel and did not vary with the z-coordinate.

The nature of the bursting process was analyzed by means of two hot wire probes and an on-line data acquisition system with the aid of an IBM 1800 analog-digital computer. An effective trigger mechanism was utilized to enable immediate data sampling at the onset of a turbulent burst. The use of a Schmitt trigger circuit is illustrated in Figure 39.

In this design the triggering circuit executes on the basis of a large negative voltage. Because a large negative spike is produced at the initiation of a turbulent burst the system utilizes this information to initiate data sampling. Figure 40 presents two graphs which depict a typical burst, one sampled automatically and the other manually. The automatic sampled data made use of the Schmitt circuit. The computer can also be made to sample data by sending a 0 to 10 volt signal to the A-D converter and this is defined as a manual operation.

Using the Schmitt trigger the time lag between the exact instant of the hot wire voltage change and the initiation of computer sampling is less than 100 microseconds. In Figure 40 the AC component of the signal



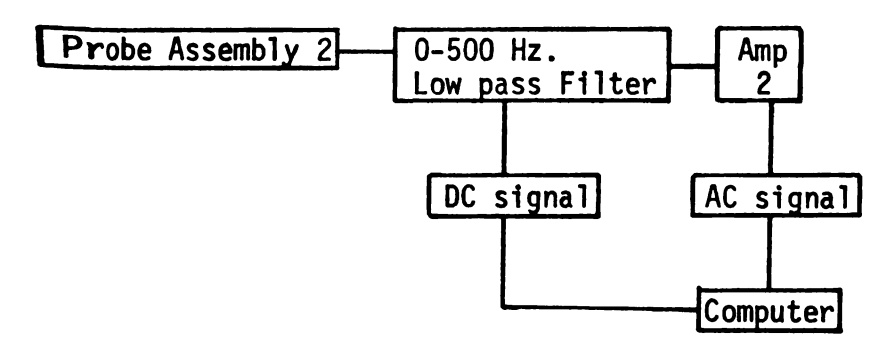
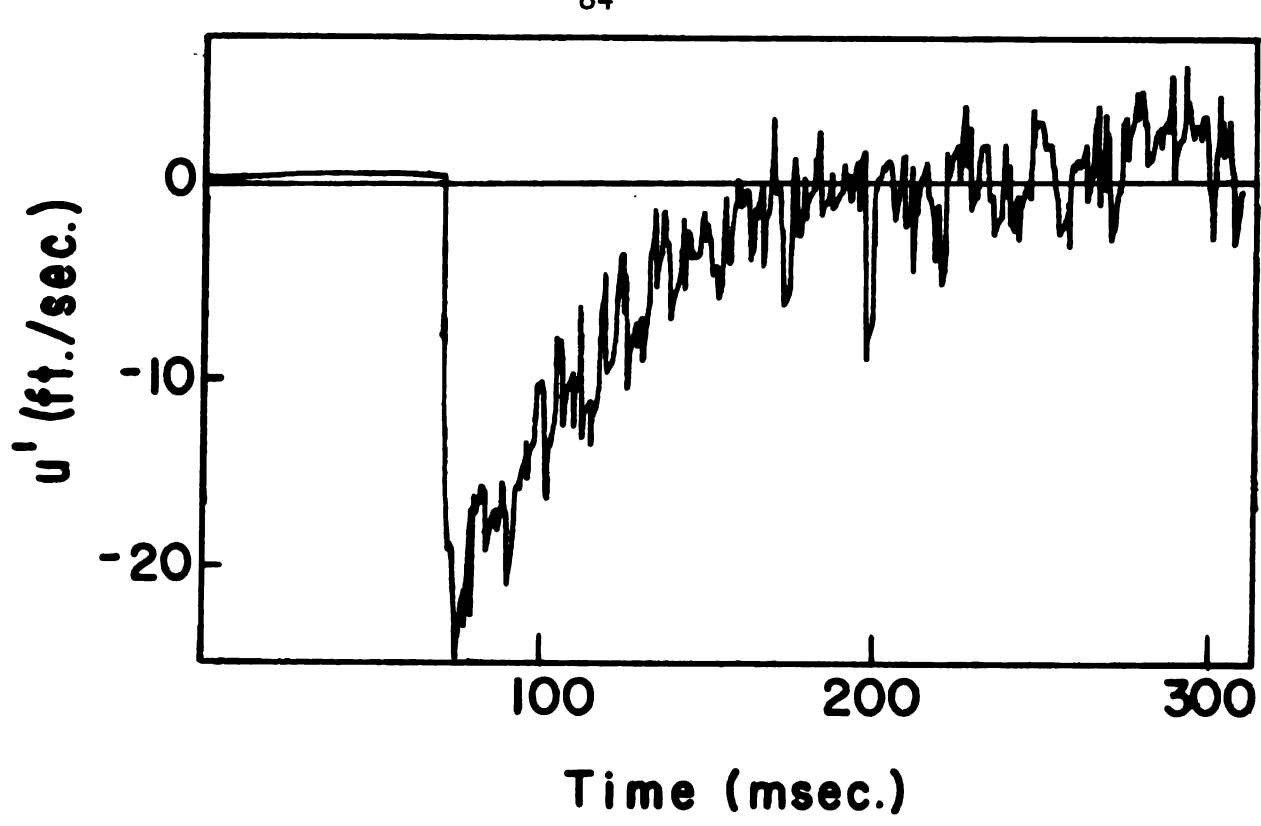


Figure 39. Illustration of Schmitt trigger circuit together with hot wire instrumentation.



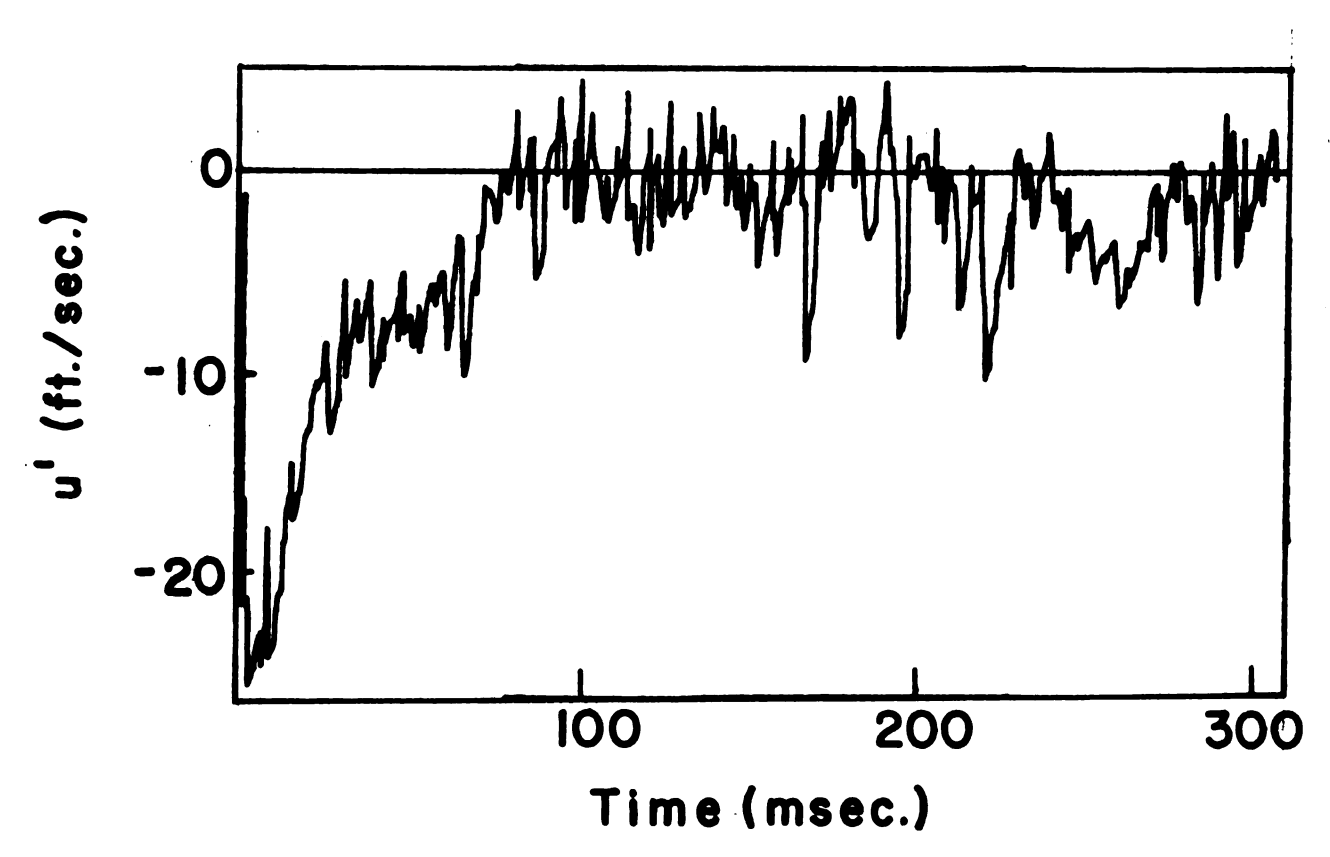


Figure 40. Comparison between automatic and manual computer sampling initiation.

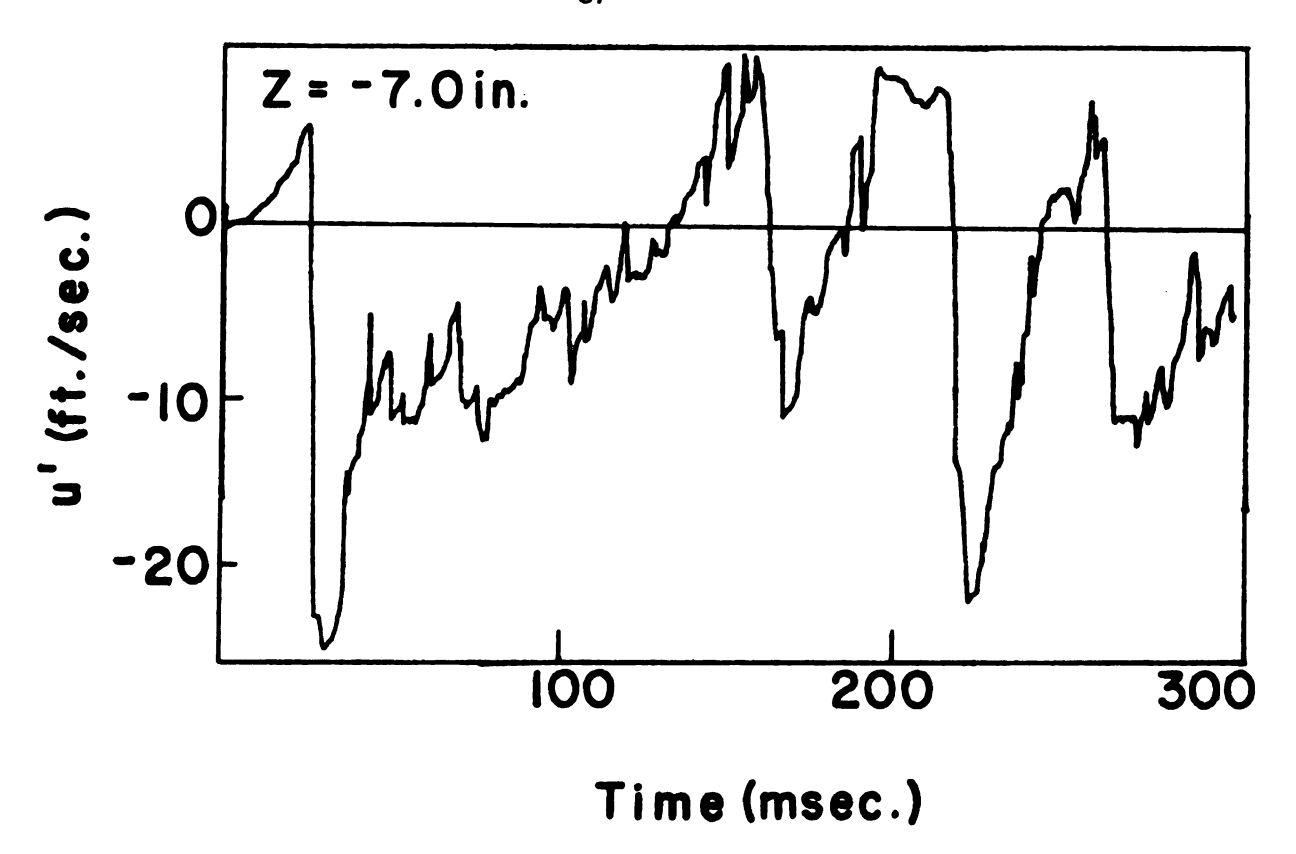
is shown with the DC portion removed. Characteristic of all bursts is an initial large spike deflected either positively or negatively depending upon the z-location of the hot wire. A similar large spike is apparent at the end of the burst process and the deflection is opposite to that observed initially. The amplitude of the spike varies with X/d location.

In order to determine the streamwise variation of the burst two probes were located at the downstream end of the channel (previous investigations determined that the burst initiates upstream of X/d=360). The probes were placed near the centerline, y=d/2, approximately 19 in. apart (Probe 1 at z=-7 in. and Probe 2 at z=12 in.). Probe 2 remained fixed while Probe 1 was pulled downstream. The trigger mechanism was applied to Probe 2. If any span-wise or streamwise variation in the turbulent slug existed as it washed downstream it would be detected as a time delay for burst detection with respect to Probe 2. For a Reynolds number of 7300 the results of this investigation are presented in Table 1.

The bursting process did not appear to be well defined or continuous across the width of the channel but isolated to particular regions. At some z-locations a number of bursts were observed at Probe 1. The characterization of these bursts could be described as "mini-bursts". An example of this unusual phenomenon is presented in Figure 41 for the location X/d = 288 with Probe 1 at z = -7.0 in. and Probe 2 at z = 10.5 in. After an initial time delay of 52.2 msec. the first burst appears and quickly dies with the generation of a second short lived burst and then another much longer burst. The number of short lived bursts and their occurence at particular locations appears to be random. Inspection of

TABLE 1
Variation of Burst Process
Along Length of Channel

Expt.	X/d Probe 1 z=-7 in. y=d/2	X/d Probe 2 z=12 in. y=d/2	# of Bursts observed at Probe 1	Time Delay (msec.) with respect to Probe 2
1	264	288	3	52.2, 177.0, 290.4
2	288	288	3	75.8, 194.6, 251.2
3	312	288	2	35.2, 131.0
4	336	288	1	62.8
5	360	288	1	96.6
6	384	288	1	100.4
7	408	288	1	155.4
8	432	288	1	160.0
9	480	288	3	9.0, 86.6, 175.4
10	52 8	288	turbulent	· -



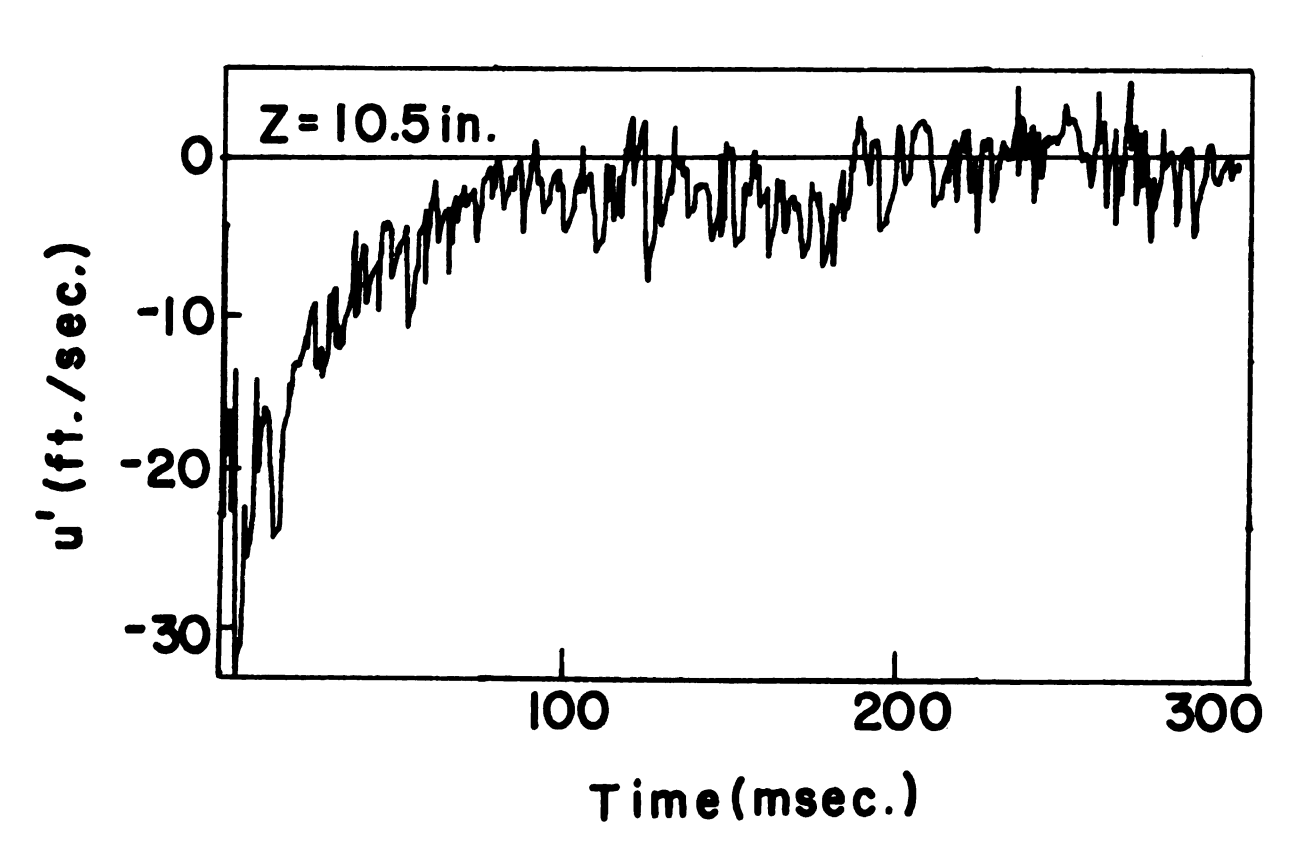


Figure 41. u' portion of computer sampled burst process at z=-7.0 in. and z=10.5 in.

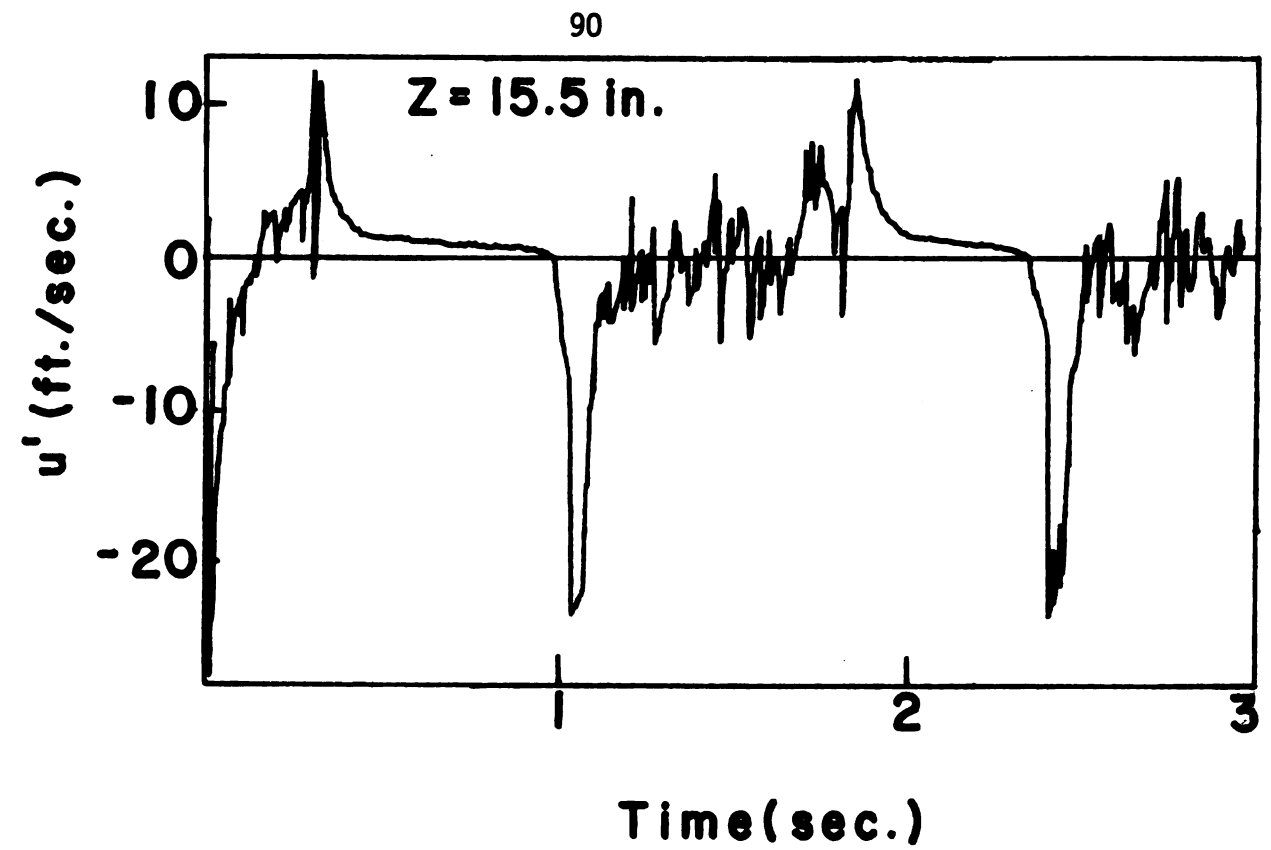
Table 1 reveals that this phenomenon is evident at 4 different locations.

The time delay between the appearance of the bursts at the two probes increases with X/d. The fact that there is a delay at Probe 1 suggests that the bursts originate at the right half of the channel, upstream of both probes. At X/d of 528 no delay is apparent since the flow is fully turbulent at this point due to the wake effects from Probe 2. In order to characterize the span-wise variation of the bursting process Probe 2 was placed near the right side wall at z = 10.5 in. and the location of Probe 1 was varied with respect to the z-coordinate. The results of the experiments at X/d of 288 are presented in Table 2. The observed time delay is with respect to Probe 2. The results indicate that the burst process is not two dimensional across the width of the channel but isolated near the right hand side. At distances greater than z = -10.0in. the burst does not appear to sweep past this region. Moving Probe 1 towards the right hand side gave rise to smaller delay times. The negative delay times in experiments 6, 7, and 8 indicate that the burst generation upstream occurs randomly at regions close to the right hand side wall.

Figure 42 depicts the burst process over 3 seconds at X/d of 288. Probe 2 is located at z=15.5 in. while Probe 1 is at z=2.0 in. The initial spikes observed at the beginning of every burst are different at the two z-locations. A large negative deflection is apparent at the extreme right hand side of the channel, whereas near the centerline a positive deflection followed by a larger negative spike is observed. This characteristic is apparent at other X/d locations.

TABLE 2
Variation of Burst Process
Across Width of Channel

Expt.	Z (in.) Probe 1 X/d=288 <u>y</u> =d/2	Z (in.) Probe 2 X/d=288 y=d/2	<u>∆Z (in.)</u>	Time Delay (msec.) with respect to Probe 2
1	-15.5	10.5	26.0	no burst on Probe
2	-9.0	10.5	19.5	no burst on Probe
3	-2.0	10.5	12.5	62. 8
4	2.0	10.5	8.5	125.0
5	4.0	10.5	6.5	9.9
6	4.0	10.5	6.5	-9.4
7	4.0	10.5	6.5	-6.3
8	4.0	10.5	6.5	3.1
9	4.0	10.5	6.5	7.9
10	4.0	15.5	11.5	11.0
11	4.0	15.5	11.5	8.6
12	11.5	15.5	4.0	10.2
13	11.5 (X/d=312)	15.5	4.0	48.0
14	11.5 (X/d=336)	15.5	4.0	turbulent



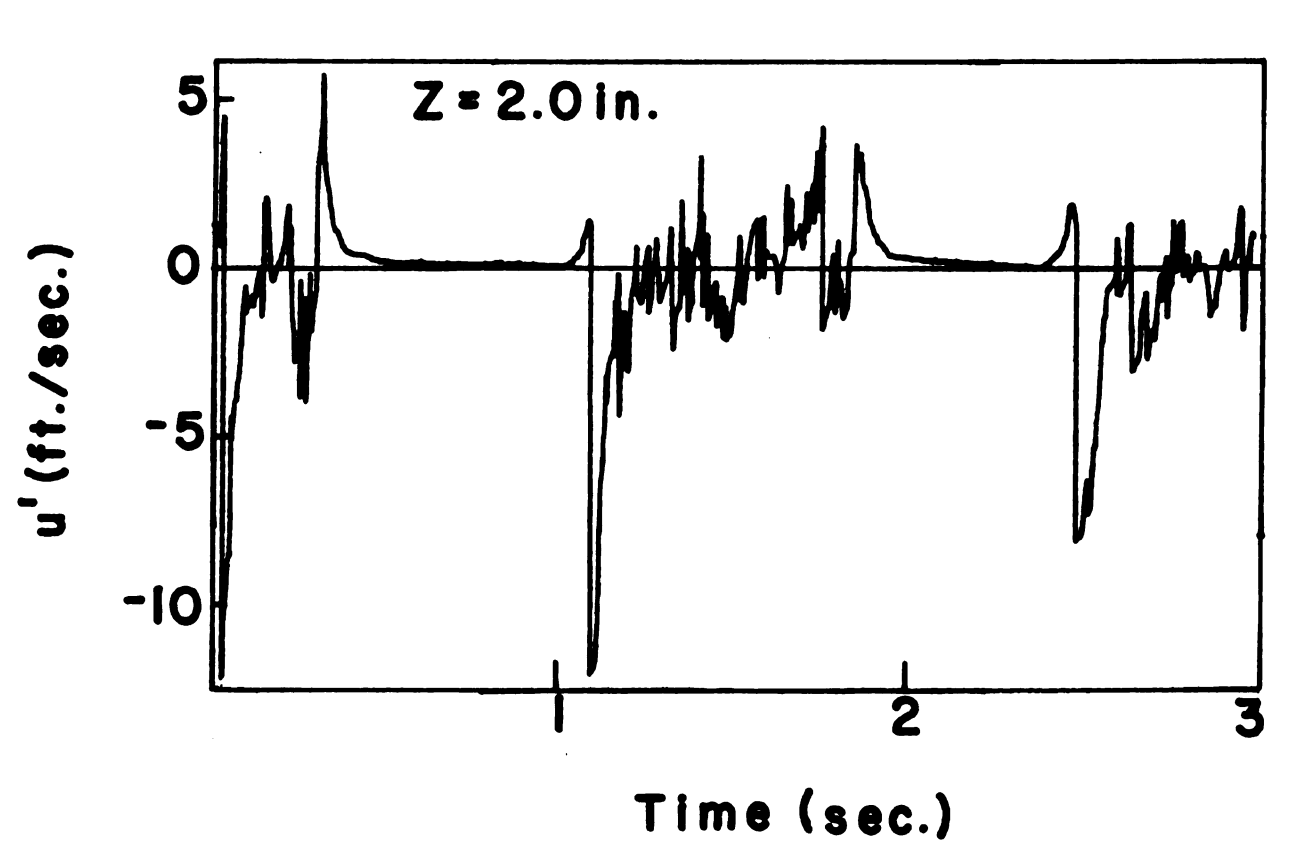


Figure 42. u' portion of computer sampled burst process at z = 15.5 in. and z = 2.0 in.

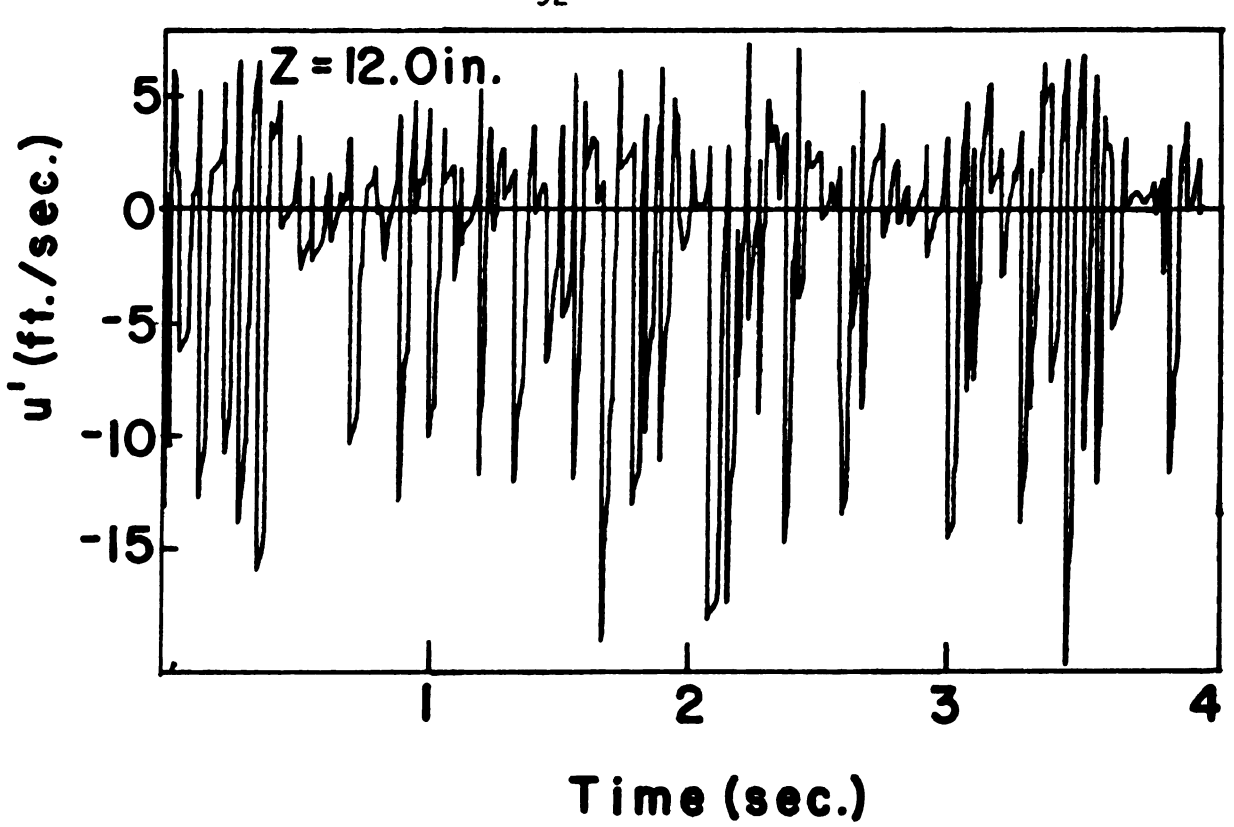
B. Location of Burst Generation

In order to establish the location of burst generation the probes were moved upstream with Probe 2 near the right side wall, z=14.5 in., and Probe 1 near the centerline, z=1.0 in. It was observed that at X/d of 96, a region where the velocity profile was still developing, the burst process was isolated to a narrow region near the right hand side wall. The Reynolds number for transition at this location was 7300. Large scale velocity spikes were first observed at z=10.0 in., growing to a maximum at z=13.5 in., and decreasing to the right side wall. The width of this unstable region is approximately 7 in. Figure 43 presents the burst process at z-locations of 12.0 in. and 9.0 in.

In order to observe the behavior of the burst process as a function of increasing X/d the two probes were pulled downstream. Figure 44 depicts the bursting at X/d of 120 for z=14.5 in. and 1.0 in. The bursting from the right hand side wall region is associated with large velocity spikes which resemble the beginning and end of a burst observed at downstream locations. The frequency of the spikes is approximately 6 to 8 Hz. The centerline region exhibits velocity fluctuations whenever large negative spikes are produced at z=14.5 in. The bursting process at X/d of 144 is displayed in Figure 45. The bursting is more defined at the side wall region with a larger burst duration time. The turbulent core region of the burst appears to be establishing itself.

C. Periodicity of the Burst Process

By placing the probes at regions close to the right and left side walls and successively measuring the burst process at every X/d location a mapping of the burst process was established. The initial burst and



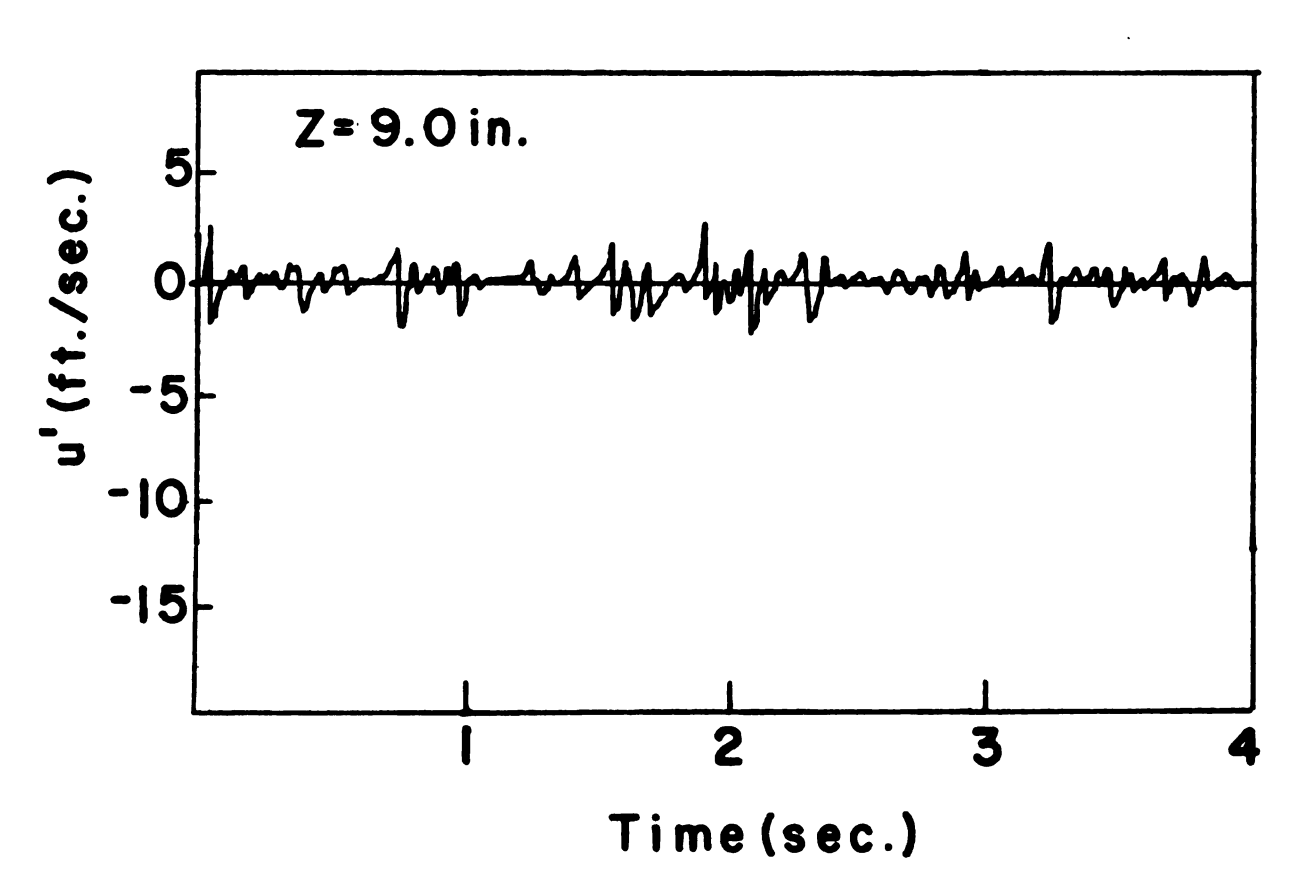
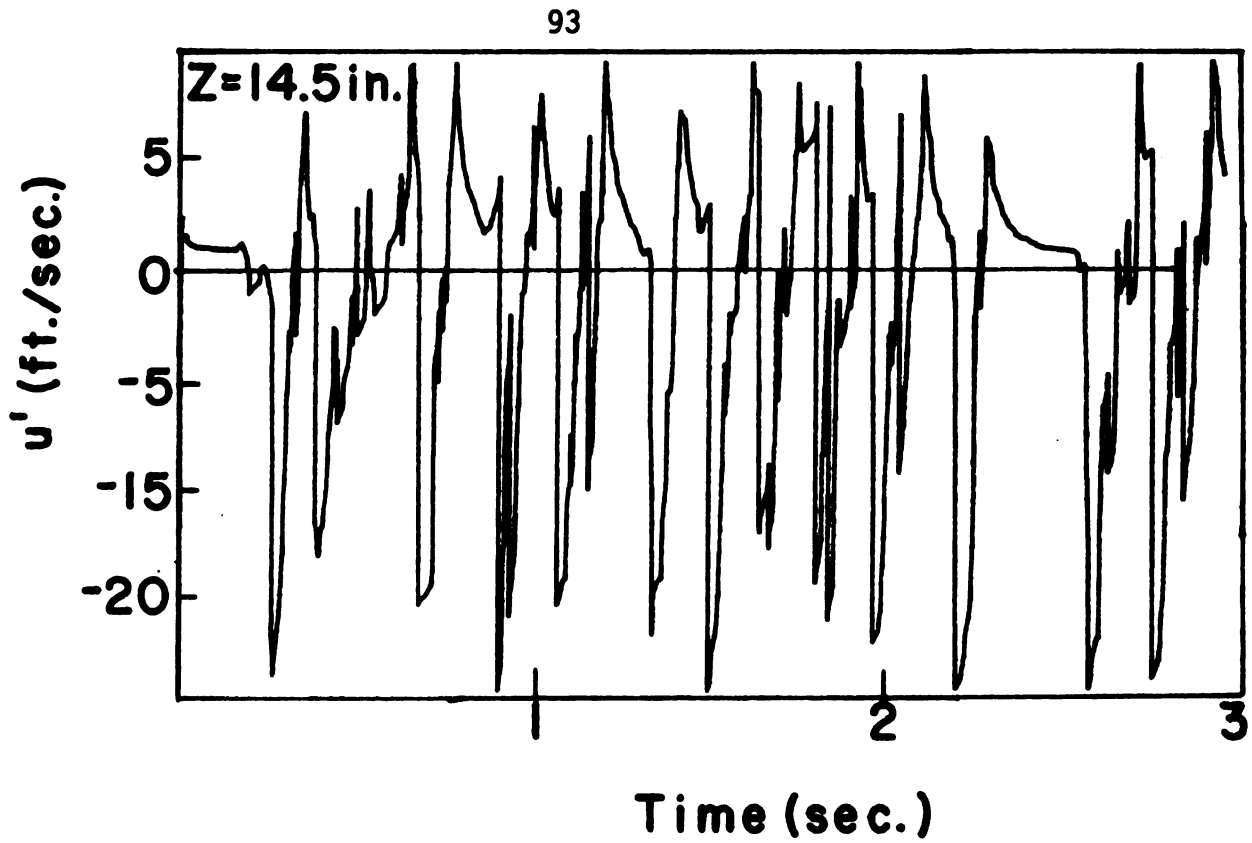


Figure 43. u' portion of computer sampled burst process at z = 12.0 in. and z = 9.0 in.; at X/d of 96.



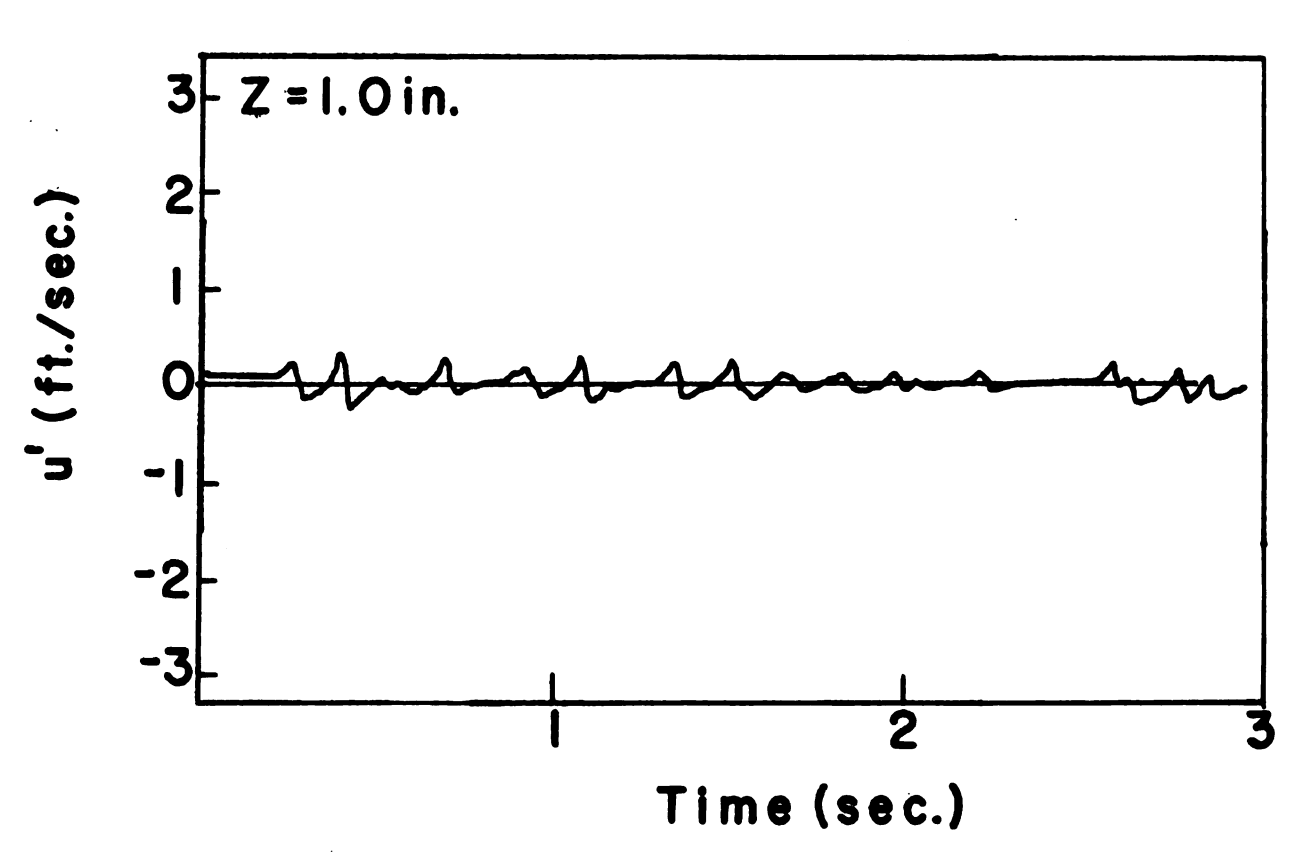
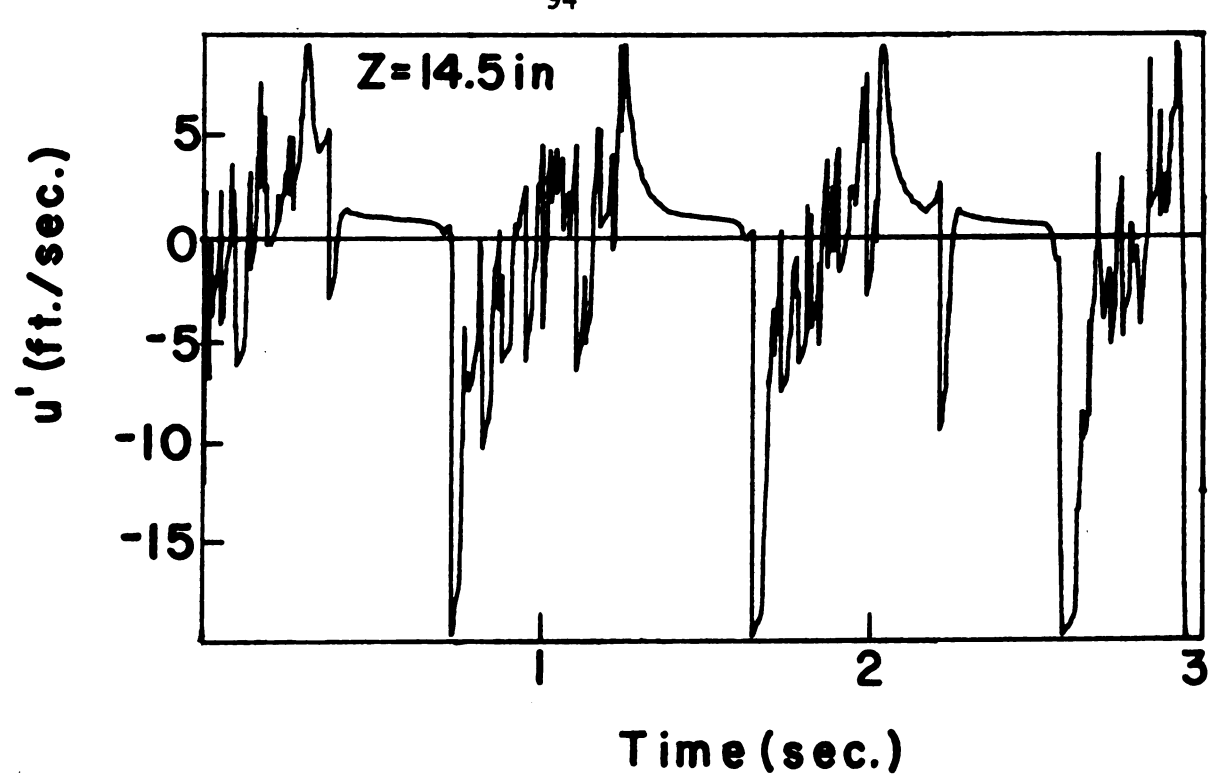


Figure 44. u' portion of computer sampled burst process at z = 14.5 in. and z = 1.0 in.; at X/d of 120



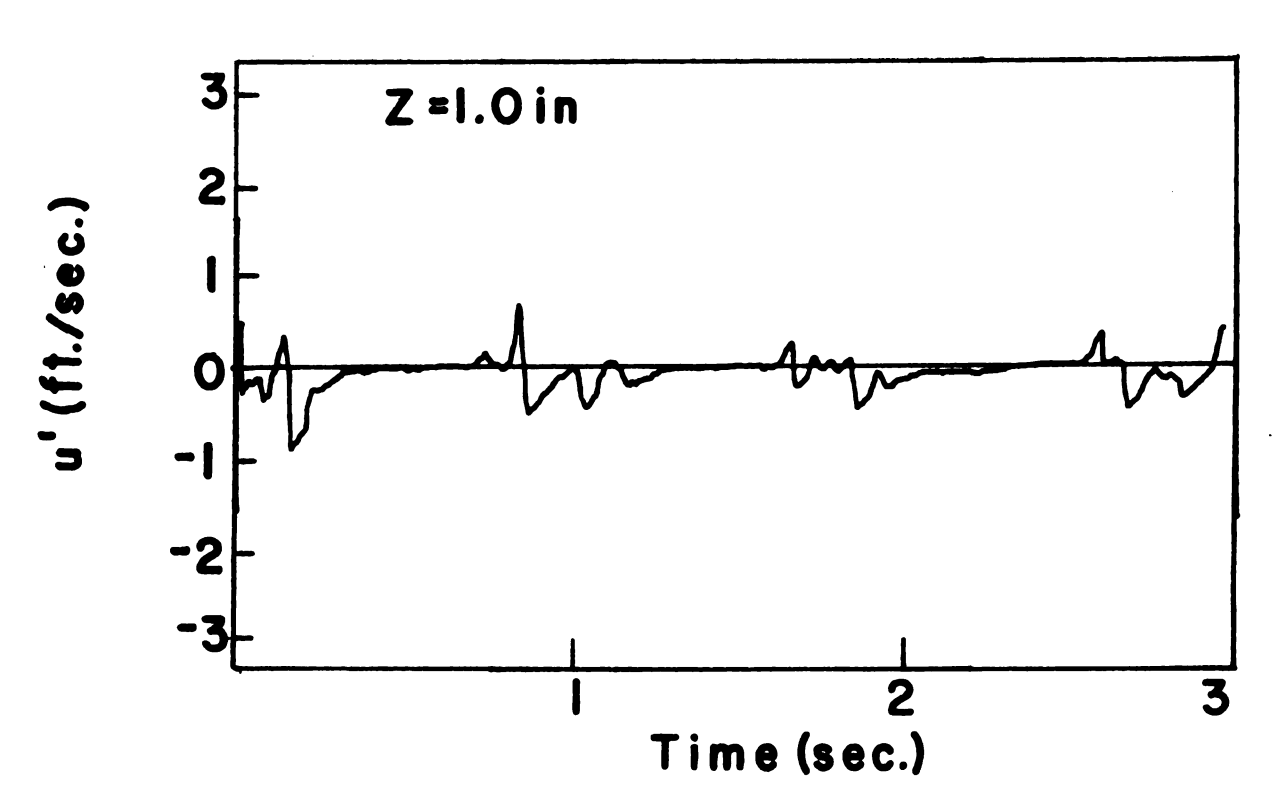


Figure 45. u' portion of computer sampled burst process at z = 14.5 in. and z = 1.0 in.; at X/d of 144.

laminar duration times including the successive burst duration times are presented in Table 3. The two probes were located at $z=\pm 13.5$ in. The duration times of the bursts and of the laminar interval between each burst increases with increasing X/d. However, this linear increase is a result of the interaction of the probes with the flow. Pulling the probes downstream causes an increase in the flow rate for a constant setting of the fan speed. Furthermore, the duration time of the first burst is always less than the time observed by the next successive burst. It is approximately 80 to 85% of the duration time of the next succeeding bursts.

The burst process generated at X/d of 96 is localized at the right side wall. From Table 3 it is observed that this burst does not sweep past Probe 1 which is situated at the far left hand side wall until X/d of 312. Utilizing this information a simple model of the burst process has been devised. This mechanism is illustrated in Figure 46. The angle of the burst wake is approximately 30 degrees. The wake fills the entire width of the channel at X/d of 336. The wavey line indicates a region of the burst wake that is dissimilar from the core of the wake. It has already been established that in this region the burst process is initiated by a positive spike, whereas the region close to the right side wall experiences a large negative spike. The two dimensional character of the burst process is not observed until X/d of approximately 450. In this region the burst process is observed to initiate with a large negative spike and end with a large positive spike.

The leading edge of the burst travels at a maximum speed of 30 to 33 ft./sec. The region surrounding the burst is laminar and the maximum

TABLE 3
Periodicity of Burst Process

	Initial Burst Duration Time (msec.) Z (in.)		Initial Laminar Duration Time (msec.) Z (in.)		Successive Burst Duration Time (msec.) Z (in.)		Successive Laminar Duration Time (msec.) Z (in.)	
X/d	<u>13.5</u>	<u>-13.5</u>	<u>13.5</u>	<u>-13.5</u>	13.5	<u>-13.5</u>	13.5	<u>-13.5</u>
96	-	-	-	-	-	-	-	-
120	160	no burst	168	no burst	328	no burst	360	no burst
144	156	no burst	164	no burst	440	no burst	352	no burst
168	160	no burst	200	no burst	4 88	no burst	496	no burst
216	232	no burst	320	no burst	376	no burst	648	no burst
264	664	no burst	616	no burst	752	no burst	440	no burst
312	720	228	568	736	920	584	368	684
360	536	264	712	992	1280	648	448	744
408	832	528	528	824	1112	1072	448	488
456	936	994	520	488	1240	1096	480	592
504	1096	1112	552	520	1312	1320	496	504
552	1256	1240	464	480	1400	1272	352	464

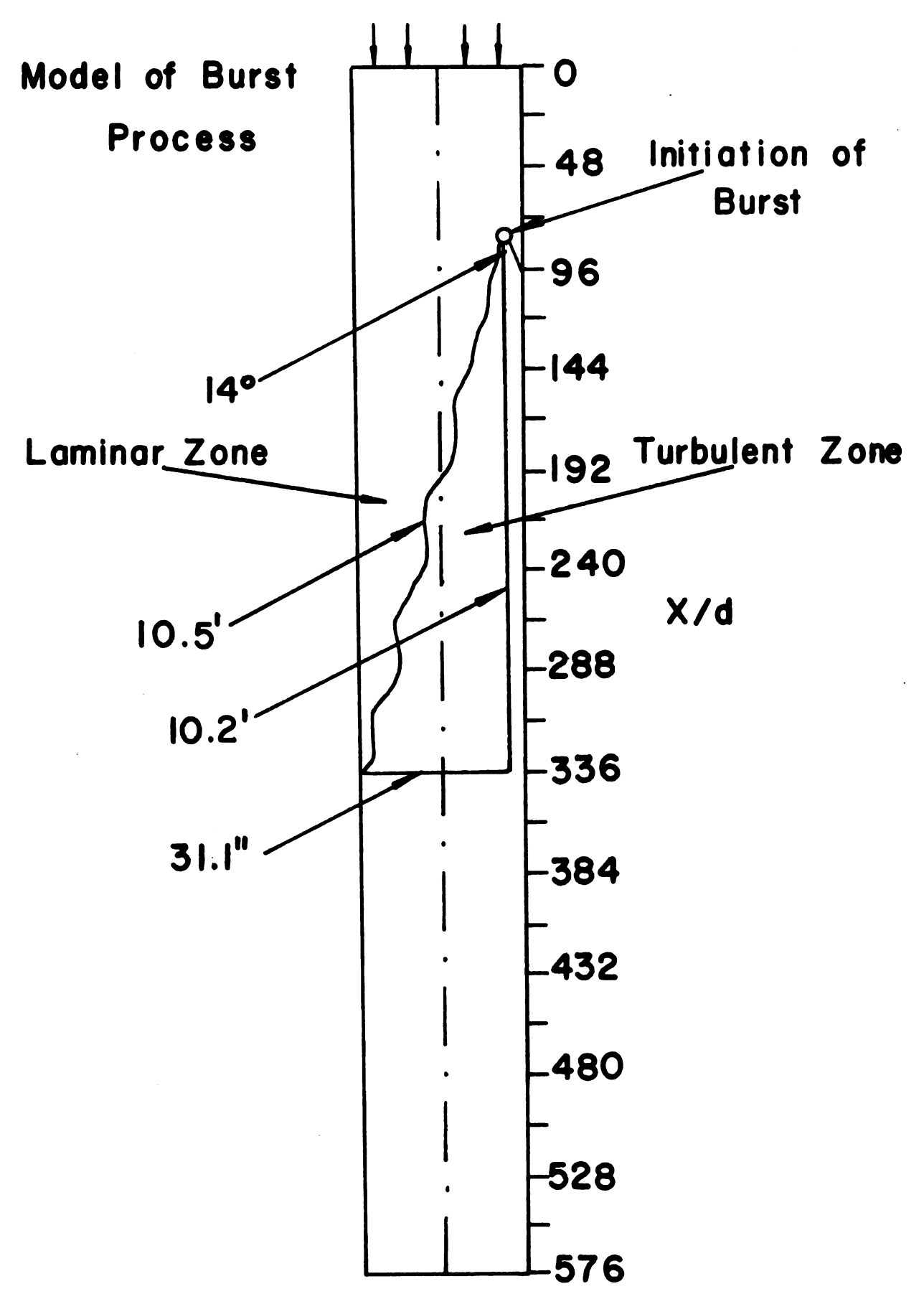


Figure 46. Mechanism of bursting process.

velocity experienced in this region is 40 to 42 ft./sec. Nevertheless, the average speed in both the turbulent and laminar regions is 28 ft./sec. The velocity of the edge of the burst wake in the z-direction is observed to be 8 to 9 ft./sec. This description characterizes the highly localized mechanism of the burst process.

In order to elucidate the cause of the localized burst generation the intensity level across the width of the channel at X/d of O was investigated. For a Reynolds number of 7100 the intensity level at the centerline, X = Y = Z = 0, was observed to be 0.12%. By variable placement of the probe with respect to the z-coordinate a high intensity region was observed at z = 13 to 15 in. A 0.23% intensity level was established in this region. Locating the probe inside the contracting region, X = -12in., established that the high intensity was generated by the filter device. At this point in the investigation the settling chamber was rebuilt, the straws removed and replaced, and the various screens aligned properly. The previous experiment was repeated and the effect of rebuilding the filter region was the elimination of the high intensity isolated at the far right hand side. Unfortunately, another high intensity region was generated on the far left side. For a Reynolds number of 5000 the intensity level at the centerline was observed to be 0.15%. Proceeding towards the left side wall the intensity level increased to a maximum of 0.19% at z = -16 in.

The bursting process was examined after the settling chamber was rebuilt and it was observed that the bursts were generated at the far left side wall, specifically at X/d of 84 and z = -13.5 in. The Reynolds number for transition was 7100. Therefore, the assymetrical intensity across

the width of the channel which was generated in the settling chamber affected transition downstream of the location of maximum intensity. If the location of maximum intensity was moved, the location of transition moved accordingly.

D. Velocity Profiles During Transition

When the Reynolds number is increased until the critical number of 7300 is achieved the flow is intermittent between a turbulent burst and a laminar flow. The intermittency of the burst process has already been established. However, the velocity profile at transition also varies between a parabola and an unknown turbulent profile ("unknown" in the sense it has never been experimentally determined). The velocity profile in the turbulent region of the burst may or may not possess the characteristics of the "one-seventh" profile. By means of conditional sampling the velocity profile was experimentally realized as the flow oscillated from a laminar condition to that of the burst condition.

For the velocity profile burst investigation the probes were placed at X/d of 360 with Probe 1 near the centerline, z = -1.0 in., and Probe 2 near the right side wall, z ' 15.0 in. The velocity profile was obtained from measurements of the centerline probe. In order to initiate each experiment the Schmitt trigger was applied to Probe 2 near the right side wall. Instantaneous on-line velocity measurements were obtained by traversing Probe 1 in the y-direction at the onset of every burst. Seventeen experiments, each representing a different y-location, were performed in order to realize an entire profile.

A mosaic of the velocity profiles during the bursting process is presented in Figure 47. Each profile is the result of 68 individual

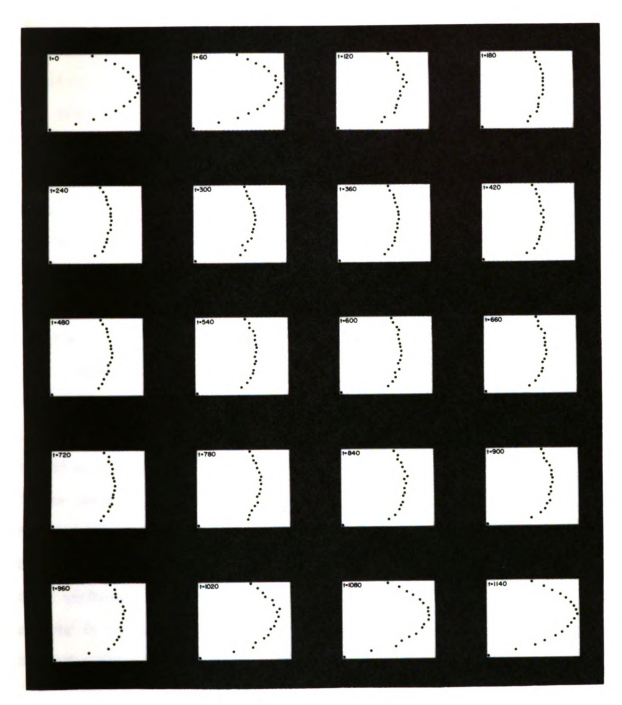


Figure 47. Mosaic of velocity profile during burst process.

experiments: a) 4 experiments at each y-location; and b) 17 experiments to cover the full height of the channel. The 4 experiments at each y-location were averaged to obtain a single point. The on-line instantaneous velocity measurements were time averaged over 60 msec. Therefore, each point represented an average over time (60 msec.) and an average over 4 individual experiments. The sampling rate of the computer was initialized for 6 msec./sample. The total number of samples for each experiment was 500 which represents a total time of 3.0 seconds. The 60 msec. time average represents 10 samples. The final task of the investigation was the registration of 17 experiments in order to create the full velocity profile.

Inspection of the mosaic in Figure 47 reveals that a parabolic velocity profile is apparent at t=0 and t=1140 msec. This represents the beginning and end of the turbulent burst. At the onset of the burst, t=60 msec., the first portion of the profile to encounter a deformation is the centerline, y=d/2. The total time in which the profile changes from a parabola to a turbulent profile is achieved within 120 msec. The turbulent profile is fully established at t=180 msec. This profile remains unchanged until t=720 msec., whereupon the change to the parabolic profile is initiated. The rate at which the turbulent profile changes to that of a parabola is a much slower process and takes approximately 360 msec. This is 3 times slower than the change from a parabola to a turbulent profile. Therefore, the mechanism that distorts the profile occurs at a faster rate at the beginning of the burst process than during the termination of the burst.

The one seventh power law is often used instead of the logarithmic

law to express the turbulent velocity profile if the Reynolds number is not very large. The relationship is expressed as

$$u = u_{max} (2y/d)^{1/7}$$
 (4.36)

Substituting this one-seventh power velocity profile in equation (4.27a) a relation is obtained between the centerline velocity and the mean velocity.

$$U_{ave} = U_{max} (0.967)$$
 (4.37)

Equation (4.36) represents the profile for one half of the channel. In order to determine whether the velocity profiles generated by the bursting process obey a one-seventh velocity profile the following equation was employed

$$u = u_{max} [1 - ABS(\frac{2y - d}{d})]^{1/7}$$
 (4.38)

This equation describes a one-seventh profile over the entire width of the channel.

The profiles represented in the mosaic of Figure 47 were curve-fitted with respect to equation (4.38). A curve-fitting routine described earlier was employed for this purpose. The results of the investigation determined that the profiles represented by times of 180 to 720 msec. obeyed the one-seventh power law profile. Experimental and theoretical values are plotted with respect to the y-coordinate in Figure 48. The residuals generated by subtracting the experimental and theoretical values are plotted in Figure 49. This plot indicates a random distribution of residuals. A standard "run" test was employed in order to test for randomness of the residuals. The experiment gave rise to a 95% confidence or random arrangement of residuals. Therefore, the result of this investigation

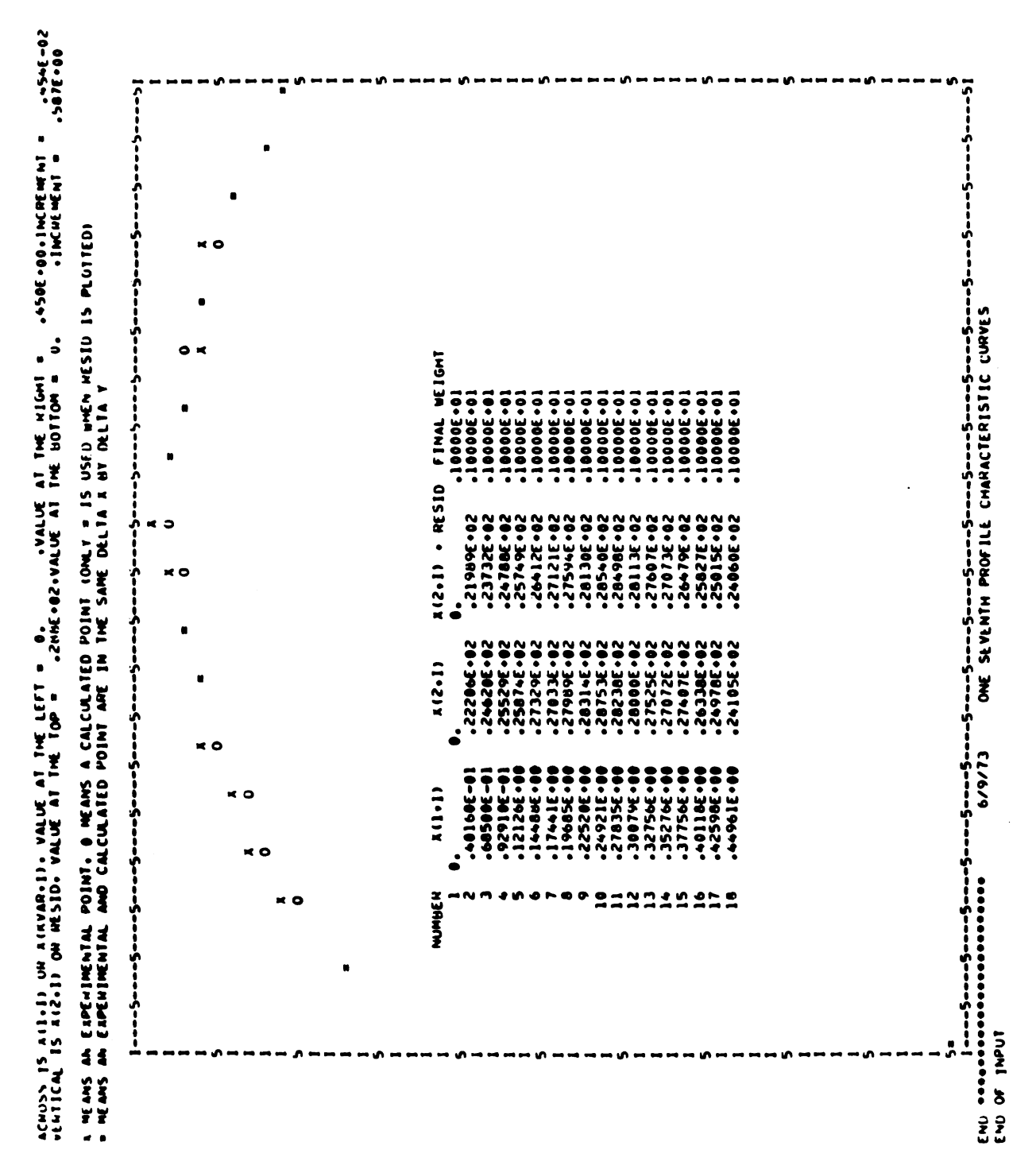


Figure 48. Computer printout of calculated and experimental velocity profiles (1/7 power law profile).

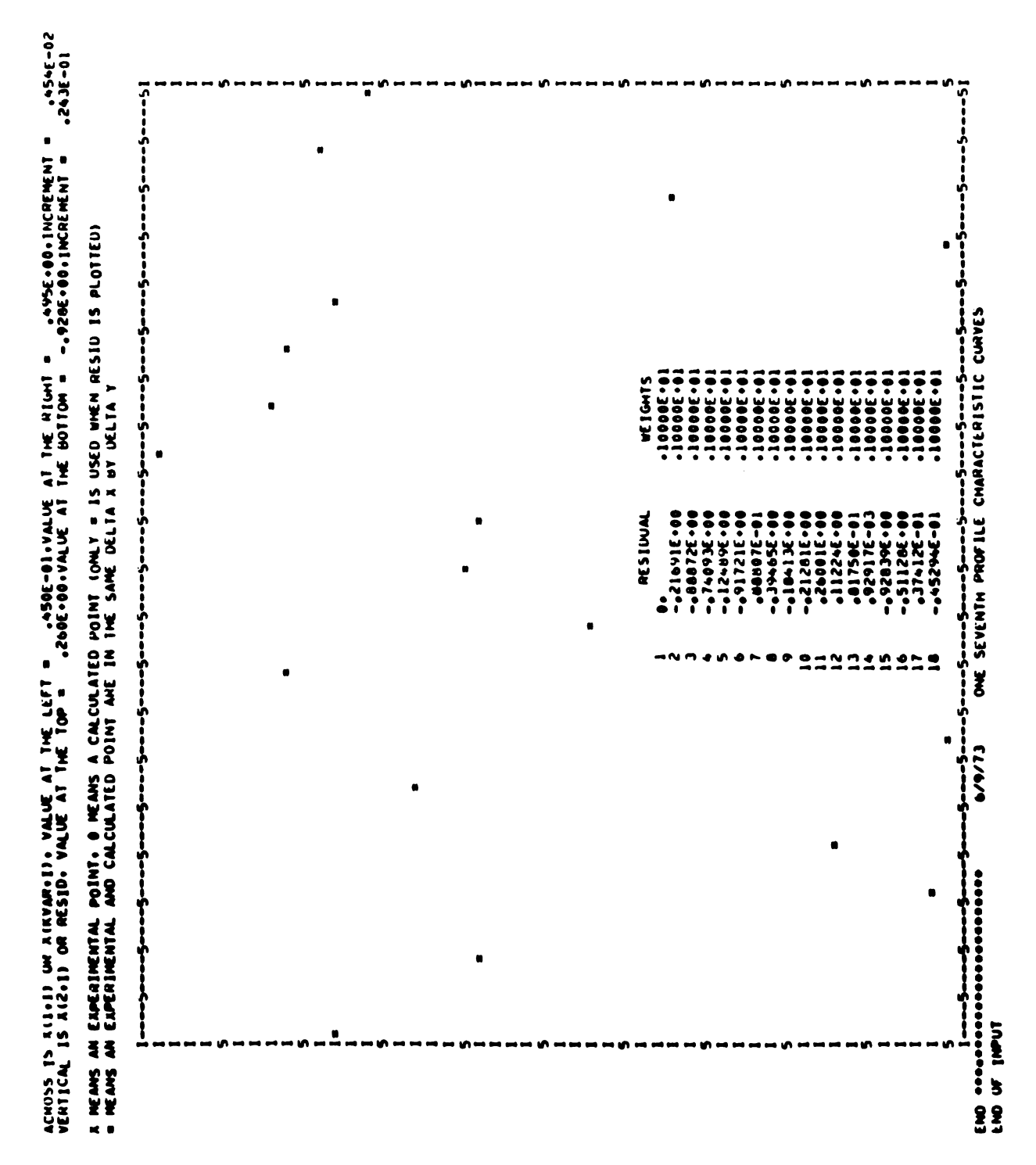


Figure 49. Computer printout of residuals.

substantiated that the velocity profiles over 70% of the turbulent burst can be described by a one-seventh power law profile.

As observed in Figure 47 the laminar to turbulent profile is quickly achieved. Regions close to the wall must undergo a sudden increase in velocity in order to maintain the one-seventh profile. Similarly, a sudden decrease in the velocity must be evident at the centerline. A schematic of this mechanism is illustrated below.

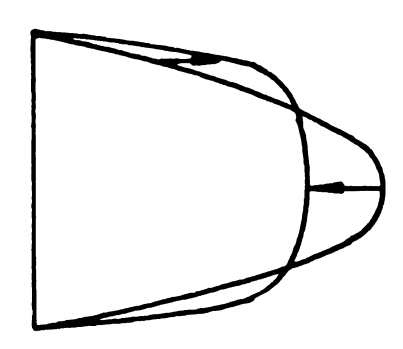
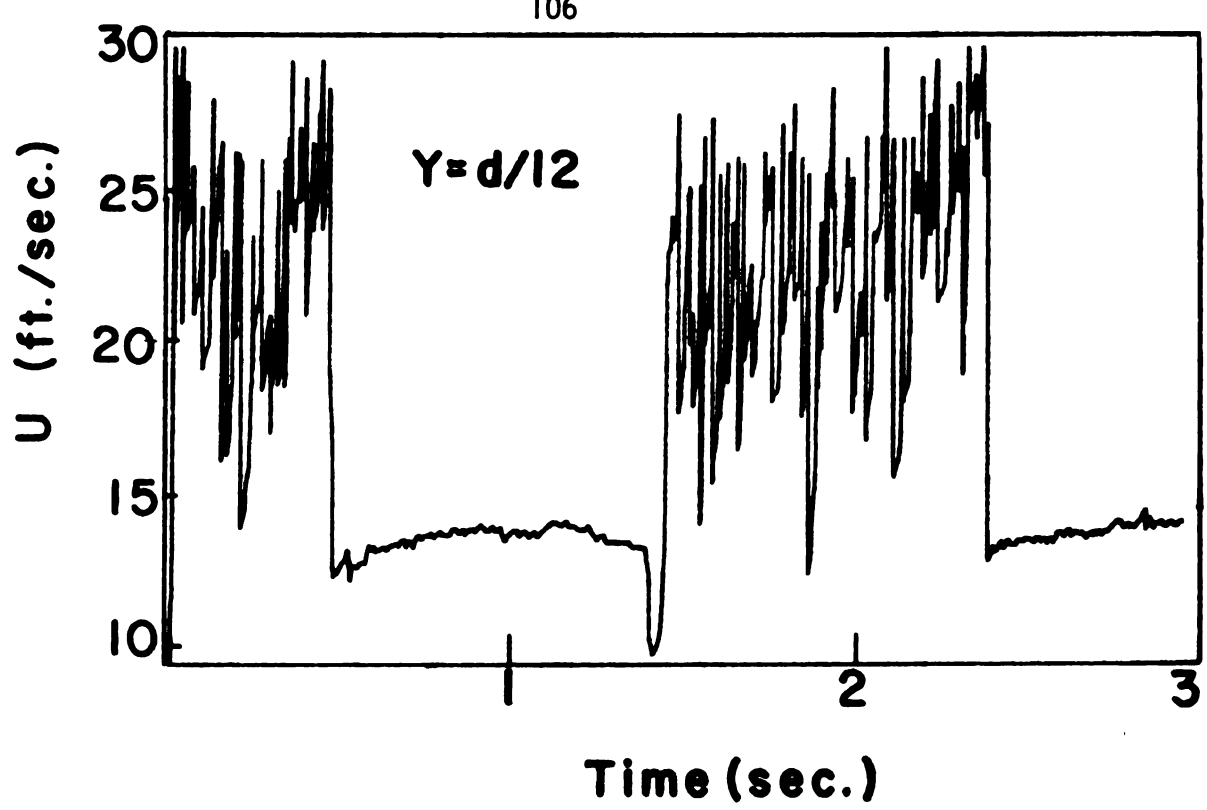


Figure 50 presents the velocity changes at two y-locations; near the wall, y = d/12, and at the centerline, y = d/2. During the bursting process the velocity increases by 17% near the wall, y = d/12, and decreases by 67% at the centerline, y = d/2.

The laminar portion of the bursting process is associated with small scale fluctuations. An indication of the level of intensity that may exist during this time is the quantity $\overline{u'}^2$. Figure 51 presents the computed fluctuations based upon the first laminar poriton of the signal in Figure 42. $\overline{u'}^2$ and $\overline{u'}^2$ are plotted versus time for the regions y = d/12 and y = d/2. It is interesting to note that at the beginning portion of the laminar signal the fluctuations decrease at a slow rate. The end of the laminar signal is associated with a very rapid increase in





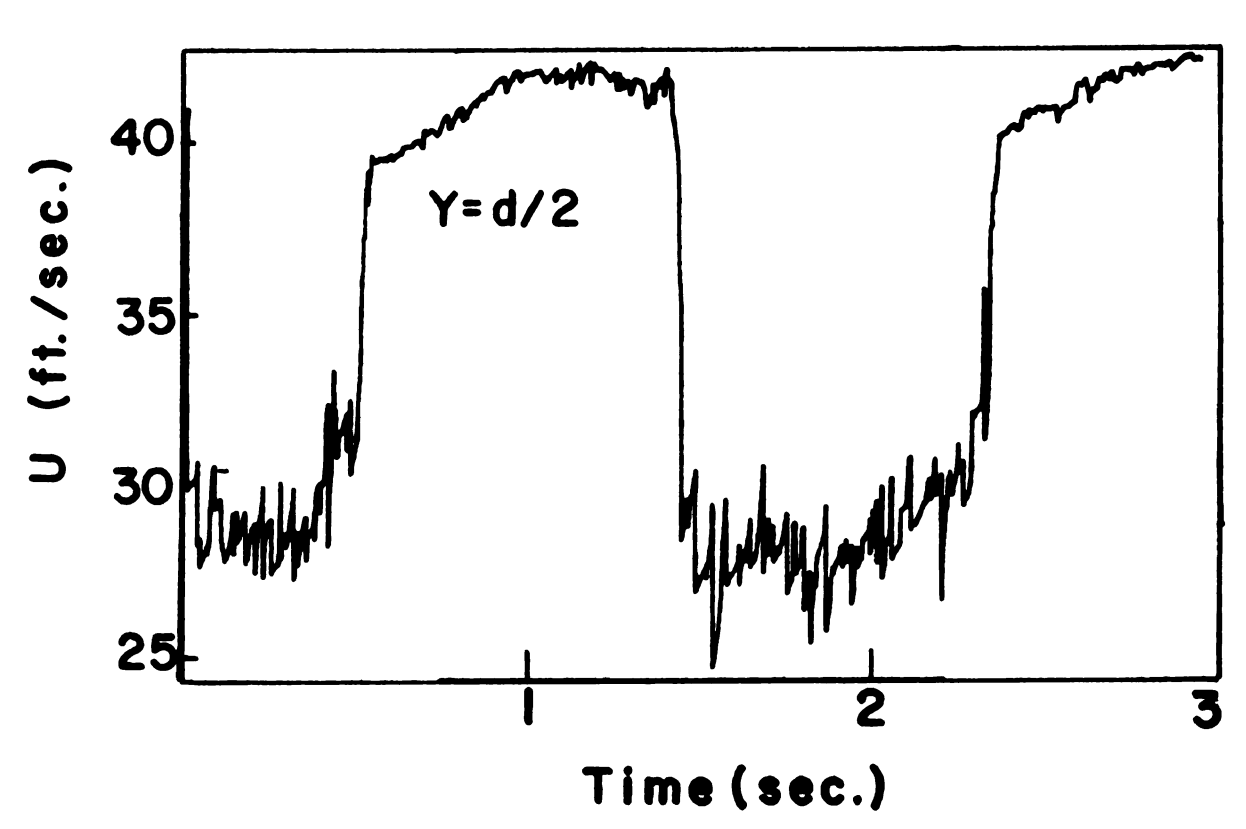
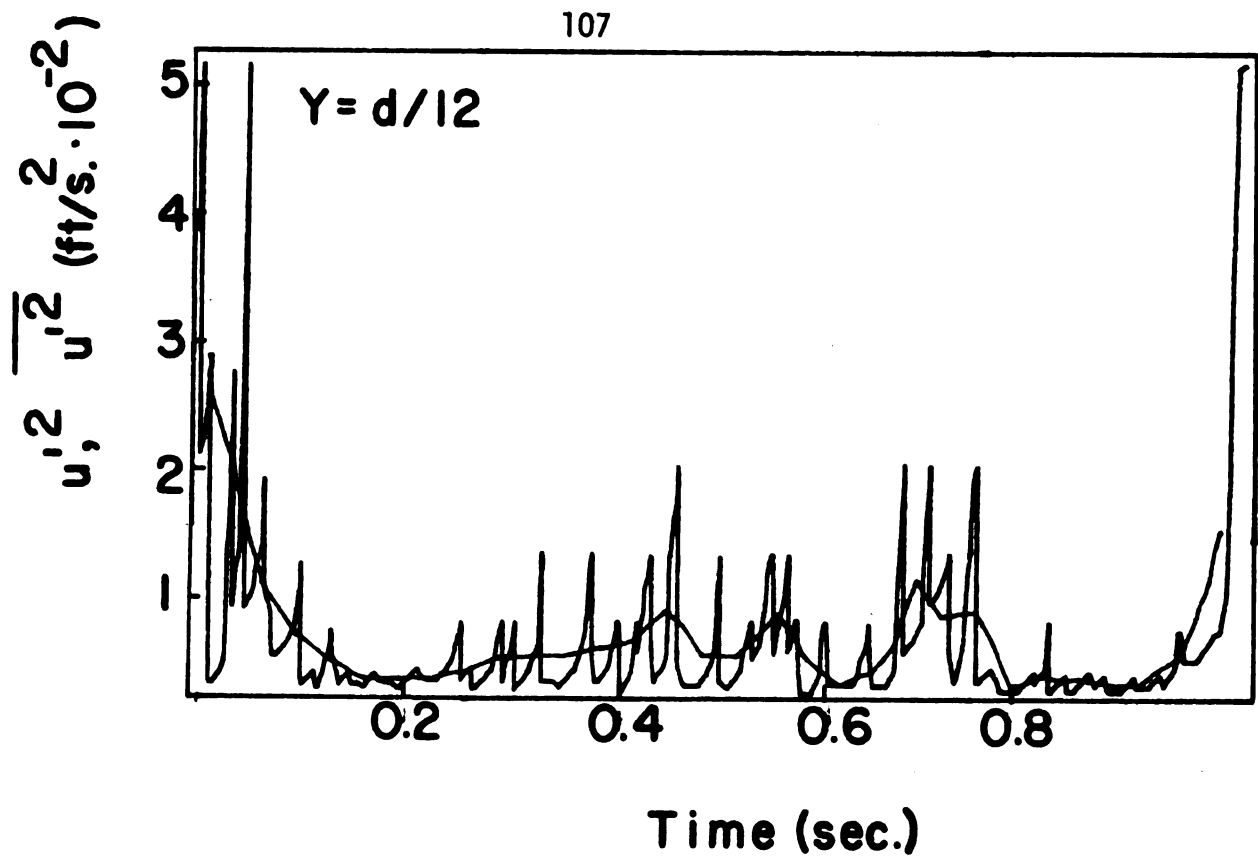
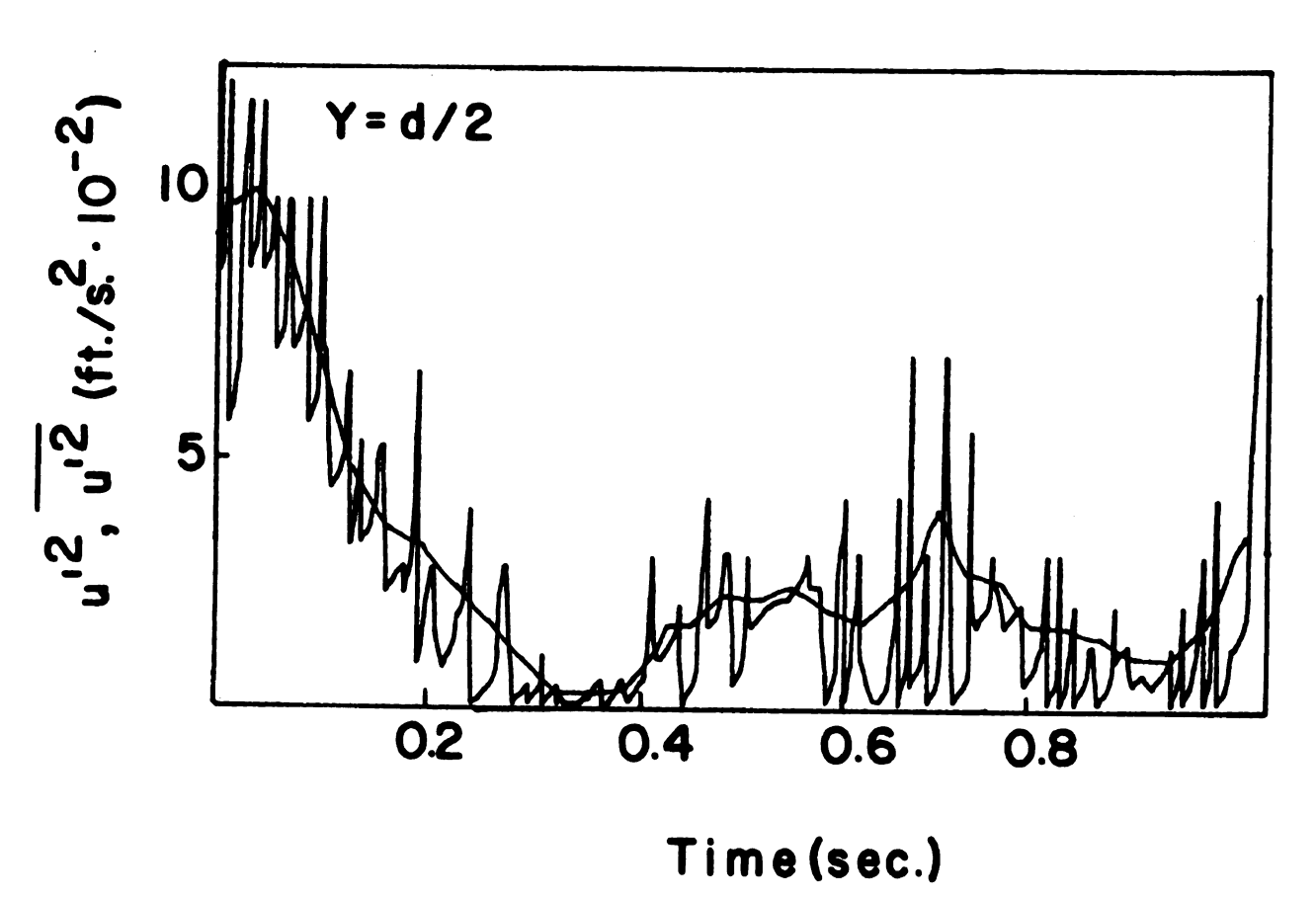


Figure 50. Velocity changes near the wall and the centerline during the burst process.





Perturbations during the laminar portion of the burst process. Figure 51.

the fluctuation level. A similar observation has been previously noted for the changing velocity profile as it moves in and out of the burst. Comparison between the region near the wall, y = d/12, and the centerline, y = d/2, shows a much larger scale of fluctuations present at the centerline.

CHAPTER 5

DISCUSSION OF RESULTS

The results of the boundary layer analysis in predicting the development of the velocity profile in the entrance region of the channel agree well with the experimental observations. Entrance lengths for the fully developed profile have been calculated for a range of Reynolds numbers. A linear relationship is observed between the entrance length and the Reynolds number. A free stream velocity distribution was calculated by means of continuity and provided a basis for the boundary layer calculations. It was observed that the free stream velocity was accurate enough to provide a good comparison between theory and experiment. The skin friction coefficient was a significant parameter that was generated by means of the boundary layer analysis. The results indicated a minimum displacement thickness and skin friction coefficient 3 in. before entry to the parallel plate channel.

The experimental results indicate that a laminar flow exists up to a critical Reynolds number of 7300 if the channel is sufficiently purified of disturbances. Developing entrance lengths have been obtained which compare well with the theoretical prediction established by Schlichting (1962). For a Reynolds number of 7300 the velocity profile is observed to be fully developed by X/d of 192. It is noted that the 6 ft. contracting region develops the flow an equivalent length of 84 channel widths for a Reynolds number of 4800.

A statistical treatment of the data was prepared to give information about the developing profile, the nature of the fully developed profile and an estimate of the channel gap width. A curve-fitting routine

was utilized to give information about deviations from a parabolic velocity profile.

Investigations in the regions of developing and fully developed flow have resulted in the experimental evidence that the wake-effects of the probe assembly result in the flow being fully turbulent in the downstream direction of the probe. The wake spreads across the entire width of the channel 2 ft. downstream of the probe assembly. This effect results in an increase of the shear stress in the turbulent region behind the probe. Since the pressure drop is a direct function of the shear stress the positioning of the probe in either the downstream or upstream direction acts as a flow meter. An equation was developed that predicted the change in the average velocity as a function of the position of the probe (for a constant setting of the fan).

A comprehensive mapping of velocity profiles in the channel assembly allowed identification of the regions of bursting and fully turbulent flow. As the probe is positioned sequentially downstream the first burst is observed at X/d of 480 for a Reynolds number of 7300. Increasing the Reynolds number resulted in the bursts being detected farther upstream. For Reynolds numbers 8000 and above the bursting region was isolated to a small region at X/d of 192. Upstream of this region the flow was laminar and downstream it was fully turbulent.

The influence of the side wall boundary layer on the mean flow was determined experimentally. The thickness of the boundary layer was measured at the centerline, y = d/2, and found to be less than 0.750 in. thick at the exit of the channel for a Reynolds number of 7300. Based on this maximum boundary layer thickness the exiting flow is two

dimensional over 96% of the width of the channel. Therefore, the influence of the boundary layer on the mean flow is minimal. It was interesting to observe that the laminar fluctuations in the side wall boundary layer increased as a function of proximity to the wall and Reynolds number. The thickness was observed to decrease and reach a minimum for a Reynolds number of 4000. However, as the Reynolds number was increased above 4000 the boundary layer increased in thickness as a result of laminar fluctuations which were induced by the high flow rates. However, the transition process did not appear to be affected by these fluctuations since bursting occurred simultaneously in the boundary layer and the mean flow.

To further establish the extent of the transition region the intensity of the finite disturbances and the frequencies of the disturbing waves were measured along the x and y-coordinates. Investigations were carried out along the centerline and locations near the wall in order to determine the symmetry of the disturbances. The results indicated that the disturbances damp as the Reynolds number is increased. For a Reynolds number range of 3000 to 6000 the fluctuation intensity is a minimum at the centerline and grows to a maximum near the wall, y = d/12. Increasing the Reynolds number range, 4000 to 7300, causes the intensity at the centerline to grow. The intensity for this range of Reynolds numbers is a maximum at y = d/12 until X/d of 336. At this location the maximum intensity is shifted to the centerline. Above the critical Reynolds number the disturbances in the regions between X/d of 0 and 192 exhibit amplification at y = d/12 and y = d/4. The centerline is most stable at this point since it has the minimum intensity.

Spectral analysis of the disturbances generated naturally in the channel showed a series of dominant waves that amplify as the flow progresses into unstable conditions. The number of these dominating waves was observed to be a maximum near the wall, y = d/12, decreasing in number to the centerline. A wave of 63 to 75 Hz. became amplified for a Reynolds number of 6800 at X/d of 144. The sudden growth of this wave strongly suggests its role in the natural transition process. The maximum intensity of the 63 to 75 Hz. wave was detected at y = d/12 and X/d of 144 for the Reynolds number range 5800 to 7000. Transition was observed to occur at X/d of 192 which implies that this particular wave must grow and amplify in 2 or 3 channel widths.

The investigation of the nature of the bursting process, analyzed by an on-line data acquisition system, gave rise to some unexpected results. It was determined that the burst process was not two dimensional across the width of the channel at the burst Reynolds number of 7300. The burst occurred in isolated regions at upstream locations where the free stream distrubance level was highest. A small region, 7 in. in width, at X/d of 96, near the right hand side wall was characterized by large velocity spikes for a burst Reynolds number of 7300. The transition occurring in this particular region was similar to the transition in a boundary layer, in that transition in a boundary layer also is a highly localized three dimensional process involving the occurrence of strong velocity spikes. Spangenberg and Rowland (1960) reported from optical studies that the turbulent spots grow rapidly during the first microseconds and appear to explode from the smooth outline of the laminar layer. Thus, the transition process is considered to be similar to that observed by

Spangenberg and Rowland. They observed a turbulent breakdown as an intermittent appearance of ripples on the outer surface of the boundary layer. As the ripples moved downstream, each divided into several segments. Each of the segments then became the source of a "shock wave". In a matter of microseconds after the appearance of these disturbances boundary layer air was "belched" from the disturbance area, and the erupted spot then grew into a turbulent spot.

In the current study the strong velocity spikes generated at a frequency of 6 to 8 Hz. at X/d of 96 appear to grow as they progress downstream. The turbulent core region between the initial large negative spike and the final positive spike becomes progressively larger at greater downstream locations. From a chaotic state of bursting at X/d of 96 the process develops into a ordered periodic structure by X/d of 384.

A description by Tani (1967) of the transition process indicates that turbulence is initiated in small localized regions in the form of "turbulence spots". These spots grow as they move downstream until they merge to form the fully developed turbulent boundary layer. The process observed at a burst Reynolds number of 7300 in the channel can be compared quite well to Tani's description. However, the dimensions are greatly increased in x and z.

The final investigation of the bursting process concerned the shape of the profile when the flow was intermittent between a turbulent slug and a laminar flow. It was observed that the mechanism distorting the parabolic profile into a turbulent one at the burst leading edge proceeded at a faster rate than the turbulent profile into a parabola at the burst trailing edge. Close examination revealed that the centerline region was

the first to be affected by the burst process. Comparison to a one-seventh power profile substantiated that the burst profile is characteristic of the common turbulent shape over 70% of the burst process.

1. Conclusions

From the present study the following conclusions can be drawn:

- a) a linear relationship has been obtained between the entrance length (the distance that is needed to achieve a parabolic velocity profile) and the Reynolds number. The experimental data was observed to correlate well with analytical predictions.
- b) For sufficiently high Reynolds numbers regions of bursting and fully turbulent flow have been identified by a comprehensive mapping of velocity profiles. The developing region between X/d of 0 to 192 was shown to be laminar at all Reynolds numbers.
- c) An experimental burst Reynolds number of 7300 has been achieved for the present channel assembly. The transition Reynolds number can be monotonically increased by decreasing the fluctuation intensity.
- d) A minimal effect of the side wall boundary layer on the mean flow was determined experimentally. For a Reynolds number of 7300 the boundary layer thickness was determined to be less than 0.750 in. at the exit of the channel.
- e) A wave of 63 to 75 Hz. was amplified as the Reynolds number was increased to 6800 at X/d of 144. The sudden growth of this wave influenced the fluctuation intensity level for regions near the wall, y = d/12 and y = d/4. The wave was not present at the centerline, y = d/2. Linear stability theory predicts a wave of 92.5 Hz. at the minimum critical Reynolds number of 7700.
- f) A close examination of the burst process revealed a three-dimensional highly localized bursting phenomenon. Strong negative

velocity spikes were observed to originate at X/d of 96 for a burst Reynolds number of 7300. A non-uniform fluctuation intensity level at the inlet of the channel influenced the origin of the burst. The location of the burst coincided with the maximum disturbance level at the inlet of the channel.

g) The shape of the turbulent profile achieved during the bursting process was observed to be the one-seventh power law profile over 70% of the burst. The mechanism distorting the parabolic profile into a turbulent one proceeded at a faster rate than the turbulent profile into a parabola.

2. Recommendations

In order to study the transition mechanism and evaluate the burst process in better detail the following recommendations are made:

- a) The settling chamber should be redesigned. Specifically, the straw chamber should be rebuilt in order to provide an even distribution of straws across the inlet. The entrance region is an important factor since the intensity level at the inlet to the channel strongly influences the origin of the burst process.
- b) Further investigations are necessary in order to elucidate the highly localized transition process. If the intensity is uniform across the width of the channel would the point of transition become random or would it remain localized?
- c) It would be of interest to traverse the boundary layer along the side walls with respect to the y and z-coordinates. This would provide a mapping of the velocity profile. The influence of high Reynolds numbers which induce large fluctuations in the boundary layer should be further investigated.
- d) Finally, another measuring device or transducer besides the hot-wire anemometry system (such as a sensitive piezo-resistive accelerometer) could be utilized in order to investigate the bursting phenomenon without grossly affecting the flow.

APPENDIX A SYMBOLS FOR BOUNDARY LAYER ANALYSIS

APPENDIX A

SYMBOLS FOR BOUNDARY LAYER ANALYSIS

```
constant used to match numerical to asymptotic solution (2.31)
             coefficients in linearized momentum equation (2.26)
C_a = 2(\delta^*/r_w) \cos \alpha , parameter related to axisymmetric flow appearing in equation (2.23)
C_f = \tau_w / \rho U^2/2, coefficient of skin friction
            coefficients in equation (2.24)
c<sub>1</sub>...c<sub>4</sub>
             gap width in the parallel plate channel
d^* = d/2 half the channel gap width
E
            modulus of elasticity
<sub>f</sub>(k)
             variables used in the Runge Kutta method, k=1,3
f' = (U-u)/U, velocity defect variable
             particular solution of equation (2.26)
             homogeneous solution of equation (2.26)
             half the gap width of the contraction at x = -6 ft. (see Fig. 1)
h
I
            moment of inertia
             length of contraction (see Fig. 1)
P = [\delta * dU/dx]/U, parameter in equation (2.16)
Q = [d(U\delta^*)/dx]/U, parameter in equation (2.16)
R = [\delta * dr_w/dx]/r_w, parameter in equation (2.16)
            radius of curvature
rw
R_{S*} = \delta*U/v, Reynolds number based on displacement thickness
r = r_w(\overline{x}) + \overline{y}\cos \alpha(\overline{x}), radius of a point in the boundary layer
```

```
parameter in asymptotic outer solution (2.33)
S
\overline{u},\overline{v}
             time average velocities in x and y directions respectively
UVT
             Reynolds stress
            wall transpiration velocity
             streamwise coordinate (see Fig. 2)
Х
             coordinate normal to wall (see Fig. 2)
У
\Delta x = x_{i+1} - x_i, numerical integration step in the streamwise direction
            angle of the tangent to the surface with respect to the axis
            boundary layer thickness
\delta^* = \int_0^\infty (U-u)/U \, dy, displacement thickness
          non-dimensional coordinate normal to the wall
\theta = \int_{-\infty}^{\infty} u(U-u)/U^2 dy, momentum thickness
     0.41 von Karman constant in the effective viscosity function
            molecular kinematic viscosity
            effective kinematic viscosity
            density
            local shear stress
     \partial (r \tau/r_{\omega} \rho U^2)/\partial \eta, non-dimensional shear stress gradient (2.24)
T
            non-dimensional effective viscosity (2.20)
            inner and outer effective viscosity functions
φ,Φ
            coordinate normal to wall in outer effective viscosity function
χ
            coordinate normal to wall in inner effective viscosity function
Subscripts
( )<sub>a</sub>
            variable evaluated at asymptotic matching point
();
            index of variable in the x direction
()
            variable evaluated at point where recalculation begins
```

() _∞	variable evaluated at the edge of the boundary layer
Supers	cripts
()'	differentiation with respect to $\eta = y/\delta^*$
(_)	denotes untransformed coordinates. Also used with functions of x only, denotes average value, [(),] + (),]/2

^APPENDIX B SYMBOLS USED IN EXPERIMENTAL RESULTS

APPENDIX B

SYMBOLS USED IN EXPERIMENTAL RESULTS

```
predicted value of parameters used in least squares analysis (4.9,\ 4.10)
             channel gap width
d^{\dagger} = du^{*}/v, normalized channel gap width
e_i = Y_i - Y_i, residual (observed minus predicted values) (4.12)
E(Y_i)
            expected value of Y;
            friction coefficient for laminar or turbulent flow
I = \sqrt{u^{2}} / U_{ave}, intensity of disturbances (4.35)
            entrance length (distance needed to achieve a parabolic
            velocity profile)
Р
            Pressure
            change in pressure (4.33)
ΔΡ
dP/dx
            pressure gradient (4.32)
R^* = 2dU_{ave}/v, Reynolds number based on twice the channel's gap width
R = dU_{ave}/v, Reynolds number based on full channel gap width
S
            sum of squares used in least squares analysis (4.15)
            time
U_{ave} = 1/d \int_{0}^{d} u(y) dy, average velocity
            average velocity at probe position x = 0 ft.
Un
            average velocity at probe position x = 23 ft.
            x-component of velocity
u^{\dagger} = u/u^{\star}, normalized velocity
u^* = \sqrt{\tau_0/\rho}, friction velocity
```

```
ū
            time-averaged velocity
u'
            perturbation in x-component of velocity
            maximum velocity
umax
X_1,Y_1
            independent and dependent variables used in least squares
            analysis (4.6)
            coordinate axes
x,y,z
y^+ = yu^*/, normalized y-component
\beta_1 \dots \beta_n
            parameters used in least squares analysis (4.6)
            error in estimating Y<sub>i</sub>
\epsilon_i
            molecular viscosity
μ
            kinematic viscosity
            density
ρ
            shear stress evaluated at the wall
ď
```

LIST OF REFERENCES

- 1. Beck, J. V., <u>Proc. of the Third International Heat Transfer Conference</u> Vol. IV. pp. 74-80 (1966), and <u>Research Proposal</u> Michigan State University.
- 2. Bodia, J. R., and Osterle, J. F., Appl. Sci. Res. 10, 265, (1961).
- 3. Boussinesq, J., Comptes Rendus, 113, 9 (1891).
- 4. Breslin, J. A., Lehigh University Technical Rep., No. 22 (1970).
- 5. Cebeci, T., and Smith, A. M. O., <u>Proc. Conf. on Computation of Turbulent Boundary Layer Prediction</u>, Stanford University, pp. 346-355 (1968).
- 6. Chen, R. Y., J. of Fluids Engineering March 153 (1973).
- 7. Elder, J. W., <u>J. Fluid Mech.</u>, <u>9</u>, 235 (1960).
- 8. Emmons, H. W., J. Aero. Sci. 18, 490 (1951).
- 9. Herring, H. J., and Mellor, G. L., N.A.S.A. CR-1564, (1970).
- 10. Karnitz, M. A., Ph.D. Diss. Michigan State University, (1971).
- 11. Kao, T. W., and Park, C., J. Fluid Mech., 43, 145 (1970).
- 12. Kao, T. W., and Park, C., J. Fluid Mech., 52, 401 (1972).
- 13. Kays, W. M., <u>Convective Heat and Mass Transfer</u> McGraw-Hill Book Co. Inc., New York (1966).
- 14. Klebanoff, P. S., Tidstrom, K. D., and Argent, L. M., <u>J. Fluid Mech.</u>, <u>12</u>, 642 (1962).
- 15. Langhaar, H. L., <u>J. Appl. Trans.</u>, <u>ASME 64</u>, A55 (1942).
- 16. Lin, C. C., Part I, II, III, Quart. Appl. Math., 3, (1945, 1946).
- 17. Mellor, G. L., and Gibson, D. M. J. Fluid Mech. 24, 225 (1966).
- 18. Mellor, G. L., and Herring, H. J., <u>Proc. Conf. on Computation of Turbulent Boundary Layer Prediction</u>, Stanford University, pp. 331-345 (1968).
- 19. Narayanan, M. A. B., and Narayana, T., <u>Z. Agnew. Math. Phys.</u>, <u>18</u>, 642 (1967).
- 20. Nicely, V. A. and Dye, J. L. Journal of Chemical Education (1971).

- 21. Pantankar, S. V., Spalding, D. B., and Ng, K. H., <u>Proc. Conf. on Computation of Turbulent Boundary Layer Prediction</u>, Stanford University pp. 356-365 (1968).
- 22. Patel, V. C., and Head, M. R., J. Fluid Mech., 38, 181 (1969).
- 23. Reynolds, W. C., and Potter, M. C., <u>J. Fluid Mech.</u>, <u>27</u>, 465 (1967).
- 24. Schiller, L., Z. angew. Math. Mech. 2, 96 (1922).
- 25. Schlichting, H., Z. angew. Math. Mech., 14, 368 (1934).
- 26. Schlichting, H., <u>Boundary Layer Theory</u> McGraw-Hill Book Co. Inc., New York (1962).
- 27. Schubauer, G. B., and Klebanoff, P. S., N.A.C.A. TN-3489, (1955).
- 28. Schubauer, G. B., and Skramstad, H. K., N.A.C.A. TR-909, (1943).
- 29. Sherlin, G. C., <u>J. Res. N.B.S. Sec. A, Phys. and Chem.</u>, <u>64A</u>, 281 (1960).
- 30. Spangenberg, W. G., and Rowland, W. R., <u>Phys. Fluids</u>, <u>3</u>, 667 (1960).
- 31. Stewartson, L. M., Stuart, J. T., and Brown, S. N., <u>J. Fluid Mech.</u> <u>51</u>, 705 (1972).
- 32. Tani, I., Phys. Fluids Supp., S11, (1967).
- 33. Tani, I., Ann. Rev. Fluid Mech., 1, 169 (1969).
- 34. Thomas, L. H., Part I, II, III, Quart. Appl. Math., 3, (1945, 1946).
- 35. Van Dyke, M., J. Fluid Mech., 44, 813 (1970).
- 36. Wilson, S. D. R., <u>J. Fluid Mech.</u>, <u>46</u>, 787 (1971).
- 37. Wygnanski, L. and Champagne, F., Boeing Scientific Res. Lab., (1970) (to be published).

